isvr Institute of Sound and Vibration Research

Model for the Control of the Sound Radiated by an Aircraft Panel Excited by a Turbulent Boundary Layer

C. Maury, P. Gardonio and S.J. Elliott

ISVR Technical Report No 287

June 2000

University of Southampton

SCIENTIFIC PUBLICATIONS BY THE ISVR

Technical Reports are published to promote timely dissemination of research results by ISVR personnel. This medium permits more detailed presentation than is usually acceptable for scientific journals. Responsibility for both the content and any opinions expressed rests entirely with the author(s).

Technical Memoranda are produced to enable the early or preliminary release of information by ISVR personnel where such release is deemed to the appropriate. Information contained in these memoranda may be incomplete, or form part of a continuing programme; this should be borne in mind when using or quoting from these documents.

Contract Reports are produced to record the results of scientific work carried out for sponsors, under contract. The ISVR treats these reports as confidential to sponsors and does not make them available for general circulation. Individual sponsors may, however, authorize subsequent release of the material.

UNIVERSITY OF SOUTHAMPTON

INSTITUTE OF SOUND AND VIBRATION RESEARCH

SIGNAL PROCESSING & CONTROL GROUP

**Model for the Control of the Sound Radiated
by an Aircraft Panel Excited by a Turbulent Boundary Layer**

by

C.Maury, P.Gardonio and S.J.Elliott

ISVR Technical Report No. 287

June 2000

Authorised for issue by
Prof S J Elliott
Group Chairman

Model for the control of the sound radiated
by an aircraft panel excited by a turbulent boundary layer

CONTENTS

List of Figures

Figure 6.23 The sound power inwardly radiated by an aircraft panel ($\varsigma = 0.0005$) before control (bold) and after cancellation of a number of **radiation** modes: the first mode (dashed), the two first modes (dash-dotted), the three first modes (dotted) and the four first modes (thin).

Figure 6.24 Attenuation in the sound power radiated by an aircraft panel ($\varsigma = 0.01$): after cancellation of the first radiation modes (dash-dotted) and after cancellation of the first structural modes (dashed).

Figure 6.25 Attenuation in the sound power radiated by a TBL-excited panel after cancellation of the first **structural** modes for different values of the damping ratio: $\varsigma = 0.0005$ (bold), $\varsigma = 0.01$ (dash-dotted), $\varsigma = 0.05$ (dashed) and $\varsigma = 0.2$ (dotted).

Figure 6.26 Attenuation in the sound power radiated by a TBL-excited panel after cancellation of the first **radiation** modes for different values of the damping ratio: $\varsigma = 0.0005$ (bold), $\varsigma = 0.01$ (dash-dotted), $\varsigma = 0.05$ (dashed) and $\varsigma = 0.2$ (dotted).

ABSTRACT

This aim of this report is to present a simplified but relevant model for predicting the vibro-acoustic response of an aircraft panel excited by a turbulent boundary layer. This analytical model provides an insight into the physical properties of the TBL-excited panel and enables the performance limitations to be derived for various idealised active control systems.

This report is divided into three main parts. The first part (sections 1-3) justifies the simplifying assumptions of the flat plate model for an aircraft panel. Furthermore, it describes how the spectral densities of the panel response can be obtained from an analysis of the system response to a harmonic deterministic excitation and a statistical model for the turbulent boundary layer.

The second part (sections 4-5) focuses on the modal formulation used to solve the flow-structure interaction problem in the frequency domain; criteria are discussed under which the cross-modal coupling of the structural modes can be neglected when excited by a turbulent boundary layer. Section 5 describes the modelling of the pressure field induced by the turbulent boundary layer which acts as a distributed random excitation field on the structure.

The third part (section 6) presents simulation results in which the verification of the approximations and the influence of the main physical parameters are discussed, together with a comparison between experimental and predicted results. The way in which the structural modes and the radiation modes of the plate contribute to the vibro-acoustic response are also examined. One important conclusion is that for subsonic turbulent flows, each structural mode radiates sound independently. A suitable strategy for the active structural acoustic control of the sound power transmitted through the panel would thus be independent feedback control of each structural mode in the low-frequency domain. It is also shown, however, that independent control of the panel's radiation modes is also possible, and that this could provide a more efficient control strategy, since a smaller number of radiation modes than structural modes needs to be controlled for a given level of performance.

1. INTRODUCTION

Noise and vibration pollution is a pervasive feature of many aspects of everyday life, such as vibration and sound transmission inside vehicles, engines and flow-noise in aeroplanes, and noise radiated by heavy fluids in pipes. Economic and quality-of-life costs are enormous, affecting vehicle design and efficiency.

In the aeronautical domain, the extensive use of propeller driven aircraft has motivated the study of the prediction and the control of the deterministic tonal noise induced, inside the cabin, by the propeller blades rotating through the air. The continual development of jet aircraft has also driven an increasing number of studies concerning the sound and the vibration generated in the cabin by the airflow developed over the fuselage under cruise conditions. More recently, the boundary layer noise induced in aircraft has received an increasing attention since the contribution of other noise sources, such as the sound radiated by jet engines, has now been significantly reduced by the use of high-bypass jet engines which are, also, more fuel efficient. Since flow-induced noise increases more rapidly with respect to the velocity than other noise sources, TBL (Turbulent Boundary Layer)-induced noise is a particularly critical problem in transsonic aircrafts.

Hence, as the flow-induced sound becomes a non-negligible part of the noise into high-speed aircraft, there is an important economic interest in reducing TBL-induced noise. This problem has to be addressed at the design stage and requires a simple model, as analytic as possible, in order to save the most computational effort and provide the best physical insight. This model should allow:

- ♦ an understanding of the mechanisms by which a turbulent boundary layer induces the vibration of a structure;
- ♦ a formulation of design criteria for the fuselage through parametric studies including different flight conditions (landing, take off and cruise);
- ♦ the investigation of possible strategies for the Active Structural Acoustic Control (ASAC) of the sound power radiated inwards the aircraft by the fuselage panels excited by the flow noise. This active control device could perhaps complement the passive reduction strategies which can exhibit poor performance at low frequencies.

Strategies of Active Structural Acoustic Control (ASAC)

The vibro-acoustic model should be formulated so that active control can be implemented through a feedback control architecture. Boundary layer noise is a random process and, thus, cannot be controlled by a feedforward control system since no suitable reference signal is generally available.

Many authors have investigated the use of feedforward techniques (Active Noise Control [1,2], Active Vibration Control [3,4]) to control the transmission of propeller noise through a fuselage, but less numerous studies have addressed the active structural acoustic control of a broadband disturbance. In order to reduce the sound power radiated by a plate excited by a turbulent boundary layer, Thomas and Nelson [5] have generalised the approach developed by Baumann *et al* [6] for a random excitation of a panel and formulated a stochastic linear regulator problem for a random excitation of the system. Another study [7] also followed this approach including aeroelastic coupling. The above mentioned feedback control strategies use a set of "coupled excitation filters", the output of which being the generalised forces exciting each structural mode of the plate.

1

In our approach, we formulate physical criteria for which the generalised forces are uncorrelated and so the amplitude of each structural mode is independent of the amplitude of any other structural mode, i.e. the modes are not correlated either by the excitation or by the fluid-loading. Hence, a suitable strategy for the Active Structural Acoustic Control of the sound power radiated inwards by the panel would be independent feedback control of each structural mode of the system in the low-frequency domain. This strategy has to be compared with the attenuations given by the active control of the sound power using radiation mode cancellation, i.e. the cancellation of velocity distributions which radiate sound independently [8,9].

Characteristics of the physical model

Most of the limited number of models describing the vibro-acoustic response of aircraft structures excited by turbulent boundary layers [5,10] have divided the fuselage skin into an array of uncorrelated simply-supported panels vibrating individually. The vertical and horizontal dimensions of these panels correspond to the distance between two adjacent frames and two adjacent stringers respectively. The validity of this model has been confirmed as representative by extensive flight test measurements carried out on the rear structure on an airplane fuselage [11,12]. These data have shown that, from 400 Hz to 5 kHz, the boundary layer noise excites the fuselage in such a way that the flow-induced vibrations are only correlated over a single fuselage bay in the streamwise direction. This is not the case for the jet noise, which produces highly correlated vibrations across several bays in the streamwise and in the spanwise direction at frequencies below about 800 Hz.

A second point concerns the geometry of the modelled subsystem. The adjacent bays are set in a cylindrical fuselage and the effects of curvature have to be considered. A recent analytical study [13] has shown that, for subsonic applications, the influence of the panel curvature on the interior sound field can be neglected only if the surrounding inner surface is sufficiently hard to appear as a baffle, but, at the same time, sufficiently absorbing to neglect the returned sound waves due to the curvature. These competing effects seem, a priori, difficult to achieve in aeronautical applications but the influence of curvature still appears to be negligible when compared with the influence of in-plane stresses acting on the boundaries of the panel [10]. These membrane tensions are due to the cabin pressurisation and lead to an increase of the typical fundamental resonance frequency of each bay by a factor of about 7. Hence, the main physical characteristics of our problem are retained by considering the simplified, but relevant model of a simply-supported flat plate stressed by tension forces.

The third point is related to the modelling of the structural damping effects. We will introduce an equivalent damping ratio ς which accounts for several effects [14]: the internal or *hysteretic* damping, the boundary damping due to the friction in the joint edges or due to the energy lost by the panel through its elastic boundaries, the friction damping for multilayered composite panels, etc...We will consider in our simulations two characteristic cases: an aluminium panel which accounts both for the hysteretic damping and the energy losses through its boundaries ($\varsigma = 0.01$) and a panel which accounts for the damping effect of a "trimmed" panel [15,16], i.e. the dissipation due to the insulating material placed between the interior and the exterior stringed frame ($\varsigma = 0.05$). However, we keep in mind that a more rigorous modelling for the trimmed panel should address the problem of a vibrating panel radiating inside a shallow cavity whose walls are covered by absorbing materials.

Previous investigations for the prediction of flow-induced structural vibration and sound radiation

One of the first investigations is due to Davies [17], who considered the case of a simply supported plate in contact with a gas and used a modal representation for the displacement and the radiated sound field of the panel. Davies simplified this representation by neglecting both the acoustic and the excitation coupling between the structural modes. Recently, a more complete investigation of this modal approach has been proposed by Robert [18] and Bano et al. [19]. However, these models use a space-frequency formulation for the turbulent excitation. Other authors [20,21] have shown the efficiency and the suitability of a wavenumber-frequency approach for asymptotics and analytical approximations of the vibro-acoustic response of a simply-supported plate randomly excited. This representation enables efficient parametric studies in the frequency range of interest, i.e. between about 200 Hz and 5kHz.

Furthermore, recent investigations [7,22] have accounted for aeroelastic structural acoustic coupling, i.e. the influence of the mean flow on both the acoustic propagation and the fluid-structure interaction at subsonic Mach numbers. These studies have pointed out a beneficial aerodynamic damping effect, leading to a decrease in the flow-induced noise transmission by the fuselage when the Mach number is increase. However, this effect is compensated to a certain extent by an increase in the levels of the sound power radiated in the cabin due to surface effects on the boundary layer pressure distribution generated over the fuselage skin, such as structural inhomogeneities and ring-stiffeners [23], the wall roughness [24] and step-like discontinuities [25].

We finally note that flow-structure interaction studies are a rather complicated subject since the difficulties of fluid dynamics (the random excitation field) add to those of structural vibrations. However, a guideline to solve this problem is to know the required precision for the modelling of the excitation field in order to describe the vibro-acoustic response of the structure with a sufficient accuracy. A significant number of publications [20,21,26,27,28] have been focussed on the choice of the modelling of the wall-pressure fluctuations with respect to the frequency range or the Mach number of interest. Section 5 of this report will discuss the influence of this choice of models of the wall-pressure field in our configurations, i.e. for high subsonic Mach number applications.

Contents of the report

This report will be organised as follows. Section 2 presents the assumptions and the governing equations of the problem. In section 3, we propose an analytic model for the vibro-acoustic response of a fluid-loaded plate under a random excitation. In this section, we define two functions: a wave-vector transfer function describing the filtering effect of the plate and a wave-vector density function quantifying the response of the plate to a stochastic excitation in terms of excitation filters. Moreover, it will be established that the statistical properties of the panel response depend on the statistics of the excitation through the response of the fluid-loaded panel to a harmonic excitation scaled on each contributing wavevector. A modal method will then be used to solve the corresponding harmonic problems.

Section 4 is devoted to the modal representation of the solution and criteria are formulated under which we can neglect both the acoustic and the excitation cross-modal coupling of the structural modes. Section 5 presents a comprehensive review of

the main turbulence modelling and justifies why a Corcos-like model is most suitable for the purpose of our analysis. The results of various parametric studies are then described in section 6. These are designed to check the main hypotheses of the model and to give a better understanding of the coupling between the dynamic behaviour of the structure and flow turbulence. Moreover, comparisons between our predictions and previous experiments are discussed. Finally, the results are presented of an initial investigation into the active control of sound radiated from a turbulent boundary layer-excited panel, in which either the structural modes or the radiation modes are suppressed.

2. STATEMENT OF THE PROBLEM

In the free-space R^3, let us consider the Cartesian set of co-ordinates (O, x, y, z). A thin elastic (or visco-elastic) plate of length a, of width b and of constant thickness $h \ll (a, b)$, occupies the open domain defined by:

$$\left\{ \mathbf{x} = (x, y, z): 0 < x < b, 0 < y < a, -h/2 < z < h/2 \right\}$$

The plate thickness h is assumed to be small compared with the wavelengths involved. For simplicity, the plate is assumed to be homogeneous and isotropic. We model its motion by using Kirchhoff's thin plate theory. All the structural quantities will therefore be defined over the mean surface Σ $(z = 0)$ of the plate. Along its boundary $\partial\Sigma$, an external normal vector $\mathbf{n}$ can be defined almost everywhere. The complement Σ' of $\overline{\Sigma}$ is defined as being a perfectly rigid baffle.

The mechanical characteristics of the plate are: a bending stiffness $D = Eh^3/12(1 - v^2)$ and a mass per unit area $m = \rho h$ where E, v and m are the Young's modulus of elasticity, the Poisson's ratio and the density of the material. The internal damping of the plate is usually modelled by a non-zero imaginary part of the Young's modulus. It will be noted η and the subsequent complex bending stiffness $D' = D(1 + j\eta)$. We will account for the cabin pressurisation effects through lateral and longitudinal complex tension terms $N'_x = N_x(1 + j\eta)$ and $N'_y = N_y(1 + j\eta)$ acting in the plane of the undeformed middle surface of the plate.

The baffled plate separates two domains Ω^+ $(z > 0)$ and Ω^- $(z < 0)$ which both contain perfect fluids which are characterised by the densities ρ^+ and ρ^- with the corresponding sound velocities c^+ and c^-. As sketched in Figure 2.1, the fluid in the domain Ω^+ is moving in the positive y-direction with the constant speed U_∞. A turbulent boundary layer develops at the interface between the fluid and the system plate-baffle. The wall-pressure fluctuations due to this turbulent boundary layer induce a vibration of the plate and an acoustic radiation in both fluid domains.

2.1 Hypothesis

(a) The model describing the interaction between the vibrating structure and the turbulent flow assumes a one-way interaction, i.e. the wall-pressure fluctuations are not modified by the vibrations of the plate. This hypothesis enables us to model the excitation term for the elastic panel in contact with a turbulent boundary layer as the wall-pressure fluctuations that would be observed on a smooth rigid wall, also called the *blocked pressure* p_b.

(b) The turbulent boundary layer is assumed fully developed when exciting the plate.

5

(c) Since the acoustic fluid load mainly depends on the mechanical properties of the fluid in the immediate neighbourhood of the plate, where the fluid flow velocity is close to zero, we can reasonably assume that the sound pressure radiated in Ω^- is not significantly affected by the fluid flow in Ω^+. So, for the acoustic wave propagation in Ω^+, we consider that the fluid is at rest.

2.2 Governing equations

In the following, we neglect the in-plane displacements of the panel with respect to its out-of-plane motions because, under the small deformation hypothesis, the membrane displacement field is not coupled with the flexural displacement field and so, does not contribute to the radiated pressure field. Let $w(\mathbf{x}; t)$ be the instantaneous flexural displacement of the mean surface of the plate at the point $\mathbf{x}$ of co-ordinates $(x, y, 0)$ and at the time t; let $p^+(\mathbf{z}; t)$ and $p^-(\mathbf{z}; t)$ stand for the acoustic pressure fields at the points $\mathbf{z}$ of co-ordinates $(x, y, z \geq 0)$ and $(x, y, z \leq 0)$ respectively in Ω^+ and Ω^- and at the time t. The pressure step $p_S(\mathbf{x}; t)$ across the plate is defined by:

$$p_S(\mathbf{x}; t) = p_S(x, y, 0; t) = \lim_{z \to 0^+} \left[p^+(x, y, z; t) - p^-(x, y, -z; t) \right]$$

The functions $w(\mathbf{x}; t)$, $p^+(\mathbf{z}; t)$ and $p^-(\mathbf{z}; t)$ satisfy, for each realisation of the process, the following system of equations:

$$\left(D'\Delta_x^2 + N'_x \frac{\partial^2}{\partial x^2} + N'_y \frac{\partial^2}{\partial y^2} + m \frac{\partial^2}{\partial t^2} \right) w(\mathbf{x}; t) = -p_b(\mathbf{x}; t) - p_S(\mathbf{x}; t), \quad \forall \mathbf{x} \in \Sigma, \quad (2.1.\text{a})$$

$$\left(\Delta - \frac{1}{c_\pm^2} \frac{\partial^2}{\partial t^2} \right) p^\pm(\mathbf{z}; t) = 0, \quad \forall \mathbf{z} \in \Omega^\pm, \quad (2.1.\text{b})$$

$$\rho_\pm \frac{\partial^2 w}{\partial t^2}(\mathbf{x}; t) + \frac{\partial p^\pm}{\partial z}(\mathbf{x}; t) = 0, \quad \forall \mathbf{x} \in \Sigma, \quad (2.1.\text{c})$$

$$\frac{\partial p^\pm}{\partial z}(\mathbf{x}; t) = 0, \quad \forall \mathbf{x} \in \Sigma', \quad (2.1.\text{d})$$

Boundary conditions for w onto $\partial \Sigma$,   (2.1.e)

Outgoing wave conditions for $p^\pm$,   (2.1.f)

Initial conditions for w, p^+ and p^-.   (2.1.g)

In the equation of motion (2.1.a), Δ_x^2 is the bilaplacian operator calculated with respect to the variables x and y. The differential elasticity operator consists of the sum of two terms: $D'\Delta_x^2$ which governs the bending motion of the plate and $\left(N'_x \partial^2/\partial x^2 + N'_y \partial^2/\partial y^2 \right)$, which accounts for inplane motion of the plate due to cabin pressurisation effects. This equation governs the structural response of the fluid-loaded plate under membrane tensions and excited by the total acoustic pressure field $p_b + p_S$,

6

consisting of the sum of the turbulent blocked pressure p_b and the acoustic pressure step p_s that would be generated by the panel motion in the absence of turbulence.

The equation (2.1.a) is completed by local boundary conditions (2.1.e) satisfied by w along its entire periphery $\partial \Sigma$. The most classical one corresponds to the case of a simply supported plate ($w = \partial_n^2 w = 0$ on $\partial \Sigma$) or the case of a clamped plate ($w = \partial_n w = 0$ on $\partial \Sigma$). But, boundary integral representations of w can take any other conditions into account [29].

The acoustic pressure fields p^+ and p^- satisfy the homogeneous d'Alembert equations (2.1.b), respectively in the fluid domains Ω^+ and Ω^-, the homogeneous Neumann boundary condition (2.1.d) on the baffle and the radiation conditions (2.1.f) at infinity. Since the fluid is supposed perfect and at rest, equation (2.1.c) expresses the continuity condition between the normal acceleration of a point vibrating on the structure and a fluid particle at its neighbourhood.

The set of equations (2.1.a-2.1.g) governs the vibrating motion of the fluid-loaded baffled plate stressed by inplane tensions and excited by wall-pressure fluctuations.

2.3 Green's representation of the displacement of the fluid-loaded plate

Because the random excitation term p_b does not possess a time-Fourier transform, the set of equations (2.1) does not possess a time-Fourier transform [30]. In order to solve the system (2.1), we introduce $\gamma(\mathbf{x}, \mathbf{x}'; \omega)$, the Green's kernel of the displacement of the fluid-loaded plate as the solution of the following system of equations, where an $e^{j\omega t}$ time dependence is assumed:

$$\left(D'\Delta_x^2 + N_x' \frac{\partial^2}{\partial x^2} + N_y' \frac{\partial^2}{\partial y^2} - m\omega^2 \right)\gamma(\mathbf{x}, \mathbf{x}'; \omega) = -\delta_{\mathbf{x}'}(\mathbf{x}) - p_S(\mathbf{x}, \mathbf{x}'; \omega), \forall (\mathbf{x}, \mathbf{x}') \in \Sigma, \text{(2.2.a)}$$

$$\left(\Delta + k_\pm^2 \right)p^\pm(\mathbf{z}, \mathbf{x}'; \omega) = 0, \quad \forall (\mathbf{z}, \mathbf{x}') \in \Omega^\pm \times \Sigma, \quad k_\pm = \frac{\omega}{c_\pm}, \quad \text{(2.2.b)}$$

$$\frac{\partial p^\pm}{\partial z}(\mathbf{x}, \mathbf{x}'; \omega) = \rho_\pm \omega^2 \gamma_\omega(\mathbf{x}, \mathbf{x}'), \quad \forall (\mathbf{x}, \mathbf{x}') \in \Sigma, \quad \text{(2.2.c)}$$

$$\frac{\partial p^\pm}{\partial z}(\mathbf{x}, \mathbf{x}'; \omega) = 0, \quad \forall (\mathbf{x}, \mathbf{x}') \in \Sigma', \quad \text{(2.2.d)}$$

Boundary conditions for $\gamma(\mathbf{x}, \mathbf{x}'; \omega)$ when $\mathbf{x} \in \partial \Sigma$, (2.2.e)

Sommerfeld conditions for p_ω^+ and p_ω^-. (2.2.f)

where $p^\pm(\mathbf{z}, \mathbf{x}'; \omega)$ is the sound pressure radiated at the point $\mathbf{z}$ in $\Omega^\pm$ due to a harmonic point force $\delta_{\mathbf{x}'}(\mathbf{x}) e^{j\omega t}$ acting normally on the plate at the point $\mathbf{x}'$, $\delta_{\mathbf{x}'}(\mathbf{x}) = \delta_{x'}(x)\delta_{y'}(y)$ being the Dirac delta function at the point $\mathbf{x}'$ of co-ordinates $(x', y', 0)$; $p_S(\mathbf{x}, \mathbf{x}'; \omega)$ is the pressure step across the plate at the point $\mathbf{x}$ on Σ and $\gamma(\mathbf{x}, \mathbf{x}'; \omega)$ represents the flexural response, i.e. the out-of-plane displacement, at the point $\mathbf{x}$ on Σ, of a finite

elastic plate coupled to two semi-infinite fluid domains $\Omega^{\pm}$ and excited by the harmonic point force previously described. ω is the angular frequency and $k_{\pm}$ is the acoustic wavenumber for each fluid domain. It can be shown that $\gamma(\mathbf{x}, \mathbf{x}'; \omega)$ only depends on the separation distance between $\mathbf{x}$ and $\mathbf{x}'$: it will then be denoted $\gamma(\mathbf{x} - \mathbf{x}'; \omega)$.

Now, we can define the time-dependent Green's kernel $\gamma(\mathbf{x} - \mathbf{x}'; t)$ of the displacement of the fluid-loaded plate as the inverse Fourier transform of the Green's kernel $\gamma(\mathbf{x} - \mathbf{x}'; \omega)$:

$$\gamma(\mathbf{x} - \mathbf{x}'; t) = \frac{1}{2\pi} \int_{-\infty}^{+\infty} \gamma(\mathbf{x} - \mathbf{x}'; \omega)\, e^{j\omega t}\, d\omega, \quad \forall (\mathbf{x}, \mathbf{x}') \in \Sigma, \quad \forall t. \qquad (2.3)$$

Therefore, the Green's kernel $\gamma(\mathbf{x} - \mathbf{x}'; t)$ leads to *an integral representation of the displacement of the fluid-loaded plate excited by the turbulent boundary layer in terms of the random excitation p_b*, as follows:

$$w(\mathbf{x}; t) = (\gamma \underset{(\mathbf{x}', t)}{*} p_b)(\mathbf{x}; t) = \int_{-\infty}^{+\infty} \iint_{R^2} \gamma(\mathbf{x} - \mathbf{x}'; t - \tau)\, p_b(\mathbf{x}'; \tau)\, d\tau\, d\mathbf{x}', \quad \forall \mathbf{x} \in \Sigma, \quad \forall t. \quad (2.4)$$

where $\underset{(\mathbf{x}', t)}{*}$ denotes a convolution product with respect to space and time variables.

3. VIBRO-ACOUSTIC RESPONSE OF AN ELASTIC PANEL TO A SPACE AND TIME STOCHASTIC EXCITATION

3.1. Derivation of a wavevector integration model for the power spectral densities associated to the vibro-acoustic response of the panel.

The excitation term $p_b(\mathbf{x}; t)$ modelling the wall pressure fluctuations due to a turbulent boundary layer is a stochastic field stationary up to order 2 with respect to the space and time variables. Consequently, the *cross-correlation function* $R_{p_b p_b}$ of the turbulent excitation p_b is defined as follows [31]:

$$R_{p_b p_b}(\mathbf{x}; t) = \mathrm{E}\big[p_b(\mathbf{x}'; t')\, p_b^*(\mathbf{x}' + \mathbf{x}; t' + t)\big], \quad \forall \mathbf{x} \in \Sigma, \quad \forall t. \tag{3.1}$$

where z^* denotes the conjugate of the complex number z. The function $R_{p_b p_b}$ admits a space-time Fourier transform, denoted $S_{p_b p_b}$, which is called the *wavenumber-frequency cross spectrum* of the excitation pressure p_b. It is given by the following expressions:

$$S_{p_b p_b}(\mathbf{k}; \omega) = \iint_{\Sigma} S_{p_b p_b}(\mathbf{x} - \mathbf{x}'; \omega)\, \mathrm{e}^{-j(\mathbf{k} \cdot (\mathbf{x} - \mathbf{x}'))}\, d^2(\mathbf{x} - \mathbf{x}'), \quad \forall \mathbf{k} \in \mathrm{R}^2, \quad \forall \omega. \tag{3.2.a}$$

$$S_{p_b p_b}(\mathbf{x}; \omega) = \int_{-\infty}^{+\infty} R_{p_b p_b}(\mathbf{x}; t)\, \mathrm{e}^{-j\omega t}\, dt, \quad \forall \mathbf{x} \in \Sigma, \quad \forall \omega. \tag{3.2.b}$$

where $\mathbf{k} = (k_x, k_y)$ is the wavenumber in the x and y directions and $S_{p_b p_b}(\mathbf{x} - \mathbf{x}'; \omega)$ is the *space-frequency cross spectrum* defined in (3.2.a) as the inverse space-Fourier transform of the wavenumber-frequency power spectrum $S_{p_b p_b}(\mathbf{k}; \omega)$.

It can also be shown that the displacement given by (2.4) is a stochastic field, which is stationary up to order 2 with respect to the time, but not stationary with respect to the space. This allows us to define the *cross-correlation function* R_{ww} of the plate displacement as follows:

$$R_{ww}(\mathbf{x}, \mathbf{x}'; t) = \mathrm{E}\big[w(\mathbf{x}'; t')\, w^*(\mathbf{x}; t' + t)\big], \quad \forall (\mathbf{x}, \mathbf{x}') \in \Sigma \times \Sigma, \quad \forall t. \tag{3.3}$$

Introducing the Green's representation (2.4) of the displacement w into the definition (3.3) leads to an integral representation of the cross-correlation function R_{ww}:

$$R_{ww}(\mathbf{x}, \mathbf{x}'; t) = \int_{-\infty}^{+\infty}\int \iint_{\Sigma} \iint_{\Sigma} \gamma(\mathbf{x} - \mathbf{x}''; t - \tau) R_{p_b p_b}(\mathbf{x}'' - \mathbf{x}'''; \tau - \tau')$$
$$\times \gamma^*(\mathbf{x}' - \mathbf{x}''; t - \tau')\, d^6\beta, \quad \forall (\mathbf{x}, \mathbf{x}') \in \Sigma \times \Sigma, \quad \forall t. \tag{3.4}$$

where $d^6\beta$ is the elementary "volume" of integration equal to $d^2\mathbf{x}''\, d^2\mathbf{x}''\, d\tau\, d\tau'$.

Since the Green's kernel γ and the auto-correlation function $R_{p_b p_b}$ admit a time-Fourier transform, the function R_{ww} admit a time-Fourier transform S_{ww}, which is called the *space-frequency cross-spectrum* of the displacement of the plate. Performing the time-Fourier transform of the expression (3.4) then yields:

$$S_{ww}(\mathbf{x}, \mathbf{x}'; \omega) = \iint_{\Sigma} \iint_{\Sigma} \gamma(\mathbf{x} - \mathbf{x}''; \omega) \, S_{p_b p_b}(\mathbf{x}'' - \mathbf{x}'''; \omega) \, \gamma^*(\mathbf{x}' - \mathbf{x}'''; \omega) \, d^2\mathbf{x}'' \, d^2\mathbf{x}''' \qquad (3.5)$$

where $\gamma(\mathbf{x} - \mathbf{x}''; \omega)$ is the time-Fourier transform of the Green's kernel $\gamma(\mathbf{x} - \mathbf{x}''; t)$ (see eq. 2.3); it is also the harmonic solution of the set of equations (2.2.a-f). The expression (3.5) has been proposed by Davies [17] and used more recently by Robert [18], Bano *et al.* [19] and Thomas *et al.* [5] to predict the vibro-acoustic response of a panel excited by a turbulent boundary layer.

More recent advances in the modelling of turbulence have provided expressions of the wall-pressure fluctuations given in the form of a wavenumber-frequency power spectrum [20,32] as presented in formula (3.2.a). In order to account for this form of modelling in the calculation of the response of the plate, it is necessary to perform an inverse Fourier transform of the expression (3.2.a) with respect to the wavenumbers (k_x, k_y) and then to substitute this inverse Fourier transform in the integral (3.5). However, this procedure involves a lot of computational effort.

A few initial considerations can reduce this large amount of calculation. According to (3.2.a), the space-frequency spectrum $S_{p_b p_b}(\mathbf{x} - \mathbf{x}'; \omega)$ can be expressed in terms of the wavenumber-frequency spectrum $S_{p_b p_b}(\mathbf{k}; \omega)$ as:

$$S_{p_b p_b}(\mathbf{x} - \mathbf{x}'; \omega) = \frac{1}{(2\pi)^2} \int_{-\infty}^{+\infty} \int_{-\infty}^{+\infty} S_{p_b p_b}(\mathbf{k}; \omega) \, e^{j\mathbf{k} \cdot (\mathbf{x} - \mathbf{x}')} \, d^2\mathbf{k}. \qquad (3.6)$$

When substituted in (3.5), we can then define a function $\Gamma_\omega(\mathbf{x}; \mathbf{k})$ as given by:

$$\Gamma_\omega(\mathbf{x}; \mathbf{k}) = \iint_{\Sigma} \gamma(\mathbf{x} - \mathbf{x}'; \omega) \, e^{-j\mathbf{k} \cdot \mathbf{x}'} \, d^2\mathbf{x}', \qquad \forall \mathbf{k} \in \mathbb{R}^2, \quad \forall \omega.$$

Hence, expression (3.5) for the plate displacement can be written in purely wavenumber terms as:

$$S_{ww}(\mathbf{x}, \mathbf{x}'; \omega) = \frac{1}{(2\pi)^2} \int_{-\infty}^{+\infty} \int_{-\infty}^{+\infty} \Gamma_\omega(\mathbf{x}; \mathbf{k}) \, S_{p_b p_b}(\mathbf{k}; \omega) \, \Gamma_\omega^*(\mathbf{x}'; \mathbf{k}) \, d^2\mathbf{k} \qquad (3.7)$$

where the cross-spectrum of the displacement of the fluid-loaded plate is now written under the form of an integral over the wavevector $\mathbf{k}$, and the wavenumber-domain Green's function $\Gamma_\omega(\mathbf{x}; \mathbf{k})$ is the displacement at position $\mathbf{x}$ on the fluid-loaded plate, calculated at the angular frequency ω, when the excitation pressure p_b scales on the

contribution of a boundary layer "eddy" of wavevector $\mathbf{k}$. $\Gamma_\omega(\mathbf{x}; \mathbf{k})$ is therefore determined by the following system of equations:

$$\left(D'\Delta_x^2 + N'_x \frac{\partial^2}{\partial x^2} + N'_y \frac{\partial^2}{\partial y^2} - m\omega^2 \right) \Gamma_\omega(\mathbf{x}; \mathbf{k}) = -e^{-j\mathbf{k}\cdot\mathbf{x}}$$

$$-\left[p_\omega^+(\mathbf{x}; \mathbf{k}) - p_\omega^-(\mathbf{x}; \mathbf{k}) \right], \quad \forall \mathbf{x} \in \Sigma, \quad (3.8.\text{a})$$

$$\left(\Delta + k_\pm^2 \right) p_\omega^\pm(\mathbf{z}; \mathbf{k}) = 0, \quad \forall \mathbf{z} \in \Omega^\pm, \quad (3.8.\text{b})$$

$$\frac{\partial p_\omega^\pm}{\partial z}(\mathbf{x}; \mathbf{k}) = \rho_\pm \omega^2 \Gamma_\omega(\mathbf{x}; \mathbf{k}), \quad \forall \mathbf{x} \in \Sigma, \quad (3.8.\text{c})$$

$$\frac{\partial p_\omega^\pm}{\partial z}(\mathbf{x}; \mathbf{k}) = 0, \quad \forall \mathbf{k} \in \Sigma', \quad (3.8.\text{d})$$

Boundary conditions for $\Gamma_\omega(\mathbf{x}; \mathbf{k})$ when $\mathbf{x} \in \partial\Sigma$, $\quad (3.8.\text{e})$

Sommerfeld radiation conditions for p_ω^+ and p_ω^-. $\quad (3.8.\text{f})$

In the next section, we will present three appropriate methods to calculate $\Gamma_\omega(\mathbf{x}; \mathbf{k})$ either analytically or numerically.

Let us note that expression (3.7) for the frequency cross-spectrum formulated in the space-frequency domain, is equivalent to the expression (3.5) formulated in the wavenumber-frequency domain. A synoptic diagram has been plotted in Figure 3.1 in order to give an overview of the methodology we have considered together with equivalent representations of the solution.

The frequency cross-spectrum $S_{p_\pm p_\pm}(\mathbf{z}, \mathbf{z}'; \omega)$ of the acoustic pressure fields radiated in the fluid domains $\Omega^\pm$ is given by the following expression, which is formally similar to (3.7):

$$S_{p_\pm p_\pm}(\mathbf{z}, \mathbf{z}'; \omega) = \frac{1}{(2\pi)^2} \int_{-\infty}^{+\infty}\int_{-\infty}^{+\infty} p_\omega^\pm(\mathbf{z}; \mathbf{k}) \, S_{p_b p_b}(\mathbf{k}; \omega) \, p_\omega^{\pm*}(\mathbf{z}'; \mathbf{k}) \, d^2\mathbf{k}, \quad \forall(\mathbf{z}, \mathbf{z}') \in \Omega^\pm, \quad \forall\omega.$$

$$(3.9)$$

The radiated sound pressures $p_\omega^\pm(\mathbf{x}; \mathbf{k})$, appearing in formula (3.9), can be computed by using their integral representation carried out by applying the Green's formula to $p_\omega^\pm$. Thus, $p_\omega^\pm$ take the form:

$$p_\omega^\pm(\mathbf{z}; \mathbf{k}) = \mp\rho_\pm\omega^2 \iint_\Sigma \mathcal{G}_\omega^\pm(\mathbf{z} - \mathbf{x}') \, \Gamma_\omega(\mathbf{x}'; \mathbf{k}) \, d^2\mathbf{x}', \quad \forall \mathbf{z} \in \Omega^\pm, \quad \forall \mathbf{k} \in \mathbb{R}^2. \quad (3.10)$$

$\mathcal{G}_\omega^\pm$ are the Green's functions of the Helmholtz equation for acoustic propagation in each half-space Ω^+ or Ω^-, which satisfy the homogeneous Neumann condition on $(z = 0)$ as well as the Sommerfeld condition at infinity.

They are given by:

$$\mathcal{G}_\omega^\pm(\mathbf{z}-\mathbf{z}') = \frac{e^{-jk_\pm r(\mathbf{z},\mathbf{z}')}}{4\pi\, r(\mathbf{z},\mathbf{z}')} + \frac{e^{-jk_\pm r(\mathbf{z},\mathbf{z}'_-)}}{4\pi\, r(\mathbf{z},\mathbf{z}'_-)}, \quad \forall(\mathbf{z},\mathbf{z}') \in \Omega^\pm \times \Omega^\pm \qquad (3.11)$$

where the co-ordinates of the points $\mathbf{z}'$ and $\mathbf{z}'_-$ are respectively (x',y',z') and $(x',y',-z')$. $r(\mathbf{z},\mathbf{z}')$ denotes the distance between $\mathbf{z}$ and $\mathbf{z}'$.

3.2. Derivation of the spectral densities involved in the power balance equation and radiation efficiency of the panel.

A natural way to obtain the expressions for the spectra associated to the power quantities of interest (boundary-layer input, radiated acoustic power and structural dissipated power) is to establish a power balance equation based upon the system (2.1.a-g) governing the vibro-acoustic response of a fluid-loaded baffled panel excited by a turbulent boundary layer. Multiplying the pressures in (2.1.a) by the out-of-plane velocity $\dfrac{\partial w^*}{\partial t}(x';t-\tau)$ (denoted $\dot{w}^*$) and evaluating the mathematical expectations (or ensemble averaging) leads to the following relation between several cross-correlation functions, the full expressions for which are given in appendix A:

$$(1+j\eta)R_{\mathcal{L}_p(w)\dot{w}}(\mathbf{x},\mathbf{x}';\tau) + mR_{\ddot{w}\dot{w}}(\mathbf{x},\mathbf{x}';\tau)$$
$$+ R_{p^+\dot{w}}(\mathbf{x},\mathbf{x}';\tau) - R_{p^-\dot{w}}(\mathbf{x},\mathbf{x}';\tau) = R_{p_b\dot{w}}(\mathbf{x},\mathbf{x}';\tau) \qquad (3.12)$$

where $\mathcal{L}_p(w)$ is the thin plate differential operator associated to the structural potential energy. It is given by:

$$\mathcal{L}_p(w) = D\left(\frac{\partial^2 w}{\partial x^2} + \frac{\partial^2 w}{\partial y^2}\right)^2 + N_x\frac{\partial^2 w}{\partial x^2} + N_y\frac{\partial^2 w}{\partial y^2}$$

The correlation functions involved in (3.12) are defined as:

$$\begin{cases}
R_{\mathcal{L}_p(w)\dot{w}}(\mathbf{x},\mathbf{x}';\tau) = \mathrm{E}\left[\mathcal{L}_p(w)(\mathbf{x}';t')\frac{\partial w^*}{\partial t}(\mathbf{x};t'+\tau)\right] \\[2mm]
R_{\ddot{w}\dot{w}}(\mathbf{x},\mathbf{x}';\tau) = \mathrm{E}\left[\frac{\partial^2 w}{\partial t^2}(\mathbf{x}';t')\frac{\partial w^*}{\partial t}(\mathbf{x};t'+\tau)\right] \\[2mm]
R_{p^\pm\dot{w}}(\mathbf{x},\mathbf{x}';\tau) = \mathrm{E}\left[\lim_{z\to 0^+}\{p^\pm(x',y',\pm z';t')\}\frac{\partial w^*}{\partial t}(x,y,0;t'+\tau)\right] \\[2mm]
R_{p_b\dot{w}}(\mathbf{x},\mathbf{x}';\tau) = \mathrm{E}\left[p_b(\mathbf{x}';t')\frac{\partial w^*}{\partial t}(\mathbf{x};t'+\tau)\right]
\end{cases}$$

Performing the time-Fourier transform of (3.12) then yields to the following relation between the corresponding frequency spectral densities:

$$(1 + j\eta)S_{\varDelta_p(w)w}(\mathbf{x};\omega) - m\omega^2 S_{ww}(\mathbf{x};\omega)$$
$$+ S_{p^+w}(\mathbf{x};\omega) - S_{p^-w}(\mathbf{x};\omega) = S_{p_bw}(\mathbf{x};\omega) \qquad (3.13)$$

The total power balance is then obtained by integrating (3.13) over the surface of the panel and equating the real parts of each quantity involved, yielding:

$$S_\Sigma(\omega) + S_{\pi^+}(\omega) - S_{\pi^-}(\omega) = S_b(\omega) \qquad (3.14)$$

where S_Σ, $S_{\pi^\pm}$ and S_b are respectively the structural dissipated power, the acoustic power radiated in $\Omega^\pm$ and the boundary-layer input power. They are given by the expressions:

$$\begin{cases} S_\Sigma(\omega) = \dfrac{\eta}{2}\Re\left[\iint_\Sigma S_{\varDelta_p(w)w}(\mathbf{x};\omega)\,d^2\mathbf{x}\right], \\[2mm] S_{\pi^\pm}(\omega) = \dfrac{1}{2}\Re\left[\iint_\Sigma S_{p^\pm w}(\mathbf{x};\omega)\,d^2\mathbf{x}\right], \\[2mm] S_b(\omega) = \dfrac{1}{2}\Re\left[\iint_\Sigma S_{p_b w}(\mathbf{x};\omega)\,d^2\mathbf{x}\right]. \end{cases} \qquad (3.15)$$

with:

$$\begin{cases} S_{\varDelta_p(w)w}(\mathbf{x};\omega) = \dfrac{1}{(2\pi)^2}\int\limits_{-\infty}^{+\infty}\int\limits_{-\infty}^{+\infty}\varDelta_p(\Gamma_\omega)(\mathbf{x};\mathbf{k})S_{p_bp_b}(\mathbf{k};\omega)\Gamma_\omega^*(\mathbf{x};\mathbf{k})\,d^2\mathbf{k}, \\[2mm] S_{p^\pm w}(\mathbf{x};\omega) = \dfrac{1}{(2\pi)^2}\int\limits_{-\infty}^{+\infty}\int\limits_{-\infty}^{+\infty}p_\omega^\pm(\mathbf{x};\mathbf{k})S_{p_bp_b}(\mathbf{k};\omega)\Gamma_\omega^*(\mathbf{x};\mathbf{k})\,d^2\mathbf{k}, \\[2mm] S_{p_b w}(\mathbf{x};\omega) = \dfrac{1}{(2\pi)^2}\int\limits_{-\infty}^{+\infty}\int\limits_{-\infty}^{+\infty}e^{i\mathbf{k}\cdot\mathbf{x}}S_{p_bp_b}(\mathbf{k};\omega)\Gamma_\omega^*(\mathbf{x};\mathbf{k})\,d^2\mathbf{k}. \end{cases}$$

The corresponding total powers can be deduced by integrating the spectral densities (3.15) over frequency.

A quantity of interest is the radiation efficiency $\sigma(\omega)$ defined as the ratio between the acoustic power radiated inwards $S_{\pi^-}(\omega)$ and the temporal and spatial average velocity of the panel.

$\sigma(\omega)$ can be also expressed in terms of the kinetic energy of the plate $S_{E_c}(\omega)$ as follows:

$$\sigma(\omega) = \frac{mS_{\pi^-}(\omega)}{\rho_- c_- S_{E_c}(\omega)} \tag{3.16}$$

where:

$$S_{E_c}(\omega) = -\frac{m\omega^2}{2} \iint_{\Sigma} S_{ww}(\mathbf{x};\omega)\, d^2\mathbf{x}.$$

3.3. The advantages of a wavenumber-frequency approach

The advantages of a wavenumber-integration modelling (Eq. 3.7) are now discussed with respect to a more classical spatial integration modelling (Eq. 3.5):

◆ The first advantage concerns the fact that a direct physical interpretation of the results can be obtained: the wavevector integration modelling (3.7-3.9) enables the plate to be represented as a wavevector filter.

Indeed, Eq. (3.7) can also be written as:

$$S_{ww}(\mathbf{x};\omega) = \frac{1}{(2\pi)^2} \int_{-\infty}^{+\infty}\int_{-\infty}^{+\infty} S_{p_b p_b}(\mathbf{k};\omega)\, T_{x,\omega}(\mathbf{k})\, d^2\mathbf{k}$$

where:

$$T_{x,\omega}(\mathbf{k}) = \Gamma_{\omega}(\mathbf{x};\mathbf{k})\, \Gamma_{\omega}^{*}(\mathbf{x};\mathbf{k})$$

is the transfer function of the displacement of the plate at the point $\mathbf{x}$ and at the frequency ω; it describes the wavevector filtering effect of the plate

We can then define a wavevector density function $D_{x,\omega}$ for the displacement of the plate at the point $\mathbf{x}$ as a measure of the response of the plate at the point $\mathbf{x}$ to one wavevector $\mathbf{k}$. It is given by:

$$D_{x,\omega}(\mathbf{k}) = \Gamma_{\omega}(\mathbf{x};\mathbf{k})\, S_{p_b p_b}(\mathbf{k};\omega)\, \Gamma_{\omega}^{*}(\mathbf{x};\mathbf{k})$$

Thus:

$$D_{x,\omega}(\mathbf{k}) = T_{x,\omega}(\mathbf{k})\, S_{p_b p_b}(\mathbf{k};\omega)$$

that is, for each angular frequency ω and for each point $\mathbf{x} \in \Sigma$, the vibrating response of the plate excited by a turbulent boundary layer can be interpreted as a shaped signal $S_{p_b p_b}(\mathbf{k};\omega)$ passed through a wavevector filter characterised by the transfer function

$T_{x,\omega}(\mathbf{k})$. Notice that a similar representation can be given on the basis of the expression (3.5), but the interpretation in terms of spatial filters is less obvious.

◆ The second advantage of the wavector approach is that recent models for turbulence are mainly formulated through a wavenumber-frequency power spectrum and this mathematical form can easily be taken into account in the expression (3.7).

◆ The third advantage of such an approach is a computational one: the calculation using the spatial-frequency approach requires a quadruple integration of a function, whose oscillations increase when the frequency increases in the expression (3.5). Hence, the numerical evaluation of the integral (3.5) may be computationally time consuming. In the wavevector approach, the formula (3.7) shows that, in this case, we have to compute a double infinite integral of a function monotonically decreasing with ω. However, it is important to notice that the wavevector density function is maximum at the origin $(k_x, k_y) = (0, 0)$ and drops very quickly when the components of the wavector increase (Figures 3.2 and 3.3). Because of this property, the major contribution to the displacement of the plate at the point $\mathbf{x}$ comes from the low-wavenumber region of the turbulent wall-pressure fluctuations spectrum. Thus, the infinite integral (3.7) converges rapidly when approximated by a finite integral defined over an increasing bounded domain centered on the origin.

All these reasons justify our choice of a wavector-frequency formulation for the response of the fluid-loaded plate.

The modelling stage of this study has thus led us to the following conclusions. The governing equations of the problem are given by the set of equations (2.1). Because the excitation is non-deterministic, the unknowns of the problem are the cross-power spectral density of the displacement of the plate, given by (3.7), together with the cross-power spectral densities of the sound pressure radiated in the fluid domains, and given by (3.9). The main result shown is that these spectral densities are obtained from the response of the system to a harmonic deterministic excitation; this latter being calculated by solving the system (3.8) of differential equations. In reference [33], the authors have solved the corresponding 1-D problem using a finite-difference method compared with a Boundary Element Method to describe the behaviour of the plate coupled to the fluid. In the next section, we will describe, as an alternative, the use of a modal representation for the unknowns of the harmonic problem.

4 MODAL REPRESENTATION OF THE HARMONIC SOLUTION AND THE DIAGONAL APPROXIMATION

Two methods can be used to solve the fluid-structure interaction problem outlined above and summarised in equation (3.8):

i. An expansion of the harmonic response of the fluid-loaded panel as a series of its *in-vacuo* eigenmodes (**modal method**). The details of this method will be given in this section using both a matrix and scalar formalism. We will show that an explicit formulation for the expansion coefficients is available only if the acoustic cross-coupling of the modes is neglected.

ii. An expansion of the harmonic response of the fluid-loaded panel as series of the **resonance modes** of the plate coupled to the fluid. It has been shown [29] that, if the series is developed in term of a small fluid-loading parameter ($\rho_{\pm}/m$), the zero-order term is exactly the modal series defined in the previous method. Higher order terms are only significant in the case of heavy fluid-loading, and so no further details will be given about this general approach since it is not the aim of this report.

4.1 Weak-coupling hypothesis

In our problem (flow-induced noise radiated inside an aircraft), the structure radiates into a light fluid. The influence of the surrounding fluid is then a small perturbating factor and so, the dynamic response of the fluid-loaded structure is very close to the corresponding *in-vacuo* one. As a consequence, it appears reasonable, as a first approximation, to assume a weak-coupling between the plate and the surrounding fluid, i.e. the dynamic behaviour of the panel is not affected by the acoustic pressures generated by the plate motion in the absence of turbulence. In paragraph 6.1.3.b, it will be verified that the acoustic pressures are negligible with respect to the turbulence fluctuating pressures.

This hypothesis is closely linked to the assumption that the vibration has no effect on the boundary layer, as stated in section 2.1, which is a standard one and has been shown to work well in a wide range of cases [10]. It is based upon the fact that the turbulence structures contributing to the wall-pressure fluctuations are almost unaffected by the acoustic motions. But this may not be correct for supersonic flows [20]. However, since we are concerned with subsonic flows, we will neglect, in equation (2.1.a), the acoustic pressure steps with respect to the turbulence pressures p_b.

4.2 Modal representation of the solution

In order to simplify rigorously the model, we will first establish the modal representation of the solution without any weak-coupling hypothesis. Second, we will give quantitative criteria which allow us to neglect either the acoustic coupling or the excitation coupling between the modes of the panel. Third, we will obtain simplified expressions for the modal expansion of the vibro-acoustic response of the plate.

4.2.1 Modal analysis

The function $\Gamma_\omega(\mathbf{x}; \mathbf{k})$, which appears in the definition (3.7) of the wavevector-frequency cross-spectrum of the displacement, can be expressed [34] in terms of the *in-vacuo* eigenmodes $\Phi_{mn}(\mathbf{x})$ of the elastic plate:

$$\Gamma_\omega(\mathbf{x}; \mathbf{k}) = \sum_{m=1}^{+\infty} \sum_{n=1}^{+\infty} w_{mn}^\omega(\mathbf{k}) \, \Phi_{mn}(\mathbf{x}) \qquad (4.1)$$

The eigenmodes $\Phi_{mn}(\mathbf{x})$ and the corresponding eigenvalues λ_{mn}^4 are defined by the following relation:

$$\Delta_x^2 \Phi_{mn}(\mathbf{x}) = \lambda_{mn}^4 \Phi_{mn}(\mathbf{x}) \qquad (4.2)$$

In the case of a simply-supported panel, $\Phi_{mn}(\mathbf{x})$ and λ_{mn}^4 are given by exact analytical expressions:

$$\left\{ \begin{array}{l} \lambda_{mn}^4 = \left[\left(\dfrac{m\pi}{b} \right)^2 + \left(\dfrac{n\pi}{a} \right)^2 \right]^2, \\[4mm] \Phi_{mn}(x, y) = \sin\left(\dfrac{m\pi\, x}{b} \right) \sin\left(\dfrac{n\pi\, y}{a} \right) = \Phi_m(x)\, \Phi_n(y). \end{array} \right. \qquad (4.3)$$

For a simply-supported tensioned plate, according to [35], the eigenmodes are not modified but the eigenvalues are given by:

$$\lambda_{mn}^4 = \left[\left(\frac{m\pi}{b} \right)^2 + \left(\frac{n\pi}{a} \right)^2 \right]^2 + \frac{N_x}{D}\left(\frac{m\pi}{b} \right)^2 + \frac{N_y}{D}\left(\frac{n\pi}{a} \right)^2 \qquad (4.4)$$

where N_m and N_n are the lateral and longitudinal plate tensions.

In the case of a panel with four edges either clamped or free, analytical approximations of λ_{mn}^4 and $\Phi_{mn}(\mathbf{x})$ have been derived by Warburton [36]. In this case, the eigenmodes of the plate are given by the product of the eigenmodes of a clamped-clamped or free-free beam along each direction parallel to the edge. A summary of these expressions can be found in [37]. However, it is clear that Warburton's method breaks down in the case of a plate whose geometrical characteristics are such that the Kirchhoff operator is not separable in the natural coordinate system of the plate.

We note that the set of eigenmodes $\{\Phi_{mn}(\mathbf{x})\}$ is a basis of the Hilbert space which the response of the plate belongs to, and so, the expansion (4.1) of the plate response as a series of its eigenmodes is convergent.

17

The trace on Σ of the sound fields $p_\omega^\pm$ radiated in $\Omega^\pm$ can also be expressed in terms of the eigenmodes of the structure:

$$p_\omega^\pm(\mathbf{x}; \mathbf{k}) = \sum_{m=1}^{+\infty} \sum_{n=1}^{+\infty} p_{mn}^\pm(\mathbf{k}; \omega)\, \Phi_{mn}(\mathbf{x}), \quad \mathbf{x} \in \Sigma. \tag{4.5}$$

with:

$$p_{mn}^\pm(\mathbf{k}; \omega) = \iint_\Sigma p_\omega^\pm(\mathbf{x}; \mathbf{k})\, \Phi_{mn}^*(\mathbf{x})\, d^2\mathbf{x} \tag{4.6}$$

The contribution of the (p, q) modal displacement $w_{pq}^\omega(\mathbf{k})$ to the (m, n) modal pressure $p_{mn}^\pm(\mathbf{k}; \omega)$ is derived from the set of equations (3.8.b-d, 3.8.f). Indeed, if we take the (x, y) spatial Fourier transform of these equations, we obtain, in the $\mathbf{k}'$ wavenumber domain, a set of equations the solution of which can easily be found.

Then if we apply an inverse spatial Fourier transform, we can derive an expression for the radiated sound field in terms of the spatial Fourier transform of the plate displacement $\Gamma_\omega(\mathbf{k}'; \mathbf{k})$, yielding:

$$p_\omega^\pm(\mathbf{z}; \mathbf{k}) = \pm \frac{j\omega^2 \rho_\pm}{(2\pi)^2} \int_{-\infty}^{+\infty}\int_{-\infty}^{+\infty} \frac{\Gamma_\omega(k_x', k_y'; \mathbf{k})e^{-j\mathbf{k}'\cdot\mathbf{z}}}{\sqrt{k_\pm^2 - k_x'^2 - k_y'^2}} dk_x' dk_y', \quad \mathbf{z} \in \Omega^\pm. \tag{4.7}$$

with:

$$\Gamma_\omega(\mathbf{k}'; \mathbf{k}) = \sum_{p=1}^{+\infty} \sum_{q=1}^{+\infty} w_{pq}^\omega(\mathbf{k})S_{pq}(\mathbf{k}'). \tag{4.8}$$

The shape functions $S_{pq}(\mathbf{k}')$ are the spatial Fourier transform of the plate eigenmodes. They are given in a separable form for a rectangular plate as follows:

$$S_{pq}(\mathbf{k}') = \left\langle e^{j\mathbf{k}'\cdot\mathbf{x}}, \Phi_{pq}(\mathbf{x}) \right\rangle = \iint_\Sigma \Phi_{pq}(\mathbf{x})\, e^{j\mathbf{k}'\cdot\mathbf{x}}\, d^2\mathbf{x} = S_p(k_x')\, S_q(k_y') \tag{4.9}$$

where:

$$\begin{cases} S_p(k_x') = \int_0^a \Phi_p(x)\, e^{jk_x'x}\, dx, \\ S_q(k_y') = \int_0^b \Phi_q(y)\, e^{jk_y'y}\, dy. \end{cases}$$

For a simply-supported panel, the shape functions are explicitly given by:

$$
\begin{cases}
S_{pq}(k'_x,k'_y) = 2\sqrt{ab}\,\dfrac{(k_p a)(k_q b)\left[1-(-1)^p e^{-jk'_x a}\right]\left[1-(-1)^q e^{-jk'_y b}\right]}{\left[(k_x a)^2-(k_p a)^2\right]\left[(k_y b)^2-(k_q b)^2\right]}, & \text{for } (k'_x,k'_y)\neq(k_p,k_q),\\[2mm]
S_{pq}(k'_x,k'_y) = -\dfrac{\sqrt{ab}}{2}, & \text{for } (k'_x,k'_y)=(k_p,k_q) \quad \text{with } k_p a = p\pi \quad \text{and}\quad k_q b = q\pi.
\end{cases}
$$

$$(4.10)$$

They can be interpreted as the wavenumber sensitivity functions of the panel. Using this convenient formalism, an analysis has been performed by Hwang and Maidanik [21] to determine the relative contribution to the coupling between a structural mode and the turbulent excitation for different wavenumber regions.

Finally, by substituting the expression (4.7) and (4.8) into (4.6), the (m,n) modal pressure $p^{\pm}_{mn}(\mathbf{k};\omega)$ can be expressed in terms of each (p,q) modal displacement as follows:

$$
p^{\pm}_{mn}(\mathbf{k}';\omega) = \pm j\omega\rho_{\pm}c_{\pm}\sum_{p=1}^{+\infty}\sum_{q=1}^{+\infty} Z^{\pm}_{mnpq}(\omega)\, w^{\omega}_{pq}(\mathbf{k}')
$$

$$(4.11)$$

with:

$$
Z^{\pm}_{mnpq}(\omega) = \frac{k_{\pm}}{(2\pi)^2}\int_{-\infty}^{+\infty}\int_{-\infty}^{+\infty}\frac{S^{*}_{mn}(k_x,k_y)S_{pq}(k_x,k_y)}{\sqrt{k_{\pm}^2-k_x^2-k_y^2}}\,dk_x\,dk_y.
$$

$$(4.12)$$

The corresponding impedance matrix is denoted $\mathbf{Z}^{\pm}_{\omega}$.

By substituting the expansion (4.1) and (4.5) into the equation of motion (3.8.a), we are lead to solve an infinite linear algebraic system:

$$
w^{\omega}_{mn}(\mathbf{k})\left\{D\lambda^2_{mn}-m\omega^2+j\omega\left[\rho_+c_+Z^{+}_{mnmn}(\omega)+\rho_-c_-Z^{-}_{mnmn}(\omega)\right]\right\}
$$
$$
+\,j\omega\sum_{\substack{r=1\\r\neq m}}^{+\infty}\sum_{\substack{s=1\\s\neq n}}^{+\infty}\left[\rho_+c_+Z^{+}_{mnrs}(\omega)+\rho_-c_-Z^{-}_{mnrs}(\omega)\right]w^{\omega}_{rs}(\mathbf{k}) = -S_{mn}(\mathbf{k}),\quad \forall(m,n)
$$

$$(4.13)$$

If we neglect the cross-terms due to the acoustic coupling between the modes in the previous system, then $Z^{\pm}_{mnrs}(\omega)=Z^{\pm}_{mnmn}(\omega)\delta^{r}_{m}\delta^{s}_{n}$ and the fully populated system becomes diagonal.

In this case, an explicit solution is given by:

$$w^{\omega}_{mn}(\mathbf{k}) = -\frac{S_{mn}(\mathbf{k})}{D_{mn}(\omega)} = \frac{F_{mn}(\mathbf{k})}{\left[\omega^2_{mn}(1+j\eta) - \omega^2 + j\omega\left(\varepsilon_+ Z^+_{mnmn}(\omega) + \varepsilon_- Z^-_{mnmn}(\omega)\right)\right]}$$

$$= \frac{F_{mn}(\mathbf{k})}{\left[\omega^2_{mn} - \omega^2 + j\omega\left(2\varsigma\omega_{mn} + \varepsilon_+ Z^+_{mnmn}(\omega) + \varepsilon_- Z^-_{mnmn}(\omega)\right)\right]} \qquad (4.14)$$

where $F_{mn}(\mathbf{k}) = -\dfrac{S_{mn}(\mathbf{k})}{\Lambda_{mn}} = \dfrac{1}{\Lambda_{mn}}\left\langle e^{j\mathbf{k}\cdot\mathbf{x}}, \Phi_{mn}(\mathbf{x})\right\rangle$, $\Lambda_{mn} = mN_{mn}$, and $\varsigma = \dfrac{\eta}{2}\dfrac{\omega_{mn}}{\omega}$ so that

$\varsigma(\omega_{mn}) = \eta/2$ for each eigenfrequency ω_{mn}. ς is then taken to be independent of frequency and for each eigenmode is equal to $\eta/2$. N_{mn} stands for the squared norm of the eigenmodes $\Phi_{mn}(\mathbf{x})$, that is: $N_{mn} = \|\Phi_{mn}\|^2$. F_{mn} represents the normalised contribution of the plane-wave excitation $e^{j\mathbf{k}\cdot\mathbf{x}}$ to the response of the plate eigenmode $\Phi_{mn}(\mathbf{x})$ of order (m,n). ε_+ and ε_- are both fluid-loading parameters defined by $\varepsilon_{\pm} = \rho_{\pm}c_{\pm}/m$.

ω^2_{mn} and ω^2 can be expressed in terms of the flexural wavenumbers of, respectively, the finite plate λ^2_{mn} and the infinite plate λ^2 as follows:

$$\begin{cases} \omega^2_{mn} = \dfrac{D\lambda^4_{mn}}{m}, \\[2mm] \omega^2 = \dfrac{D\lambda^4}{m}. \end{cases} \qquad (4.15)$$

Let us note that the modal series (4.1) is finite for all ω since the damping of the plate (either due to radiation into the fluid or internal relaxation) has been taken into account.

If we do not neglect the acoustic cross impedance in (4.13), we are left with an infinite full linear system, the solution of which can only be found numerically. Nevertheless, we can write a formal expression for the solution as follows:

$$w^{\omega}_{mn}(\mathbf{k}) = -\sum_{r=1}^{+\infty}\sum_{s=1}^{+\infty} Y_{mnrs}(\omega) S_{rs}(\mathbf{k}) \qquad (4.16)$$

in which the structural modal mobilities $Y_{mnrs}(\omega)$ are implicit functions of ω. The corresponding matrix is denoted $\mathbf{Y}_{\omega}$.

On using the definition (3.14) for the spectra involved in the power balance equation (3.13) and expressing the pressure and displacement as modal sums (4.5, 4.1), we find:

$$
\left\{
\begin{aligned}
S_\Sigma(\omega) &= \frac{1}{2}\mathrm{Tr}\!\left[\mathbf{C}_\Sigma\,\mathbf{Y}_\omega\,\mathbf{\Psi}_\omega\,\mathbf{Y}_\omega^H\right], & C_\Sigma(m,n,p,q) &= D\eta\,\lambda_{mn}^4\,\delta_m^p\,\delta_n^q, \\
S_{\pi^\pm}(\omega) &= \frac{1}{2}\Re\!\left\{\mathrm{Tr}\!\left[\mathbf{C}_\omega^\pm \mathbf{Z}_\omega^\pm(\mathbf{Y}_\omega\,\mathbf{\Psi}_\omega\,\mathbf{Y}_\omega^H)\right]\right\}, & C_\omega^\pm(m,n,p,q) &= j\omega\rho_\pm c_\pm \delta_m^p\delta_n^q, \\
S_b(\omega) &= \frac{1}{2}\Re\!\left\{\mathrm{Tr}\!\left[\mathbf{\Psi}_\omega\,\mathbf{Y}_\omega^H\right]\right\}.
\end{aligned}
\right.
\tag{4.17}
$$

in which the superscript ^{H} denotes the Hermitian (complex conjugate transpose) and Tr[A] is the trace of the matrix A (the sum of its diagonal elements). In (4.17), the element $\Psi_{mn}^{pq}(\omega)$ of the modal excitation matrix $\overline{\Psi}_\omega$ are defined in terms of the wavenumber-frequency power spectrum of the turbulent pressure $S_{p_b p_b}(\mathbf{k};\omega)$ as follows:

$$
\Psi_{mn}^{pq}(\omega) = \iint_{R^2} S_{mn}(\mathbf{k})\; S_{p_b p_b}(\mathbf{k};\omega)\; S_{pq}^*(\mathbf{k})\; d^2\mathbf{k}
\tag{4.18}
$$

On using Parseval's formula, the modal excitation term $\Psi_{mn}^{pq}(\omega)$ can be expressed, in the spatial domain, as:

$$
\Psi_{mn}^{pq}(\omega) = \left(4\pi^2\right)\iint_\Sigma\iint_\Sigma \Phi_{mn}(\mathbf{x})\; S_{p_b p_b}(\mathbf{x}-\mathbf{x}';\omega)\; \Phi_{pq}^*(\mathbf{x}')\; d^2\mathbf{x}\,d^2\mathbf{x}'
\tag{4.19}
$$

In order to save some computational cost, it would be convenient if the cross-terms could be neglected in expression (4.17).

4.2.2 Conditions under which the coupling can be neglected

In the expression (4.17) for the spectra of the power quantities, two coupling terms may be neglected: the acoustic cross-coupling terms (then, $Z_{mnpq}^\pm(\omega) = Z_{mnmn}^\pm(\omega)\delta_m^p\,\delta_n^q$) and the excitation cross-coupling terms (then, $\Psi_{mn}^{pq}(\omega) = \Psi_{mn}^{mn}(\omega)\delta_m^p\,\delta_n^q$).

From the system (4.13), it appears clearly that, if the acoustic cross-coupling terms are neglected, then the cross structural mobilities can be neglected, i.e. $Y_{mnpq}(\omega) = Y_{mnmn}(\omega)\delta_m^p\,\delta_n^q$. However, some authors [17,38] neglect the cross structural mobilities without neglecting the acoustic cross-coupling terms in the radiated sound power S_Σ (4.17). This situation may arise only for the cases of light fluid-loaded structures with a high modal density for which the acoustic cross-coupling terms are of the same order as the acoustic self-coupling terms $Z_{mnmn}^\pm(\omega)$, but both terms are negligible with respect to the structural coefficients that appear in the system (4.13). In

this case, only the neglect of the excitation cross-coupling terms can lead to a simplified expression for S_Σ.

Before performing the diagonal approximations on the expression (4.17), it is recommended to know for which frequency ranges these simplifications are valid.

4.2.2.a Conditions under which the acoustic cross-coupling terms can be neglected

Leppington *et al.* [39] have shown that these terms could be reasonably neglected for frequencies above the critical frequency of the modes contributing to the plate response, the radiation efficiency of these modes being largely independent of their order. When the inefficient modes contribute also to the system response in the very low frequency domain, Mkhitarov [40] has derived a quantitative criteria for which the acoustic coupling may be negligible. It is based on an iterative method starting from the solution obtained with the diagonal approximation and is given by ($N_\pm \eta \omega / \varepsilon_\pm \gg 1$) where $N_\pm^2 = k_\pm^2 (a^2 + b^2)$. More restrictive conditions have been obtained by Graham [41] through investigating the plate response when only two inefficient modes interact, giving ($N_\pm^2 \eta \omega^2 / \varepsilon_\pm^2 \gg 1$). The last condition provides a minimum frequency ω_{ac} above which the acoustic cross-coupling terms may be neglected.

This frequency depends on the fluid-loading parameter $\varepsilon_\pm$, the structural damping η and the size of the plate (a, b) as follows:

$$\omega_{ac} = \left(\frac{\rho_\pm c_\pm^2}{m \eta \sqrt{a^2 + b^2}} \right)^{\frac{1}{3}} \tag{4.20}$$

The underlying idea is that the fluid-loading terms can be neglected in the governing modal equation (4.13) with respect to the structural terms above this critical frequency and thus, the system (4.13) becomes diagonal. It is well known, indeed, that, when the frequency increases, the structural properties dominate the dynamic of a system with respect to its acoustic interaction with the surrounding fluid. Though the fluid-loading terms cannot be neglected with respect to the structural terms in the low-frequency domain, the weak modal overlapping between the resonance allows the cross-coupling terms to be neglected with respect to the self-coupling terms and thus the diagonal approximation still applies.

4.2.2.b Conditions under which the excitation cross-coupling terms can be neglected

In the previous paragraph, we have formulated criteria to neglect the acoustic coupling between the modes: these are general criteria related to any fluid-structure interaction problem. Further simplifications can be obtained in the case of a structure excited by wall-pressure fluctuations.

Dyer [42] and Davies [17] have derived similar criteria to neglect the coupling between the modes by a turbulent forcing field. From the expression (4.19) of the modal

excitation terms written in the spatial domain, Davies has shown that, if the correlation lengths in both the streamwise and the spanwise directions are largely much smaller than the dimensions of the plate in the respective directions, then the spatial-frequency spectrum of the turbulent excitation $S_{p_b p_b}(\mathbf{x} - \mathbf{x}'; \omega)$ almost becomes a Dirac function $\delta_x(\mathbf{x}')$ and the integral (4.19) then expresses the orthogonality relationship between the eigenmodes of the plate. The correlation lengths L_x and L_y of the turbulent excitations in both directions will be introduced in the next section. They are formally given by:

$$\begin{cases} L_x = U_c / \alpha_x \omega \\ L_y = U_c / \alpha_y \omega \end{cases} \tag{4.21}$$

where U_c is the convection velocity and (α_x, α_y) are empirical constants. They represent the spatial decay in both directions due to the changes of the pressure eddy patterns when they are convected from one point to another.

Hence, Davies suggests a lower limit ω_l of the frequency for which the excitation cross-coupling terms can be neglected:

$$\text{If } \omega \gg \omega_l, \text{ then } \Psi_{mn}^{pq}(\omega) \ll \Psi_{mn}^{mn}(\omega) \quad \forall (m,n) \neq (p,q),$$

$$\text{where: } \omega_l = \text{Max}\left(U_c / c_y a, U_c / c_x b \right). \tag{4.22}$$

Let us notice that, even if there exist a strong coupling between the modes by the forcing field below this frequency, the excitation cross-coupling terms may still be neglected if the resonance frequencies are widely separated as it is the case for the lightly damped structures. However, this point is rigorously true at the first resonance or for a third-octave analysis over a frequency band with a low modal density, mainly influenced by the levels at the peak resonance. Otherwise, it has to be checked with attention on each special case before performing a diagonal simplification for the excitation.

Having pointed out for which values of the physical parameters can be neglected the acoustic or the excitation coupling between the modes, reduced expressions for the spectral densities of the displacement, the radiated pressure field and the power quantities can then be derived.

4.2.3 The diagonal approximation

We first aim to compute the spectral densities (3.7, 3.9, 3.14) within a frequency range over which the acoustic coupling can be neglected. On substituting the modal series (4.1) with the explicit coefficient (4.14) into the cross-power spectrum of the displacement (3.7), the cross-spectrum of the plate displacement becomes:

$$S_{ww}(\mathbf{x}, \mathbf{x}'; \omega) = \frac{1}{(2\pi)^2} \sum_{m=1}^{+\infty} \sum_{n=1}^{+\infty} \sum_{p=1}^{+\infty} \sum_{q=1}^{+\infty} \frac{\Psi_{mn}^{pq}(\omega)\, \Phi_{mn}(\mathbf{x})\, \Phi_{pq}^*(\mathbf{x}')}{D_{mn}(\omega) D_{pq}^*(\omega)}, \quad \forall (\mathbf{x}, \mathbf{x}') \in \Sigma \times \Sigma. \tag{4.23}$$

23

An expression similar to (4.23) for the cross-spectrum of the acoustic pressure fields radiated in both domains $\Omega^{\pm}$ is easily obtained when substituting the modal series (4.5) into the formula (3.9). With a wavenumber representation of the pressure fields, it is found:

$$S_{p_{\pm}p_{\pm}}(\mathbf{x},\mathbf{x}';\omega) = \frac{\omega^2\rho_{\pm}^2 c_{\pm}^2}{(2\pi)^2}\sum_{m=1}^{+\infty}\sum_{n=1}^{+\infty}\sum_{p=1}^{+\infty}\sum_{q=1}^{+\infty}\frac{\Psi_{mn}^{pq}(\omega)Z_{mnmn}^{\pm}(\omega)Z_{pqpq}^{\pm^*}(\omega)\,\Phi_{mn}(\mathbf{x})\,\Phi_{pq}^*(\mathbf{x}')}{D_{mn}(\omega)D_{pq}^*(\omega)} \quad (4.24)$$

or, with a spatial representation of the pressure fields:

$$S_{p_{\pm}p_{\pm}}(\mathbf{x},\mathbf{x}';\omega) = \frac{\rho_{\pm}^2\omega^4}{(2\pi)^2}\sum_{m=1}^{+\infty}\sum_{n=1}^{+\infty}\sum_{p=1}^{+\infty}\sum_{q=1}^{+\infty}\frac{\Psi_{mn}^{pq}(\omega)}{D_{mn}(\omega)D_{pq}^*(\omega)}\left(\iint_{\Sigma}\mathcal{G}_{\omega}^{\pm}(\mathbf{x}-\mathbf{x}'')\,\Phi_{mn}(\mathbf{x}'')\,d^2\mathbf{x}''\right)$$
$$\times\left(\iint_{\Sigma}\mathcal{G}_{\omega}^{\pm}(\mathbf{x}'-\mathbf{x}''')\,\Phi_{mn}(\mathbf{x}''')\,d^2\mathbf{x}'''\right)^* \quad (4.25)$$

In the case of far-field pressure, (4.25) simplifies into:

$$S_{p_{\pm}p_{\pm}}(\mathbf{x},\mathbf{x}';\omega) = \frac{\rho_{\pm}^2\omega^4}{(2\pi)^4}\frac{e^{jk_{\pm}\|\mathbf{x}\|}}{\|\mathbf{x}\|}\frac{e^{jk_{\pm}\|\mathbf{x}'\|}}{\|\mathbf{x}'\|}$$
$$\times\sum_{m=1}^{+\infty}\sum_{n=1}^{+\infty}\sum_{p=1}^{+\infty}\sum_{q=1}^{+\infty}\frac{\Psi_{mn}^{pq}(\omega)}{D_{mn}(\omega)D_{pq}^*(\omega)} \quad (4.26)$$
$$\times S_{mn}(k_{\pm}\sin\theta_P\cos\varphi_P, k_{\pm}\sin\theta_P\sin\varphi_P)$$
$$\times S_{pq}^*(k_{\pm}\sin\theta_{P'}\cos\varphi_{P'}, k_{\pm}\sin\theta_{P'}\sin\varphi_{P'})$$

in which $\mathbf{x}$ is described by $\left(\|\mathbf{x}\|\sin\theta_x\cos\varphi_x, \|\mathbf{x}\|\sin\theta_x\sin\varphi_x, \|\mathbf{x}\|\cos\theta_x\right)$ in the rectangular co-ordinate system of the plate (O,x,y,z) and by $\left(\|\mathbf{x}\|,\theta_x,\varphi_x\right)$ in the associated spherical co-ordinate system. The corresponding co-ordinates of $\mathbf{x}'$ are then easily deduced.

Quantities of interest are the spectra of the powers defined by (3.15). Under the acoustic diagonal approximation, the expressions (4.17) simplify into:

$$\begin{cases} S_{\Sigma}(\omega) = \dfrac{\eta}{2}\sum_{m=1}^{+\infty}\sum_{n=1}^{+\infty}\dfrac{D\lambda_{mn}^4}{\left|D_{mn}(\omega)\right|^2}\Psi_{mn}^{mn}(\omega), \\[3mm] S_{\pi^{\pm}}(\omega) = \dfrac{\omega\rho_{\pm}c_{\pm}}{2}\sum_{m=1}^{+\infty}\sum_{n=1}^{+\infty}\dfrac{\Re\left(Z_{mnmn}^{\pm}(\omega)\right)}{\left|D_{mn}(\omega)\right|^2}\Psi_{mn}^{mn}(\omega), \\[3mm] S_b(\omega) = \dfrac{1}{2}\sum_{m=1}^{+\infty}\sum_{n=1}^{+\infty}\Re\left(\dfrac{1}{D_{mn}^*(\omega)}\right)\Psi_{mn}^{mn}(\omega). \end{cases} \quad (4.27)$$

The radiation efficiency $\sigma(\omega)$ of the plate has been defined at the end of the previous section (3.16) and has been expressed in terms of both the radiated acoustic

power $S_\Sigma(\omega)$ and the kinetic energy $S_{E_c}(\omega)$. Thus, a simplified expression of $\sigma(\omega)$ can also be deduced.

Let us notice that further simplifications can be obtained for the cross-spectra of both the displacement (4.23) and the radiated pressure fields (4.24-26) if, moreover, we neglect $\Psi_{mn}^{pq}(\omega)$ for $(m,n) \neq (p,q)$, i.e. the excitation cross-coupling between the modes. However, no further simplifications will appear if we apply this hypothesis to the power spectra (4.27).

Hence, the cross-power spectrum of the displacement (4.23) reduces to:

$$S_{ww}(\mathbf{x}, \mathbf{x}'; \omega) = \frac{1}{(2\pi)^2} \sum_{m=1}^{+\infty} \sum_{n=1}^{+\infty} \frac{\Psi_{mn}^{mn}(\omega) \, \Phi_{mn}(\mathbf{x}) \, \Phi_{mn}^*(\mathbf{x}')}{\left| D_{mn}(\omega) \right|^2} \tag{4.28}$$

The cross-power spectrum (4.24) for the acoustic pressure fields radiated in $\Omega^\pm$ simplifies into:

$$S_{p_\pm p_\pm}(\mathbf{x}, \mathbf{x}'; \omega) = \frac{\omega^2 \rho_\pm^2 c_\pm^2}{(2\pi)^2} \sum_{m=1}^{+\infty} \sum_{n=1}^{+\infty} \frac{\Psi_{mn}^{mn}(\omega) \left| Z_{mnmn}^\pm(\omega) \right|^2 \Phi_{mn}(\mathbf{x}) \Phi_{mn}^*(\mathbf{x}')}{\left| D_{mn}(\omega) \right|^2} \tag{4.29}$$

4.2.4 Methodology for the choice of the useful eigenmodes

The modal excitation terms $\Psi_{mn}^{pq}(\omega)$, defined by (4.19), appear in the expressions (4.23-26). They correspond to the projection of the excitation field on the eigenmodes. The self-modal excitation terms $\Psi_{mn}^{mn}(\omega)$ of the first structural modes of the plate have been plotted on Figures 4.1 and 4.2. At a given frequency, the contribution of a mode to the panel response is all the more important that the modal excitation term is high. This will occur, in the wavenumber domain, for frequencies for which the maximum peak of the modal shape function nearly coincides with the convection peak of the turbulent pressure field (*hydrodynamic coincidence effect*). Hence, for each frequency, we can deduce from the plots 4.1 and 4.2 the number of modes that will contribute significantly in the modal representation of the solution because the choice of the eigenmodes to be accounted for is governed by the bandwidth of the excitation.

Indeed, it is *a priori* obvious that the useful eigenmodes are those which are necessary for an accurate expansion of the excitation, i.e. of the function $S_{p_b p_b}(\mathbf{x}; \omega)$, an expansion of which is given, under the diagonal approximation, by:

$$S_{p_b p_b}(\mathbf{x}; \omega) = \sum_{m=1}^{+\infty} \sum_{n=1}^{+\infty} \Psi_{mn}^{mn}(\omega) \left| \Phi_{mn}(\mathbf{x}) \right|^2 \tag{4.30}$$

The eigenmodes which have a negligible contribution in the excitation representation (4.30) will have a negligible contribution in the system response (4.23-29). This property provides a methodology for the choice of the useful eigenmodes to be accounted for since the expansion (4.30) is easy to compute once a model has been

chosen for the excitation. Let us note that this methodology can be applied whatever the nature of the excitation.

For the panel of interest (described at section 6), all the modes up to order 7 and 11 respectively in the spanwise and streamwise directions were required to describe with a good accuracy the power spectral density of the displacement of the plate. It can be verified on Figures 4.3 and 4.4. The figure 4.3 represents the power spectral density of the kinetic energy of the panel when increasing the number of structural modes accounted for. The figure 4.4 compares, for an increasing number of modes, the evolution of the normalised quantities corresponding to the panel kinetic energy and to the excitation pressure field. These quantities have been normalised in order to provide the same scale [0,1] for the comparison.

First, we notice that the modal expansion for the power spectral density of the plate kinetic energy is a convergent series (Figs. 4.3-4.4). Second, below the convergence limit, increasing streamwise mode numbers has a significant effect on the spectrum levels over a wide frequency range whereas increasing spanwise mode numbers has a reduced effect (Fig. 4.3). This can be understood through the Figure 4.2. Third, the Figure 4.4 confirms our methodology for the choice of the useful eigenmodes. The discontinuities for the convergence curves are only due to our choice for "ordering" the modal numbers.

4.3 Conclusions

The first conclusion which can be drawn is that when the plate is excited by a turbulent boundary layer, the sound power radiated by the plate above the frequency ω_t can be expressed as a sum of uncorrelated structural modes. This is an important statement for active control, since we are certain to reduce the sound power radiated by the plate if we manage to reduce the amplitude of any structural mode provided the amplitudes of the other structural modes are not affected. *A priori*, this would not be the case for a general harmonic excitation.

A second conclusion can be formulated from the expression of $S_{\pi^{\pm}}(\omega)$ that is given in the set of equation (4.27). It can then be seen that the contribution of a given mode (m,n) to the sound power radiated depends on several conditions:

- whether it is resonant or not ($\left| D_{mn}(\omega) \right|^2$ minimum, if resonant);

- whether it is highly excited or not ($\Psi_{mn}^{mn}(\omega)$ maximum at the hydrodynamic coincidence);

- whether it radiates efficiently ($\Re\left(Z_{mnmn}^{\pm}(\omega)/\rho_{\pm}c_{\pm}\right)$ asymptotes to one when the frequency is above the acoustic coincidence frequency (Fig. 6.11)) or not.

Because of these competing effects, it is *a priori* difficult to determine which kind of mode will be preponderant in the system response: resonant and highly excited but inefficient modes or resonant and efficient, but weakly excited by the turbulent field. To answer this question, a detailed study of the modal distribution of the structure together with the behaviour of the wall-pressure field both in the convective and in the subconvective region are required. This latter point will be discussed in section 6.

26

5. MODELS FOR TURBULENT WALL-PRESSURE FLUCTUATIONS

Numerical predictions (Direct Numerical Simulations) of TBL pressure fluctuations are limited to low Reynolds number simple flows and, in any other case one has to rely on semi-empirical models fitted to experimental data. A large number of these models have been developed to describe the wall-pressure fluctuations on a rigid plane wall due to a turbulent boundary layer. A comprehensive review of the most classical models may be found in [20]. In the following, we mainly focus our attention on Corcos and Chase models. But, as a prelude to this discussion, some general comments are made about the "typical evolution" of the wavenumber-frequency power spectrum of the wall-pressure fluctuations on a rigid surface. The thin curve in Figure 5.1, which corresponds to the Chase model for compressible fluids as explained below, is characterised by two main peaks:

♦ The higher peak, corresponding to the convective ridge, occurs for streamwise wavenumbers of order ω/U_c, where U_c is the eddy convection velocity, and for spanwise wavenumbers k_x near 0. It separates the low-wavenumber region ($k_k U_c / \omega < 1$) from the high-wavenumber region ($k_k U_c / \omega > 1$).

♦ The second peak, not described by the Corcos model, is located in the low-wavenumber region for a modulus of $\mathbf{k} = (k_x, k_y)$ near the acoustic wavenumber $k_+ = \omega/c_+$. When $\mathbf{k}$ tends to $\mathbf{0}$, the power spectrum becomes a wavenumber-white spectrum, about 40 dB lower than the level at the convective peak.

5.1 The Corcos model

5.1.1 Formulation in the space-frequency domain

One of the first model has been introduced by Corcos [43] to discuss problems of spatial resolution for pressure transducers at high frequency. First, Corcos assumes that the cross-correlation function of the wall-pressure fluctuations can be expressed in a separable form:

$$S_{p_b p_b}(\xi_x, \xi_y; \omega) = \Phi_0(\omega) \, C_x(\xi_x; \omega) \, C_y(\xi_y; \omega) \tag{5.1}$$

where $\xi_x = x - x'$ and $\xi_y = y - y'$ denote the spanwise and the streamwise distance coordinates, respectively along the x and y directions. $\Phi_0(\omega)$ is the point-power spectrum defined as:

$$\Phi_0(\omega) = \frac{1}{(2\pi)^2} \int\limits_{-\infty}^{+\infty}\int\limits_{-\infty}^{+\infty} S_{p_b p_b}(k_x, k_y; \omega) dk_x dk_y$$

where $S_{p_b p_b}(k_x, k_y; \omega)$ is the spatial Fourier transform of $S_{p_b p_b}(\xi_x, \xi_y; \omega)$ and has been defined in (3.2.a).

Different non-dimensional models of the point-power spectrum $\Phi_0(\omega)$ are plotted in Figure 5.2. For which the Chase model (dash-dotted) is given by:

$$\Phi_0(\omega) = a_+(1+\gamma)\rho_+^2 U_\tau^4\ \omega^{-1}$$

where ρ_+ is the mass density of the flow. The values of the constants are: $a_+ = 0.766$, $\gamma = 0.389$. The friction velocity U_τ is simply related to the free-stream speed U_∞ of the fluid flow by $U_\tau = 0.03 U_\infty$. More sophisticated expressions are provided in the literature for larger band expressions [32,44]. We have noticed that the semi-empirical model (bold line in Fig. 5.2) proposed by Cousin [45] achieved an excellent fit with measured data. Nevertheless, we have chosen for the simulations presented in section 6 the Efimtsov model (thin line in Fig. 5.2) valid up to high Reynolds number ($U_\infty \approx 306$ m/s) and given [27] as a function of the Strouhal number $Sh = \omega\delta/U_\infty$ by:

$$\Phi_0(\omega) = \frac{\tau_w^2 \delta}{U_\tau} \frac{0.01\pi}{\left(1+0.02 Sh^{2/3}\right)}, \quad U_\tau = \sqrt{\frac{\tau_w}{\rho_+}}$$

where δ is the boundary layer thickness and τ_w is the mean wall shear stress. We notice [46] that the point-power spectrum not only depends on U_∞ via the Strouhal number, but also via δ and τ_w (Fig. 6.10).

At this step, the unknown spanwise and streamwise correlation functions C_x and C_y are to be determined from experimental data and are approximated, in terms of their corresponding coherence lengths $L_x = U_c/\alpha_x\omega$ and $L_y = U_c/\alpha_y\omega$, by an exponential behaviour, as follows:

$$\begin{cases} C_x(\xi_x;\omega) = e^{-\alpha_x|\omega\,\xi_x/U_c|} \\ C_y(\xi_y;\omega) = e^{-\alpha_y|\omega\,\xi_y/U_c|}\ e^{-j\omega\,\xi_y/U_c} \end{cases} \tag{5.2}$$

where α_x and α_y are constants derived from experiments. Various values for these constants are reported in the literature, but most authors [20,46] provide values of α_y scattering around 0.1-0.3 and $\alpha_x \approx 7\alpha_y$. It is clear that the most reliable values for α_y and α_x can only be derived from the most extensive series of measurements on aircraft boundary layers. For this reason we have chosen those values suggested by Blake ($\alpha_y = 0.1$ and $\alpha_x = 0.7$) [46].

In the expression (5.2) for the correlation functions, the eddy convection velocity U_c is introduced. U_c is usually expressed in terms of the free-stream velocity U_∞ through the ratio U_c/U_∞ which depends, a priori, on the angular frequency ω and on the streamwise distance co-ordinate ξ_x. Indeed, measurements [47] have shown that:

◆ For all ξ fixed, the convection velocity decreases slightly with frequency. It means that the convection velocity of larger eddies, associated with the low-frequency domain and developed near the free-stream, is higher than the smaller eddies, corresponding to the high-frequency domain and developed near the wall. This drop in the velocity profile when the distance to the wall tends to zero is due to the fact that, for a turbulent flow, the convection velocity of the smaller eddies is more and more restrained by the fluid viscosity when approaching the wall.

◆ For a fixed frequency, the ratio U_c/U_∞ increases as ξ increases. It is explained by the fact that, if we increase the spacing between two pressure transducers measuring the convection velocity, we will increase the filtering effect on the contribution of the smaller eddy structures since they will vanish rapidly. We will then measure a convection velocity mainly governed by large eddies which are convected at a greater speed than smaller structures.

Nevertheless, there is not a great scattering for the values of the ratio U_c/U_∞ which is usually found to be between 0.7 and 0.8. In this report, the convection velocity U_c is taken to be equal to $0.7\,U_\infty$.

5.1.2 Formulation in the wavenumber-frequency domain

If we take the spatial-Fourier transform of the expression (5.1), we obtain the Corcos wavenumber-frequency power spectrum, expressed as follows:

$$S_{p_b p_b}(\mathbf{k};\omega) = \Phi_0(\omega)\left(\frac{U_c}{\omega}\right)^2 \hat{C}_x\left(\frac{U_c k_x}{\omega}\right)\hat{C}_y\left(\frac{U_c k_y}{\omega}\right) \tag{5.3}$$

with:

$$\left\{
\begin{array}{l}
\hat{C}_x\left(\dfrac{U_c k_x}{\omega}\right) = \dfrac{\alpha_x}{\pi\left\{\alpha_x^2 + \left(\dfrac{U_c k_x}{\omega} - 1\right)^2\right\}}, \\[4ex]
\hat{C}_y\left(\dfrac{U_c k_y}{\omega}\right) = \dfrac{\alpha_y}{\pi\left\{\alpha_y^2 + \left(\dfrac{U_c k_y}{\omega}\right)^2\right\}}.
\end{array}
\right.$$

The wavenumber-frequency power spectrum given by (5.3) is plotted in Figure 5.1 (bold). By comparisons with measurements, Blake [46] has shown that the Corcos model provided a good estimate of the power spectrum of flow-noise near the convective ridge. This model is particularly useful for high flow speeds applications like aircraft boundary layers since, in this case, the convective wavenumber ω/U_c nearly coincides with the first modal wavenumbers of the plate. This is the hydrodynamic coincidence effect. An accurate modelling of the convective domain will be required for aeronautical applications because it will mainly contribute to the excitation of the radiating supersonic components of the panel.

The second advantage of the Corcos model, as it will be shown below, is that it is simple enough to provide closed-form analytical expressions for the modal excitation term $\Psi_{mn}^{pq}(\omega)$ either in the space-frequency domain [17,18] or in the wavenumber-frequency domain [10]. Thus, extensive parametric studies can easily be handled over a wide frequency range without a lot of computational effort.

5.1.3 Limitations of the Corcos model

The major limitations of the Corcos model are the following:

♦ First, it is assumed that the coherence lengths L_x and L_y do not depend on the boundary layer displacement thickness δ^*, which is only true for small values of the separation coordinates ξ_x and ξ_y. On the other cases, the Corcos model underestimates dramatically the width of the convective peak and δ^*-corrections for streamwise and spanwise correlation lengths must be taken into account. For this purpose, empirical expressions for $L_x(\delta^*)$ and $L_y(\delta^*)$ have been proposed by Efimtsov [27] for different ranges of Mach numbers.

♦ Second, the Corcos model presents a white low-wavenumber behaviour and, thus, fails to exhibit the theoretically required $\|\mathbf{k}\|^2$ dependency when $\|\mathbf{k}\| \ll 1/\delta^*$ (the Phillips-Kraichnan theorem). However, instead of proposing a new theoretical formulation including this property and leading to new unknown constants, Hwang *et al.* [21] have modified the empirical Corcos model so as to satisfy the $\|\mathbf{k}\|^2$ constraint (together with an integral normalisation condition). Although the Corcos model has thus been improved, it always suffers from its lack of dependence on the boundary layer thickness, for which the similarity variable is given by the Strouhal number Sh.

♦ The last inconvenient for the Corcos model is closely related to the previous one: it concerns the overestimation of the low-wavenumber levels for the power spectrum which, then, exhibits a white wavenumber spectrum from 20 to 40 dB above the measured spectrum in the subconvective region down to the compressible (or acoustic) domain (see Figure 5.1). Unfortunately, in most low Mach number applications, such as underwater acoustics, for which the structural wavenumbers are usually much lower than the convective wavenumber, large eddy scales of turbulence contribute as a major part to the vibro-acoustic response of the structure and, hence, require a more rigorous model than the Corcos description for the low-wavenumber region.

5.2 The Chase model

In 1980, Chase derived a theoretical model for an incompressible fluid [44], introducing new parameters which would enable, if suitably chosen, the correct prediction of levels for the wall-pressure fluctuations spectrum in the low-wavenumber frequency domain ($\omega/c_+ \le k_y \le \omega/U_c$) (see Figure 5.1, dash-dotted). Moreover, the $\|\mathbf{k}\|^2$ dependency of the spectral density is taken into account in this model when $\|\mathbf{k}\| \ll 1/\delta^*$.

For this purpose, in 1987, Chase reformulated his model [32] to include the effect of compressibility and, thus, to describe spectral elements of the flow noise down to and

near the acoustic wavenumber (see Figure 5.1, thin). The Chase wavenumber-frequency power spectrum is given as follows:

$$S_{p_b p_b}(\mathbf{k};\omega) = S^m_{p_b p_b}(\mathbf{k};\omega) + S^t_{p_b p_b}(\mathbf{k};\omega) \qquad (5.4)$$

where $S^m_{p_b p_b}$ represents the contribution of the mean-shear to the wall-pressure fluctuations spectrum:

$$S^m_{p_b p_b}(k_x, k_y; \omega) = \frac{C_m \rho^2_+ \upsilon^3_* k^2_y}{\left[\dfrac{(\omega - k_y U_c)^2}{(h_m \upsilon_*)^2} + \|\mathbf{k}\|^2 + \dfrac{1}{(b_m \delta^*)^2} \right]^{5/2}}$$

and $S^t_{p_b p_b}$ concerns the contribution of the pure turbulence to the wall-pressure fluctuations spectrum:

$$S^t_{p_b p_b}(k_x, k_y; \omega) = \frac{C_t \rho^2_+ \upsilon^3_* |\vec{k}|^2}{\left[\dfrac{(\omega - k_y U_c)^2}{(h_t \upsilon_*)^2} + \|\mathbf{k}\|^2 + \dfrac{1}{(b_t \delta^*)^2} \right]^{5/2}}$$

The parameters recommended by Chase are:

$$C_t = 3r_t a_+ / 2\pi h_t, \quad C_m = (C_t + r_m)/r_t,$$
$$h_m = \mu_m U_c / \upsilon_*, \quad h_t = \mu_t U_c / \upsilon_*,$$
$$r_t = 0.389, \quad r_m = 0.611,$$
$$a_+ = 0.766, \quad \mu_m = \mu_t = 0.176,$$
$$b_m = 0.756, \quad b_t = 0.378.$$

Blake [46] has shown that both semi-theoretical formulations proposed by Chase reasonably agreed with measured data within a wide range of subconvective wavenumbers down to $k_y \approx 0.4/\delta^*$.

The main limitations of the Chase model are discussed below. However, for the purposes of this report, these are minor limitations:

♦ First, the Strouhal number dependency of the power spectrum has been recently contested by Witting [48] and is not yet clearly established.

♦ Secondly, the Chase model does not take into account the spectral elements of the flow noise with a supersonic speed ($k_x \leq \omega/c_\pm$), whose behaviour is dominated by compressible effects. This last point is of particular interest when studying the acoustic contamination of an incoming signal by the sound generated by supersonic turbulent structures in marine applications.

31

5.3 Choice of the excitation model

In summary, the Chase and Corcos models are complementary. The Corcos power spectrum of the excitation provides a good estimation for the levels of the wall-pressure fluctuations near and at the convective peak which is of fundamental importance for aircraft boundary layers. On the other hand, the Chase power spectrum agrees reasonably well with experimental data for the subconvective domain down to the acoustic wavenumber. It is therefore more suitable for low-speed flow applications where the strongest flow-structure interaction occurs in the low-wavenumber region. For the case considered in section 6, with a Mach number of 0.7, it is thus the Corcos model which is the most suitable.

6. RESULTS FOR THE PREDICTION AND THE CONTROL OF THE VIBRO-ACOUSTIC RESPONSE OF A TBL-EXCITED PANEL

In this section, simulation results are presented for the response of an aircraft panel to the excitation by a turbulent boundary layer. We will first give some general comments about the main hypothesis underlying our simplified model. In a second part, we will examine the influence of the main physical parameters on the vibro-acoustic response of a TBL-excited plate: the structural dissipation, the hydrodynamic coincidence effects and the radiation efficiency, as it has been pointed out at the end of section 4. In a third part, comparisons will be presented between numerical predictions and experimental results. In a final part, a suitable strategy will be discussed for the active structural acoustic control of the sound power transmitted through an aircraft panel.

For a typical aircraft panel and otherwise stated, the geometrical and mechanical parameters are given in the Table 6.1.

Table 6.1 Geometrical and physical parameters for a typical aircraft panel

Parameters	Value
Free-stream velocity	$U_\infty = 225$ m / s
Convection velocity	$U_c = 0.7 U_\infty$
Boundary layer thickness	$\delta = 0.1$ m
Panel thickness	$h = 0.001$ m
Panel Young's modulus	$E = 7.24 \times 10^{10}$ Pa
Panel longitudinal tension	$N_m = 29300$ N / m
Panel lateral tension	$N_n = 62100$ N / m
Panel Poisson's ratio	$v = 0.33$
Panel mass density	$\rho_p = 2800$ kg / m^3
Panel damping ratio	$\varsigma = 0.01$ or $\varsigma = 0.05$
Panel dimensions	$a = 0.414$ m, $b = 0.314$ m
Sound speed in fluid	External fluid: $c_+ = 300$ m / s
	Internal fluid: $c_- = 340$ m / s
Fluid density	External: $\rho_+ = 0.44$ kg / m^3
	Internal : $\rho_- = 1.42$ kg / m^3

6.1. General considerations

The eigenfrequencies of the flat panel without membrane effects are given in the Table 6.2 (third column), together with the corresponding critical frequencies (sixth column), for which the structural wavelength equals to the acoustic wavelength. In the fourth column, the eigenfrequencies of the aircraft panel described by the parameters given in Table 6.1, i.e. the flat tensioned plate, have been reported and the fifth column

shows the eigenfrequencies of a panel with transverse curvature, such as that due to the cylindrical geometry of the fuselage in the spanwise direction.

Table 6.2. Resonance and critical frequencies of the panel

m	n	f_{mn}^{res} (Hz) Flat panel	f_{mn}^{res} (Hz) In-plane tensions	f_{mn}^{res} (Hz) Curved + in-plane	f_{mn}^{crit} (Hz) Flat panel
1	1	38.7	270.2	307.9	679.5
1	2	80.9	351.9	451.0	983.6
2	1	112.2	502.8	505.3	1158.0
1	3	151.4	465.3	575.8	1345.6
2	2	154.5	556.6	575.9	1359.0
2	3	225.0	642.6	681.9	1640.1
3	1	234.7	759.3	759.6	1675.3
1	4	250.1	602.5	704.4	1729.4
3	2	277.1	802.5	806.6	1820.0
2	4	323.7	757.6	808.4	1967.3
3	3	347.7	874.2	886.6	2038.5
1	5	377.0	761.6	850.4	2123.3
4	1	406.3	1039.3	1039.4	2204.2
3	4	446.3	974.4	995.7	2309.9
4	2	448.6	1078.1	1079.2	2316.1
4	3	519.2	1143.1	1147.4	2491.4
1	6	532.2	942.8	1018.8	2522.6

6.1.1. Effect of membrane stresses on the sound power radiated

The influence of in-plane tension on the sound transmission through the panel has also been considered. Figure 6.1 shows the result of a calculation for the internal sound power radiated from a flat untensioned panel subject to a TBL excitation, as well as that calculated taking into account the influence of membrane stresses due to the cabin pressurisation, for the typical parameters given in Table 6.1. According to the Table 6.2, these membrane tensions lead to an increase of the fundamental eigenfrequency of the panel by a factor of about 7. Moreover, the order of the corresponding eigenfrequencies for the individual modal values (m, n) associated with each structural mode are modified. The corresponding mode shapes are, however, still the same as the untensioned plate. Hence, it is clear that we cannot neglect the influence if the in-plane tension even in a simplified model.

6.1.2 Effect of circumferential curvature on the panel structural properties

The first eigenfrequencies of the curved aircraft panel are reported in the Table 6.2 and have been obtained from analytical approximations given by Blevins [49]. We have used a typical circumferential radius of 2 m [12]. It can be seen that the curvature raises the natural frequencies of a curved panel above that of an analogous flat plate of a

factor of up to about 1.3, but in a non-uniform way. Indeed, it can be noticed, as expected, that the eigenfrequencies that are weakly raised (less than 1%) are only those associated to the very first modal order in the streamwise axial direction. Hence, the influence of curvature on the structural properties of an aircraft panel appears negligible when compared with the influence of cabin pressurisation. Other investigations have been carried out to determine the effect of panel curvature on the sound field inwardly radiated [13] (discussed in section 1) as well as on the wall-pressure fluctuations [50].

6.1.3 Verification of the main simplifications

6.1.3.a Neglection of the cross-excitation terms

In Figures 6.2 and 6.3, a comparison is shown of the prediction of the power spectral density of the displacement of an aircraft panel between the full solution given by the expression (4.22) and the approximate one given by the expression (4.27), which is obtained by neglecting the cross modal excitation terms with respect to the diagonal terms. It is clearly seen that, for moderate values of the structural damping ($\varsigma = 0.01$, Fig. 6.2), the cross-modal excitation terms can be neglected to predict the vibrating response of the turbulent excited plate over the frequency range of interest. Indeed, the geometrical criteria (4.21), proposed by Davies [17], suggests a critical value corresponding to the frequency above which the coherence lengths of the turbulent forcing field $L_x = U_c / \alpha_x \omega$ and $L_y = U_c / \alpha_y \omega$ are respectively "negligible" with respect to the size b and a of the plate (Eq. 4.22), which in our case is above 290 Hz. However, for the characteristics of our problem, the cross-coupling terms can also be neglected below 290 Hz because there is not a great modal overlap in this frequency range.

The situation is somewhat different concerning the case when $\varsigma = 0.05$ (Fig. 6.3), where we account for the damping effect of a trimmed panel: neglecting the excitation cross-coupling leads to an overestimation of the levels of the structure response over the whole frequency range.

It seems that, for highly damped structures, a mechanical counterpart of the geometrical criteria (Eq. 4.22) should be formulated, accounting for the structural properties of the plate, as follows: find the frequency range and the structural parameter region for which

$$\frac{\Psi_{mn}^{pq}(\omega)}{D_{mn}(\omega)D_{pq}^*(\omega)} << \frac{\Psi_{mn}^{mn}(\omega)}{\left|D_{mn}(\omega)\right|^2} \quad \forall(m,n) \neq (p,q).$$

Such a criterion needs to be more thoroughly analysed. It will not affect the main physical trends we are going to point out, however, because, in the following we will consider the full solution for the case when $\varsigma = 0.05$.

6.1.3.b Neglection of the radiation damping effects

In Figures 6.4 and 6.5 the sound power inwardly radiated by the panel has been plotted for $\varsigma = 0.01$ and $\varsigma = 0.05$, with or without the radiation damping terms which

appear in expression (4.14) for the frequency response $D_{mn}(\omega)$ of mode (m,n). First, only the levels at the very first resonance are modified by the radiation damping terms: they decrease when the higher damping ratio is used. The effect is dramatically diminished with increasing frequency and structural damping. This is due to the fact that, in these cases, the radiation damping effect becomes less and less important with respect to the structural damping effect. Thus, we will neglect the radiation damping effect in the following analysis for both $\varsigma = 0.01$ and $\varsigma = 0.05$.

6.2. Effects of the mechanical and/or geometrical parameters on the vibro-acoustic response of the panel.

6.2.1 Effects of the structural damping

♦ In Figures 6.6 and 6.7, power quantities involved in the balance energy equation (3.14) are shown for $\varsigma = 0.001$ and $\varsigma = 0.05$. First, we notice that, in all cases, only a small fraction of the power input by the TBL contributes to the radiated sound power, most of the boundary layer input power being either dissipated within the structure or transmitted through the boundaries. Second, this effect becomes more significant with increasing frequency, since the radiation damping decreases with frequency so that, above 1 kHz (Fig. 6.6), the structural dissipation becomes the dominant effect. Third, this effect is obviously accentuated for $\varsigma = 0.05$ (Fig. 6.7) with a significantly higher structural damping.

♦ In Figure 6.8, the effect of changing the structural damping ratio from 1% to 5% has been considered on the sound power inwardly radiated by the aircraft panel. As expected, it is the levels at the resonant peaks that are mainly affected and a reduction of about 10 dB has been achieved in the overall total sound power radiated by increasing the structural damping from 1% to 5%. Moreover, we notice that the influence of the structural damping increases with frequency. Hence, the accurate prediction of the panel response will require a more precise model of structural dissipation as the analysis frequency increases. Although the increase in damping ratio shown in Fig. 6.8 has a beneficial influence on the sound power radiated, further increases in the damping ratio (Fig. 6.9) for highly dissipative panels do not seem to affect the radiated sound power levels to the same degree [16].

6.2.2 Effects of hydrodynamic coincidence

♦ A straightforward influence of the flow velocity on the panel response is that the levels of sound power inwardly radiated by the plate increase over the whole frequency range with the flow speed, i.e. the aircraft speed, because of the influence of the convection velocity on the point power spectrum $\Phi_0(\omega)$ (Fig. 6.10). However, if the "boundary layer growth" along the flow direction is accounted for as in the Efimtsov model, this evolution is not uniform over a broad frequency range: the radiated sound power scales onto U_c^3 in the low-frequency domain whereas it scales onto $U_c^{11/3}$ for higher frequencies.

♦ A more subtle effect due to flow velocity has been pointed out in Figure 6.11, where we have plotted the evolution, for three values of the flow velocity, of the sound power inwardly radiated by the panel and scaled onto independent parameters of the turbulent flow so that the effect of the term $\Phi_0(\omega)$ no longer appears. It can be seen that the bandwidth within which the radiated energy is concentrated increases slightly with flow velocity. This is not due to the increase of the bandwidth of the turbulent excitation as, up to 2 kHz, the spectrum of the pressure fluctuations can be considered as essentially flat (Fig. 6.10). The explanation lies in the hydrodynamic coincidence effect that occurs when the phase velocity of the excitation (ω/k_y) matches the flexural phase velocity (ω/λ) where λ is the flexural wave number and is defined by Eq. (4.15). In other words, it appears when the convective scale of the turbulent excitation, where the main fluctuating energy lays, coincides with the scale of a structural mode.

This phenomenon can be clearly understood from Figure 6.12. the eigen-frequencies associated with the first structural modes of the panel are plotted in terms of the streamwise mode number n for different spanwise mode numbers m together with the hydrodynamic matching lines $\omega/U_c = n\pi/a$ for the three Mach numbers considered in Fig. 6.11. The structural modes located in the neighbourhood of the matching lines will be highly excited by the TBL: this is what we observe in Fig. 6.11 where, as the flow velocity increases, the higher order modes are more and more excited since they are closer to the hydrodynamic line. As illustrated in Fig. 6.12, the low order modes are less sensitive to changing in the flow velocity.

Finally, it appears that in our configuration and for high-speed subsonic flows, hydrodynamic coincidence exists up to 1-1.5 kHz. It is thus the convective peak of the wall-pressure wavenumber-frequency spectrum that determines the levels of sound radiated over this frequency range. This clearly justifies our choice of a wall-pressure model that gives correct levels in the convective region.

6.2.3 Modal radiation properties

♦ The third major effect which governs the amplitudes of the resonant peaks for the sound radiated concerns the radiation efficiency of each structural mode. From Table 6.2, it is clear that most of the modes which contribute to the response of the system are inefficient radiators at their resonant frequencies. This means that, below their critical frequency, these modes have large differences in their contribution to the far-field radiated pressure, the less efficient modes being the even-even modes (Fig. 6.13). Above their critical frequency, however, these modes radiate sound independently, with an efficiency that asymptotes to one for all modes (Fig. 6.13). For instance, we notice in Figure 6.1 that, below 500 Hz for the untensioned panel, the resonant modes with the highest contribution to the sound power radiated are odd-odd inefficient modes. However, the (2,2) mode that does not contribute to the sound power radiated by the untensioned panel at its natural frequency of 154 Hz, because it is so inefficient, begins to radiate efficiently when the panel is tensioned and its natural frequency is raised to 556 Hz. This evolution is clearly illustrated in Fig. 6.13 where $ka = 1.2$ at the resonant frequency of the (2,2) mode for the untensioned plate and $ka = 4.3$ at the resonant frequency of this mode for the tensioned plate.

In order to plot the radiation efficiency of each structural mode as a function of frequency, we must compute the real part of the modal impedance integrals (4.12), also named the radiation resistance. Although analytical approximations have been derived for this quantity [39,41,51], we have used a numerical approach, based upon the Clenshaw-Curtis adaptive quadrature [52].

♦ An important point is that the sound field radiated by any structural mode couples with any other structural mode, as illustrated by the thin curve in Fig. 6.13. This means that *a priori* the cross-terms of the radiation matrix $\Re(\mathbf{Z}_\omega^\pm)$ are not zero-valued. However, as presented by Elliott et al. [9], it is possible to define a new basis for the solution that diagonalize $\Re(\mathbf{Z}_\omega^\pm)$. It is relevant that the corresponding frequency-dependent eigenvectors or *radiation modes* do not depend on the mechanical properties of the plate. Mathematical details about their construction are given in appendix B. The radiation efficiencies of the radiation modes are proportional to the eigenvalues of the radiation matrix. The radiation efficiencies of the first four radiation modes are plotted in Fig. 6.14 as a function of normalised frequency. The mode shapes of the first six radiation modes are plotted in Fig. 6.15 for two excitation frequencies: 250 Hz and 1000 Hz, which correspond to $ka = 1.9$ and $ka = 7.6$.

We notice that the first radiation mode can be considered as a piston-like mode up to 600 Hz and its amplitude can thus be approximated by the volumetric contribution of the structure velocity. This uniform shape is slowly transformed into a "dome" shape for larger values of ka.

By definition, there are no cross-dependent terms and the radiation modes radiate sound independently. Using this new set of basis functions, the sound power radiated by the plate can thus be seen as the sum of independent contributions due to each radiation mode. This means that the sound pressure radiated by the plate vibrating with a surface velocity proportional to one of the radiation modes will not reexcite the other (radiation) modes. As we have noticed, this is not the case with the structural modes since the sound power radiated by each structural mode is partially reabsorbed by the other (structural) modes.

♦ At this stage, an important conclusion for control strategies can be drawn: we are certain to reduce the total sound power radiated by the plate if we manage to reduce the amplitude of any radiation mode. Previous studies have, however, shown that under a general harmonic excitation, reducing the amplitude of a structural mode does not necessarily guarantee a decrease in the sound power radiated. Nevertheless, when the plate is excited by a TBL, the sound power radiated by the plate can be expressed as a sum of uncorrelated structural modes (section 4). In contrast to harmonic excitation, reducing the amplitude of any structural mode should guarantee an attenuation of the sound power radiated while also reducing the vibration or near-field pressure levels provided the amplitudes of the other structural modes have not been affected. This conclusion will be checked in section 6.4.

6.3 Comparisons with experimental results

In this section, the predictions from the current model will be compared with experimental results obtained in the anechoic wind-tunnel of the LMFA (Ecole Centrale

de Lyon, France) for the vibration of a flat plate excited by a turbulent boundary layer [18].

A thin (1mm thick) rectangular untensioned plate made of stainless steel is clamped on the rigid wall of a wind-tunnel test section. Although the measurements have been realised for a fluid velocity varying from 40 m/s to 130 m/s, we will only present the results obtained for the highest flow speed. Indeed, the use of a Corcos-like model to describe the turbulent excitation is relevant to predict the structure response only when the hydrodynamic coincidence effect occurs and this effect is all the more preponderant over a broader bandwidth that the flow velocity is high (par. 6.2.2).

The plate is flush-mounted far downstream from a rectangular pipe inlet in order to achieve conditions of homogeneity and stationarity for the airflow when developped over one side of the plate. The anechoic tunnel has been designed to prevent the effects of acoustic contamination from the centrifugal blower and the ambient noise. Nevertheless, the wall-pressure fluctuations usually exhibit an undesirable acoustic component apart from the turbulent component below 200 Hz: this is due to the contribution of longitudinal acoustic modes that are excited in the pipe between the inlet and the outlet. Signal processing methods have been reported to cancel the acoustic component from the power spectral density of the wall-pressure fluctuations like the temporal substraction method [53] and the coherent output technique [54]. They are all based on the principle that the acoustic field is more coherent than the turbulent field in the spanwise direction. We have to keep in mind that no noise cancellation techniques have been applied for the measurements herein presented and could lead, to a certain extent, to inaccuracies as for the measurements below 200 Hz.

The plate acceleration is measured by very light Bruël and Kjaer accelerometers attached to the structure. As the surface mass of the plate is high (7.8 kg/m^2), the added mass effect introduced by the accelerometers can be neglected. The geometrical and mechanical characteristics of the system under study are summarised in the Table 6.3.

Table 6.3. Physical characteristics of the TBL-excited panel

Panel parameters	Flow parameters
Dimensions : $a \times b \times h = 0.30 \times 0.15 \times 0.001 \, \text{m}^3$	Boundary layer thickness : $\delta = 0.03$ m
Mass density : $\rho_p = 7800 \, \text{kg} / \text{m}^3$	Mass density : $\rho_+ = \rho_- = 1.3 \, \text{kg} / \text{m}^3$
Young's modulus : $E = 221 \text{GPa}$	Sound speed : $c_+ = c_- = 340 \, \text{m} / \text{s}$
Modal damping ratio : $\varsigma = 0.005$	Free stream velocity : $U_\infty = 130 \, \text{m} / \text{s}$
Poisson's ratio : $v = 0.3$	

In the Table 6.4, the first successive measured modal frequencies of the plate are compared with those calculated from analytical approximations [37] for two values of the

Young's modulus. Because of uncertainties concerning the bending rigidity of the structure, we have first computed the eigenfrequencies of the plate from an estimated value of the Young's modulus for steel material: $E = 221\,\text{GPa}$ (Table 6.4, middle column). We notice that the predicted eigenfrequencies are greater than the measured one. This shift can be corrected by adjusting the Young's modulus in our model in order to get the best fit with the experimental data. This leads to $\tilde{E} = 200\,\text{GPa}$ and the corresponding eigenfrequencies are given in the right column of Table 6.4. The measured and predicted eigenfrequencies of the clamped plate then agree within a few percent, but in practice may be due to tensioning.

Table 6.4. Experimental and theoretical eigenfrequencies of the clamped plate.

f_{mn}^{res} (Hz) Measured	f_{mn}^{res} (Hz) Comp., $E = 221\,\text{GPa}$	f_{mn}^{res} (Hz) Comp., $\tilde{E} = 200\,\text{GPa}$
240.	280.	267.
340.	364.	346.
480.	512.	487.
700.	725.	695.
740.	813.	774.
880.	952.	906.
960.	999.	950.
1100.	1152.	1097.
1260.	1332.	1268.
1300.	1406.	1338.
1360.	1415.	1347.
1480.	1490.	1418.

In Fig. 6.16, we have plotted the measured and predicted ($\varsigma = 0.005$) power spectral density of the plate velocity at the point R1 with coordinates $x = 0.08\,\text{m}$ and $y = 0.16\,\text{m}$, i.e. near the center of the plate. The numerical results (bold line) have been obtained with the modal formulation detailed in section 4. The overall levels at the peaks are correctly described by our model.

The differences concerning the position of the resonant peaks are mainly due to the errors inherent to the measurements of the mechanical parameters of the plate. Some small peaks have been detected and predicted above 800 Hz: they correspond to even-even modes that poorly contribute to the vibrating response of the plate measured at a centered point (R1).

Measurements have also been performed at another point R2 with coordinates $x = 0.09\,\text{m}$ and $y = 0.27\,\text{m}$, i.e. located near one corner of the plate. In this case, a larger number of modes are observed (Fig. 6.17) and this is configuration is thus of more interest in the assessment of our model. In fact, we have a better agreement with these experimental data than with the previous one, not only concerning the overall levels, but also when we compare the relative contribution of each peak to the vibrating response.

In Fig. 6.16 and 6.17, the thin line of the top figure represents predictions obtained with a Boundary Integral Equation Method developped in the CNRS-LMA (Marseille, France) [55]: there is also a good agreement with the experimental data, but the levels at the peaks tend to be overestimated for increasing modal orders. Although the discrepancies have not been clearly identified, it has been shown that they could not be explained by the influence of the flow velocity on the acoustic propagation in Ω^+ since this latter phenomenon involves a "damping" effect on the structure response, but to a lesser extent.

It is important to notice that our simulations have been carried out within a few seconds on a Pentium III processor. Such a low computational cost is a consequence of the analytical model (Eq. 4.28) used to predict the velocity of the plate and simplified under the diagonal approximation. Although the modal excitation term Ψ_{mn}^{mn} of the clamped panel chould have been numerically computed, we have kept the exact analytical expression that has been derived in [41] for a simply-supported panel. Because the mode shapes of a clamped panel only differ from the mode shapes of a simply-supported panel in the vicinity of the plate boundaries, there is only a small difference between the corresponding modal excitation terms as long as the first modes are considered: our approximation is therefore justified.

A plot similar to Fig. 6.12 would have shown that, in this configuration, the bandwidth of efficiently excited modes (because of the hydrodynamic coincidence) extends up to 1000 Hz: this explains the flat evolution for the mean levels of the vibrating response of the plate over this frequency range in Fig. 6.16 and 6.17.

6.4 Sound power attenuation: structural modes versus radiation modes cancellation

The reduction of the sound power radiated by the plate can be achieved either by means of passive control techniques (modifying the properties of the radiating sources or the transmitting paths) or by means of active secondary sources in order to cancel the contribution due to the primary sources. In the following section, we will focus on the second method of control, which is expected to be most efficient in the low-frequency domain. Passive techniques show a poor efficiency over this frequency domain [56] unless an unrealistic amount of insulating material is used.

In order to define a suitable control strategy, we first examine how the first structural modes or radiation modes of the plate contribute to the vibro-acoustic response by cancelling their participation in the modal expression (Eq. 4.27) for the sound power radiated. Physically, it can be interpreted as an ideal case of feedback control in which a matched actuator/sensor pair is designed with a sensitivity chosen to detect or control each kind of mode [57].

Figures 6.18 to 6.23 show the effect of cancelling either the first few structural modes or the first few radiation modes on the sound power radiated by the lightly-damped tensioned panel ($\varsigma = 0.01$, Figs. 6.18 and 6.19; $\varsigma = 0.2$, Figs. 6.20 and 6.21; $\varsigma = 0.0005$, Figs. 6.22 and 6.23). The attenuation achieved for the total sound power radiated up to 1 kHz by accounting for the cancellation of a limited number of the higher order structural or radiation modes is summarised in Figure 6.24 ($\varsigma = 0.01$). Figures 6.25 and 6.26 show the effect of increasing values of the damping ratio on the attenuation achieved for the

total sound power radiated up to 1 kHz by accounting for the cancellation of a limited number of the higher order structural or radiation modes.

From Figs. 6.18, 6.20 and 6.22, we verify that each structural mode contributes independently to the sound power radiated by the TBL-excited panel. Although the cancellation of any radiation modes ensures a reduction for the total sound power radiated (Figs 6.19, 6.21 and 6.23), their contribution to the panel response is less obvious. However, some general trends can be observed. Removing the contribution from the piston-like radiation mode (dashed line) involves a reduction of the first resonant peaks associated to the odd-odd structural modes (monopole contributions). Furthermore, we can notice similar effects between the rocking modes and the first odd-even or even-odd structural modes (dipole contributions), as well as between the quadrupole-type mode and the first even-even structural modes. This suggests that the shapes of each radiation modes can be expressed as a set of structural modes with suitable amplitudes (see Appendix B and [59]).

From Fig. 6.24, it can be noted that approximately the same level of attenuation (about 6.5 dB) is observed by cancelling the first radiation mode or structural mode of the plate. When the higher order modes are cancelled, however, sound power reductions are achieved more efficiently when suppressing the contribution of the radiation modes compared with the structural modes. Indeed, cancelling the first three radiation modes leads to 13 dB of attenuation whereas six structural modes must be cancelled in order to achieve the same level of attenuation.

In Figs. 6.25 and 6.26, it can be seen that increasing the structural damping from $\varsigma = 0.0005$ to $\varsigma = 0.2$ does not affect significantly the attenuation of the overall sound power radiated after cancellation of the first structural or radiation mode. However, we notice that, as expected, the performances of both strategies are degraded when increasing the damping ratio, but only to a limited extent. This is related to the fact that we have assumed in paragraph 4.2.1 a constant value for the modal damping ratio ς whatever the modal order.

7. CONCLUSIONS

A simple model has been developed for predicting both the displacement and the acoustic radiation of a thin baffled plate, simply supported along its boundaries, stressed by in-plane tensions and excited by a turbulent boundary layer. This simplified modelling describes reasonably well the dynamic behaviour of the cylindrical part of an aircraft fuselage as a network of adjacent panels excited by wall-pressure fluctuations under subsonic cruise conditions and vibrating individually in the frequency range of interest (up to 1 kHz).

The spectral densities of the system response have been expressed, in the wavenumber-frequency domain, in terms of the spectral density of the turbulent excitation filtered by the transfer function of the plate, which is deduced from the plate response to a harmonic excitation. This latter quantity being expanded in terms of the plate eigenmodes, a modal analysis of the spectral densities has been performed and has lead to a power balance equation between the turbulent, the dissipated and the radiated power spectra. Physical criteria have been proposed to simplify these expressions. These

42

approximations assume the excitation and the acoustic modal coupling to be neglected over a defined frequency range. They have been checked *a posteriori*.

Parametric studies have pointed out the influence of the structural dissipation together with the hydrodynamic coincidence on the sound power inwardly radiated by the panel. First, increasing the structural damping reduces the levels of noise inwardly radiated, but only to a limited extent. Second, increasing the flow velocity contributes significantly to increasing the radiated sound power, but more subtle effects underlie this phenomenon, i.e. the dominant contribution comes from the highly excited resonant modes whose structural phase speed matches the turbulent convection velocity, also called the hydrodynamical coincidence effect.

The important conclusion we have drawn is that the structural modes of each panel radiate sound independently and a suitable strategy for the active structural acoustic control of the sound power inwardly radiated by the panels would be independent feedback control of each structural mode of each panel in the low-frequency domain. We have shown (Fig. 6.20) that this strategy could provide attenuation of up to 13 dB with six independent controllers.

As an alternative, a strategy based on the cancellation of the radiation modes has also been investigated. We have noticed that cancelling the first structural mode or the first radiation mode provides similar attenuation in the total sound power radiated up to 1 kHz. We have also noted that the cancellation of a limited number of the higher order radiation modes was more efficient than the cancellation of the same number of structural modes for the control of the sound power radiated by such panels.

Because perfectly matched sensors and actuators have been assumed in this paper, the performance would not been degraded by any *spillover* effects. In practice, with discrete actuators and sensors, these effects will always occur and degrade the results. However, the object here was to derive the performance limitations due to the physical properties of the TBL-excited panel, rather than a particular actuator-sensor arrangement, and so the assumption of idealised matched transducers is justified.
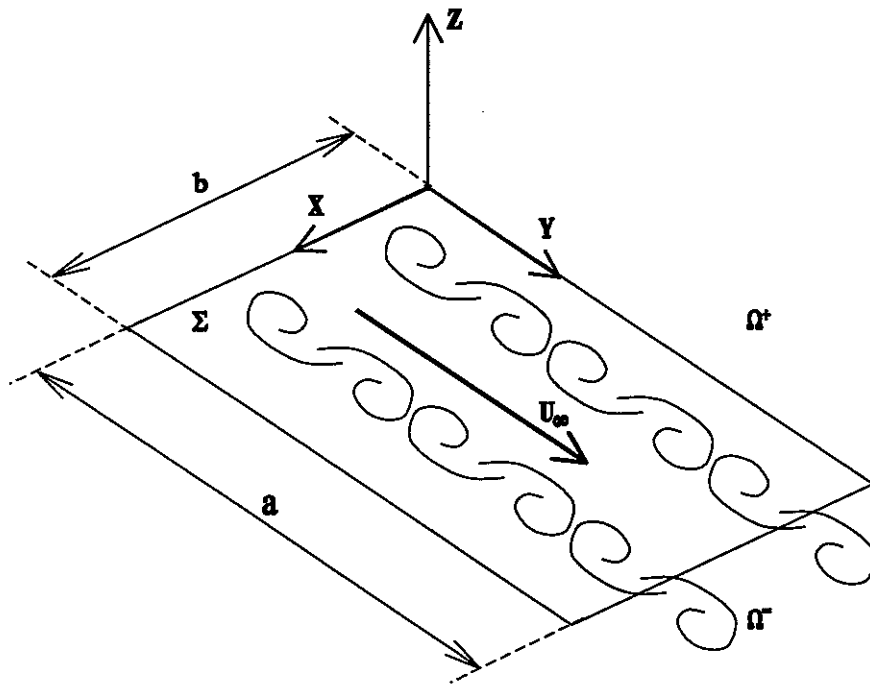
Figure 2.1 Geometry of the model, a flat panel inserted in an infinite baffle and excited on one side by a turbulent airflow with the free-stream velocity U_∞.
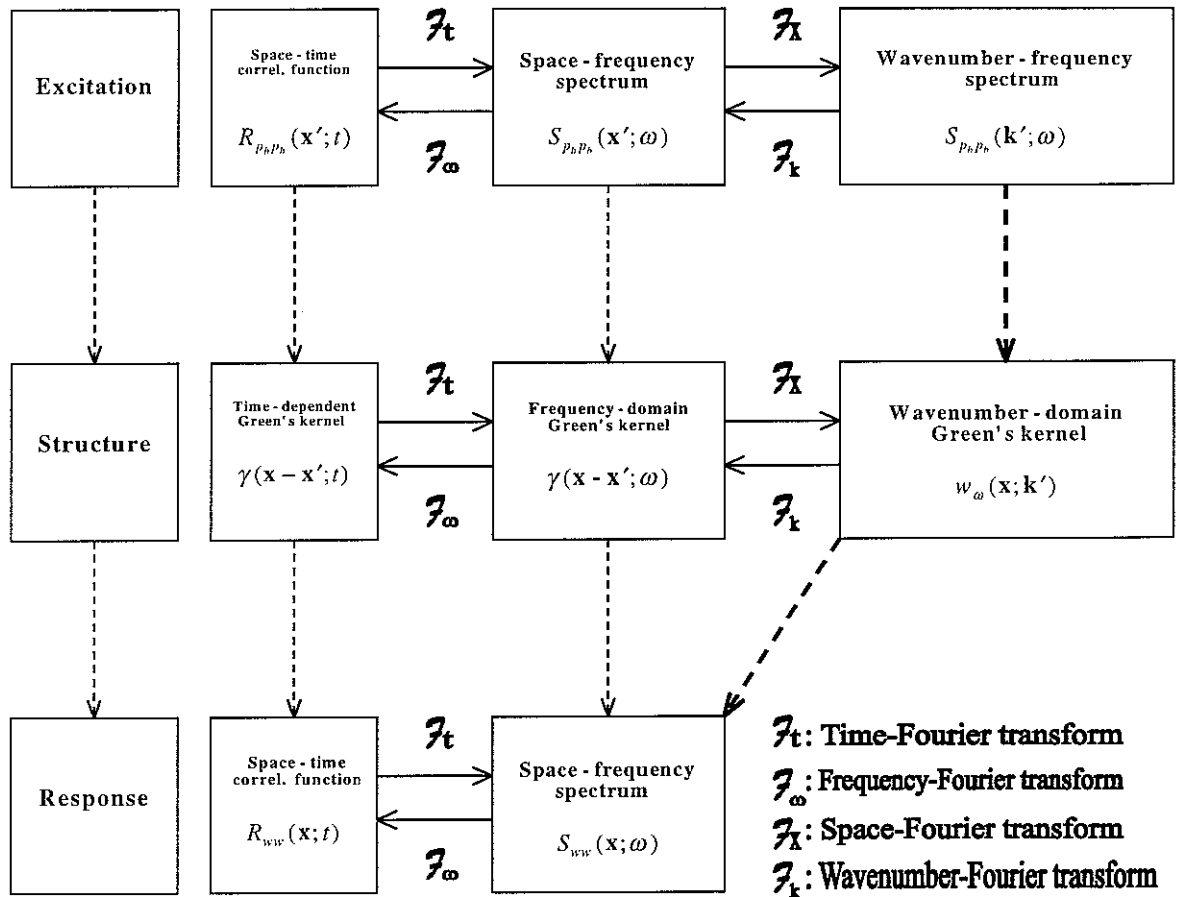
Figure 3.1 Schematic overview of the theoretical formulation for the derivation of the displacement response of a plate excited by a turbulent boundary layer.
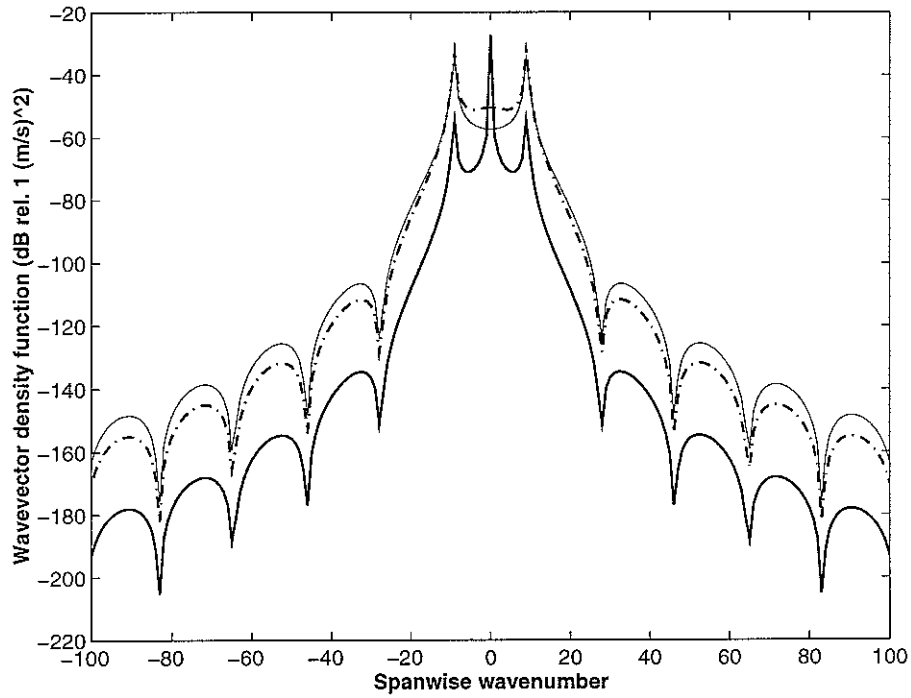
Figure 3.2 Contribution of the first mode to the wavevector density function $\left|w_{11}^{\omega}(k_x,0)\Phi_{11}(b/2,a/2)\right|^2 S_{p_b p_b}(k_x,0;\omega)$ *for the displacement at the middle of the plate and in the spanwise direction* $k_y = 0$ *for three analysis frequencies:* $f = 1$ Hz *(bold),* $f = 200$ Hz *(dash-dotted) and* $f = 1000$ Hz *(thin).*
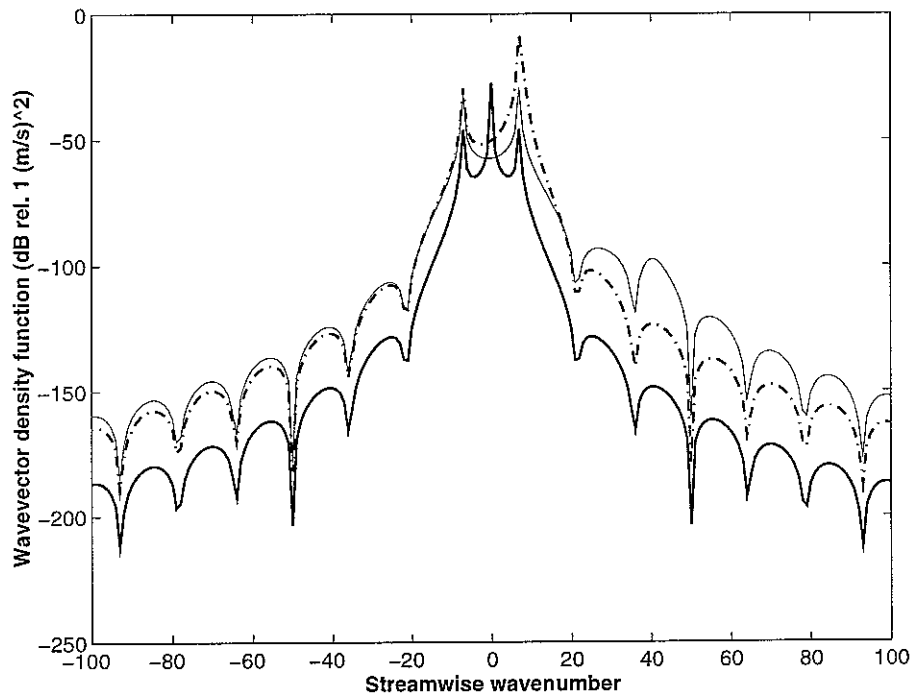
Figure 3.3 Contribution of the first mode to the wavevector density function $\left|w_{11}^{\omega}(0,k_y)\Phi_{11}(b/2,a/2)\right|^2 S_{p_b p_b}(0,k_y;\omega)$ *for the displacement at the middle of the plate and in the streamwise direction* $k_x = 0$ *for three analysis frequencies:* $f = 1$ Hz *(bold),* $f = 200$ Hz *(dash-dotted) and* $f = 1000$ Hz *(thin).*

46
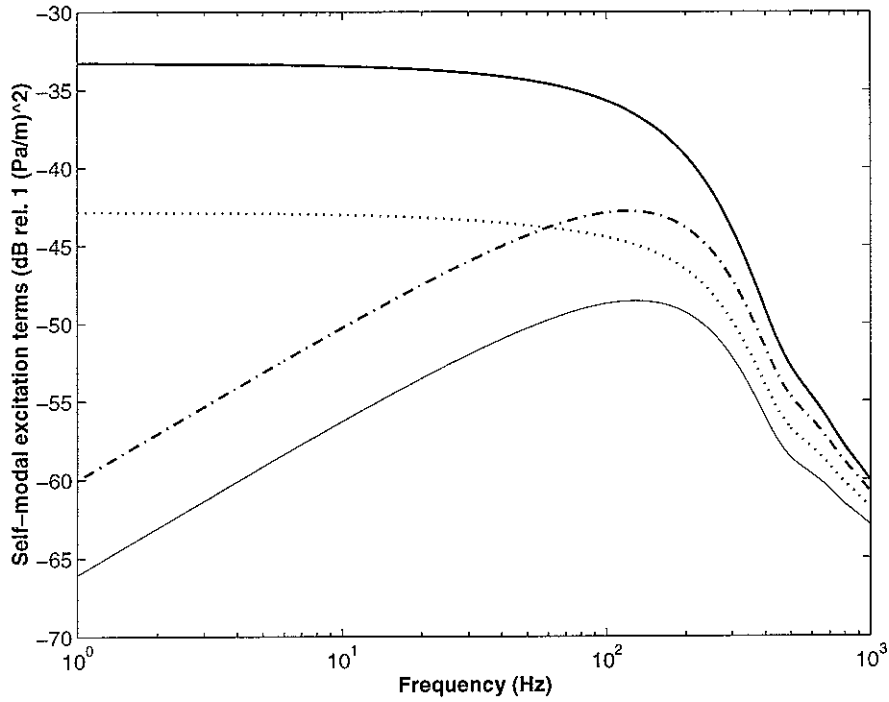
Figure 4.1 The self-modal excitation terms $\Psi_{mn}^{mn}(\omega)$ *as a function of the frequency for increasing* **spanwise** *mode numbers: (1,1), bold; (2,1), dash-dotted; (3,1), dotted and (4,1), thin.*
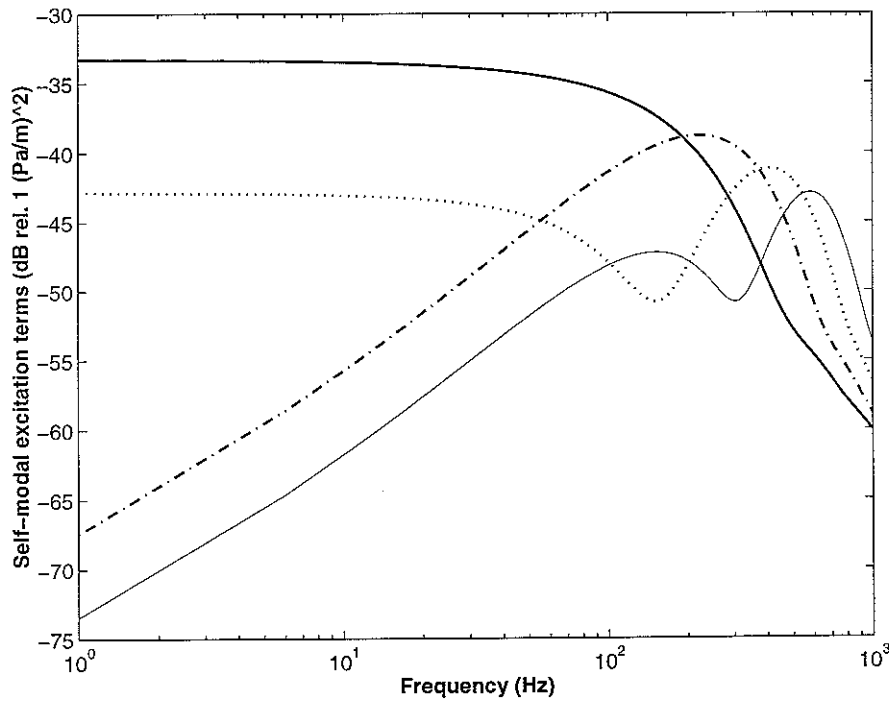
Figure 4.2 The self-modal excitation terms $\Psi_{mn}^{mn}(\omega)$ *as a function of the frequency for increasing* **streamwise** *mode numbers: (1,1), bold; (1,2), dash-dotted; (1,3), dotted and (1,4), thin.*
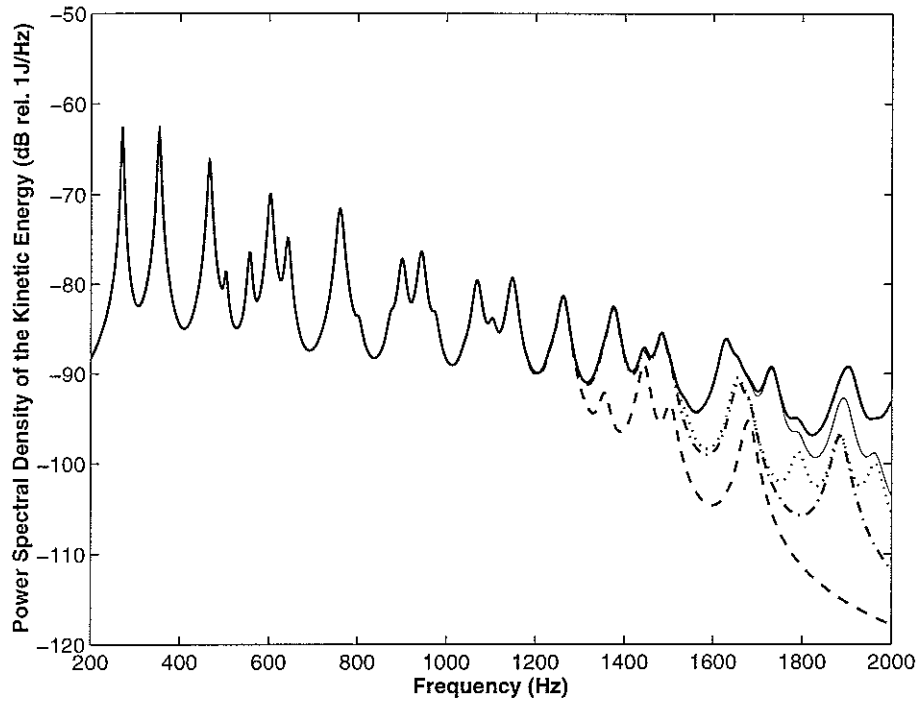
Figure 4.3 The power spectral density of the kinetic energy as a function of the frequency when an increasing number of structural modes is accounted for: (4,7), dashed; (4,8), dash-dotted; (5,8), dotted; (5,9), thin and (7,11), bold.
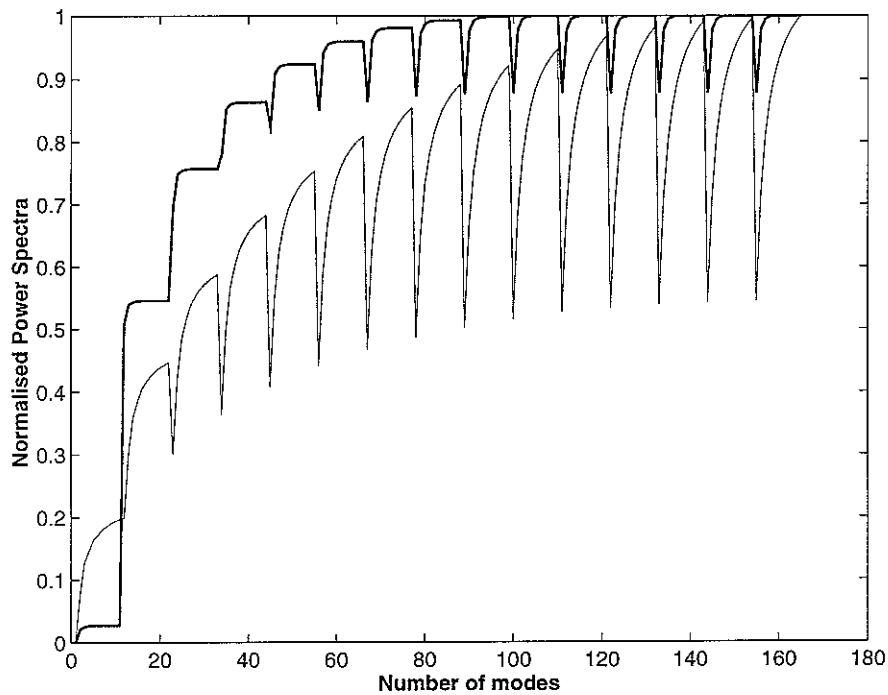
Figure 4.4 The normalised power spectra corresponding to the excitation pressure field (thin) and the kinetic energy (bold) as a function of the total number of structural modes accounted for in their modal expression.

48
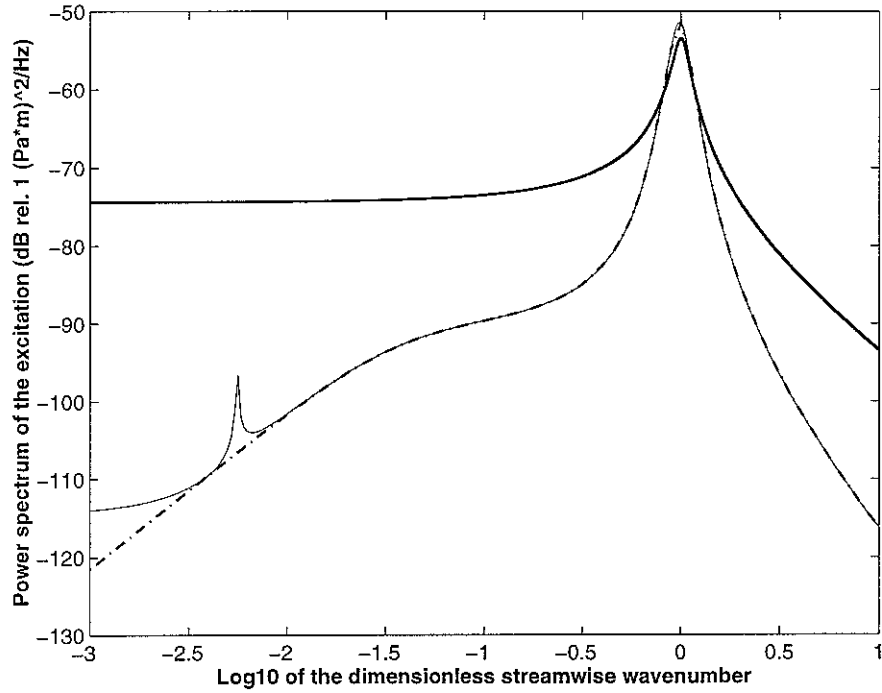
Figure 5.1 The excitation spectrum $S_{p_b p_b}\left(0, k_y; \omega\right)$ *as a function of the logarithm of the dimensionless streamwise wavenumber* $k_y U_c / \omega$; *bold: Corcos model, dash-dotted: Chase model (incompressible), thin: Chase model (compressible).*
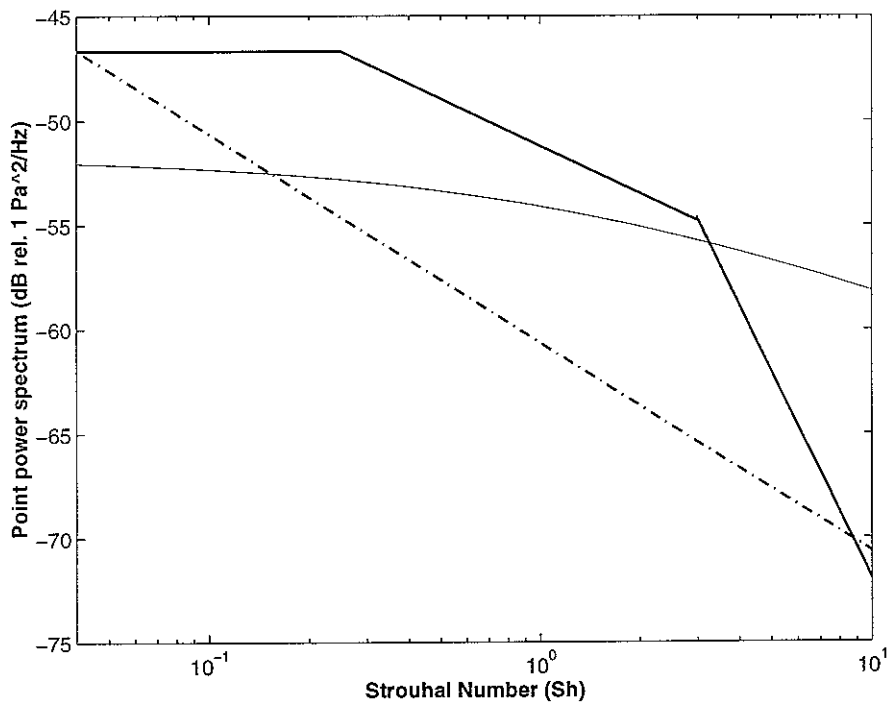
Figure 5.2 Different models for the turbulent boundary layer point power spectra $\Phi_0(\omega)$ *in terms of the Strouhal number* $Sh = \omega\delta/U_\infty$ *with* δ *the boundary layer thickness* ($\delta = 0.1\,\mathrm{m}$) *and* $U_\infty = 225\,\mathrm{m/s}$; *bold: Cousin model (semi-theoretical), dash-dotted: Chase model (theoretical), thin: Efimtsov model (theoretical).*

49
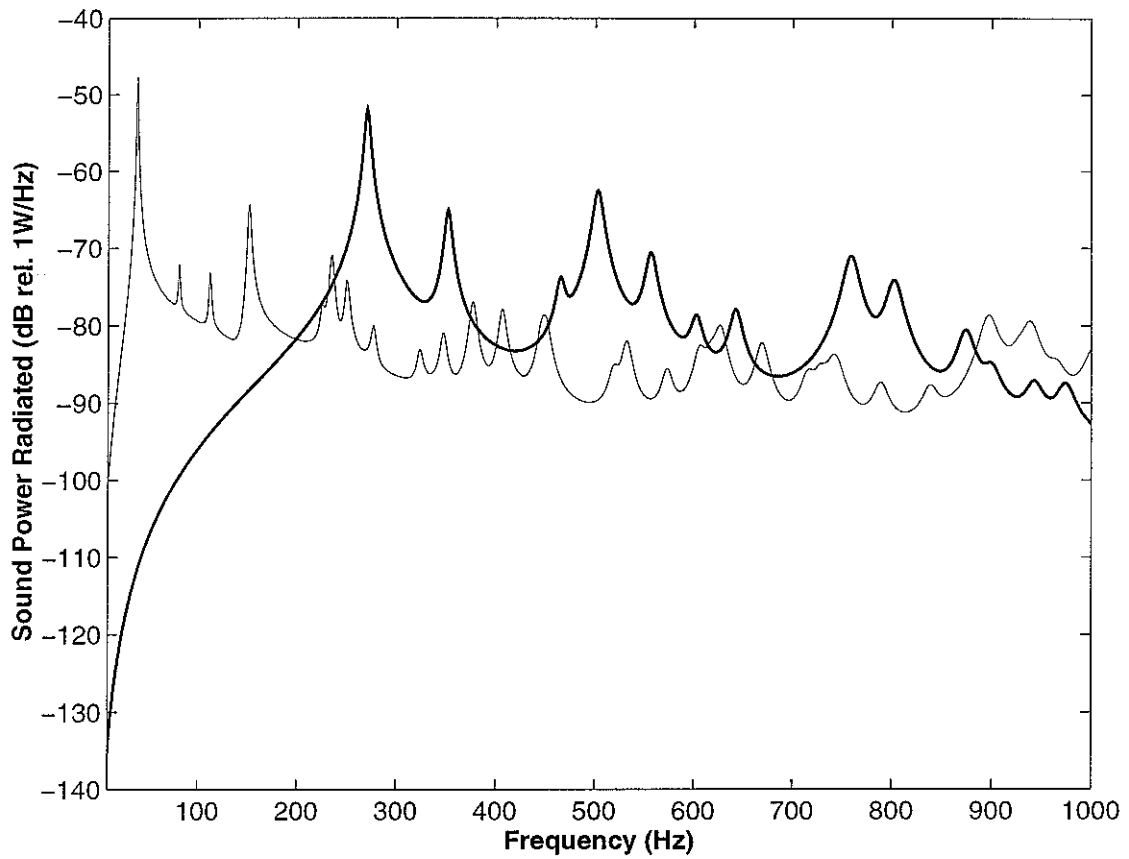
Figure 6.1 The sound power inwardly radiated by a tensioned plate (bold) and an untensioned plate (thin); $\varsigma = 0.01$ *and when excited by a TBL pressure field.*
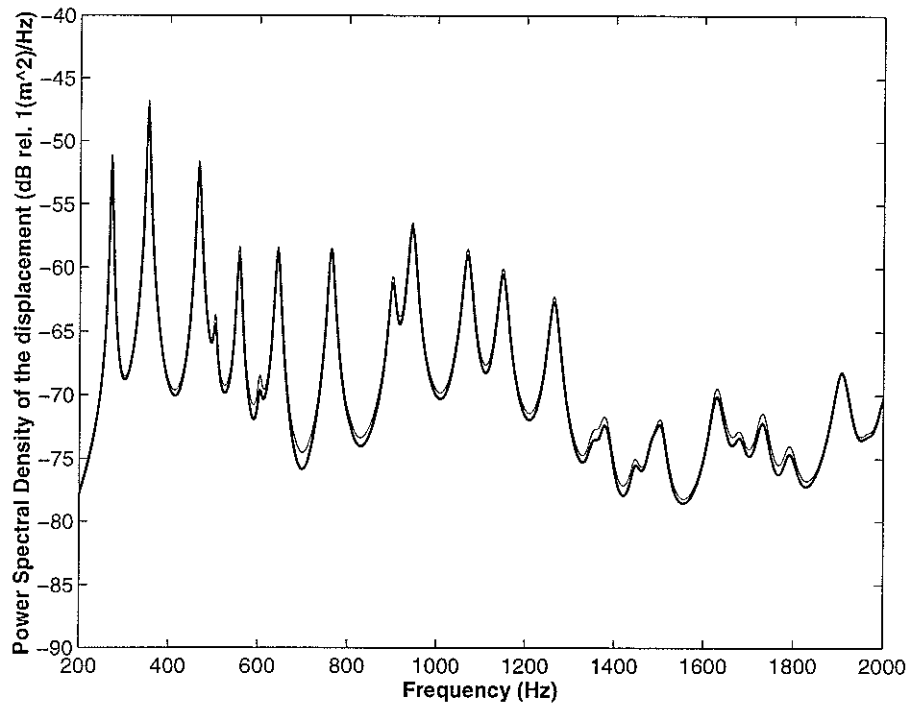
Figure 6.2 Comparison between the full solution (bold) and the diagonal solution (thin) for the power spectral density of the displacement of an aircraft panel ($\varsigma = 0.01$) at the point $(x, y) = (0.1, 0.1)$.
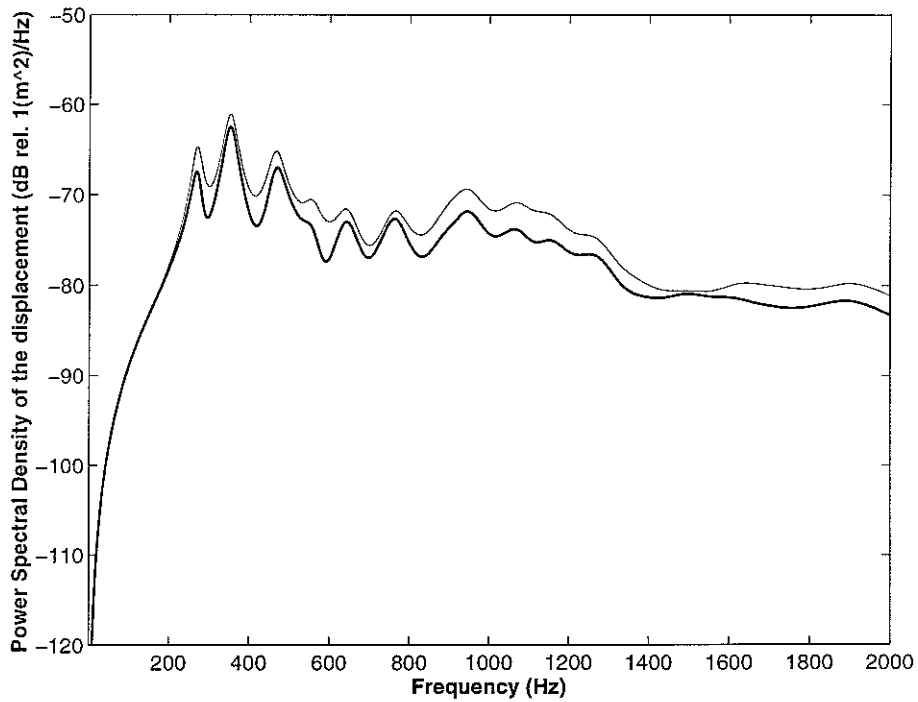
Figure 6.3 Comparison between the full solution (bold) and the diagonal solution (thin) for the power spectral density of the displacement of an aircraft panel ($\varsigma = 0.05$) at the point $(x, y) = (0.1, 0.1)$.
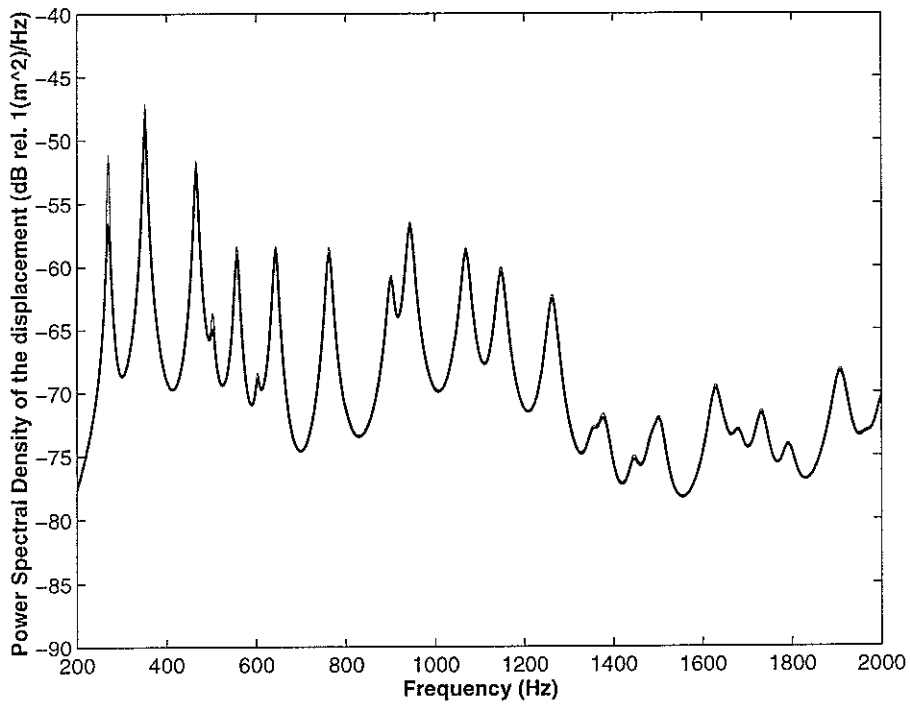
Figure 6.4 Fluid-loading effect on the vibrating response of an aircraft panel ($\varsigma = 0.01$): power spectral density of the displacement at the point $(x, y) = (0.1, 0.1)$ with fluid-loading (bold) and without fluid-loading (thin).
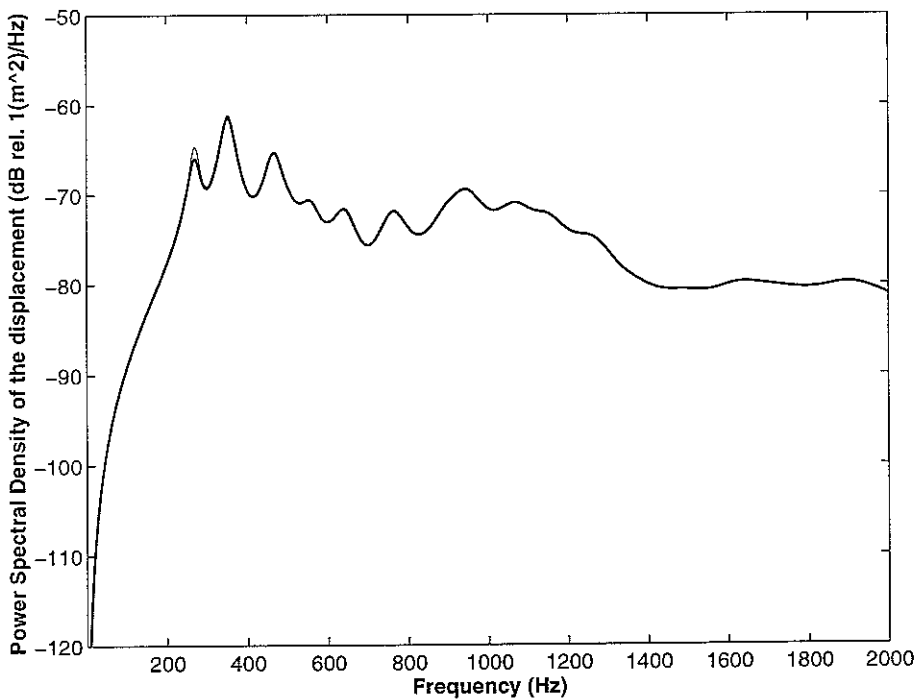
Figure 6.5 Fluid-loading effect on the vibrating response of an aircraft panel ($\varsigma = 0.05$): power spectral density of the displacement at the point $(x, y) = (0.1, 0.1)$ with fluid-loading (bold) and without fluid-loading (thin).
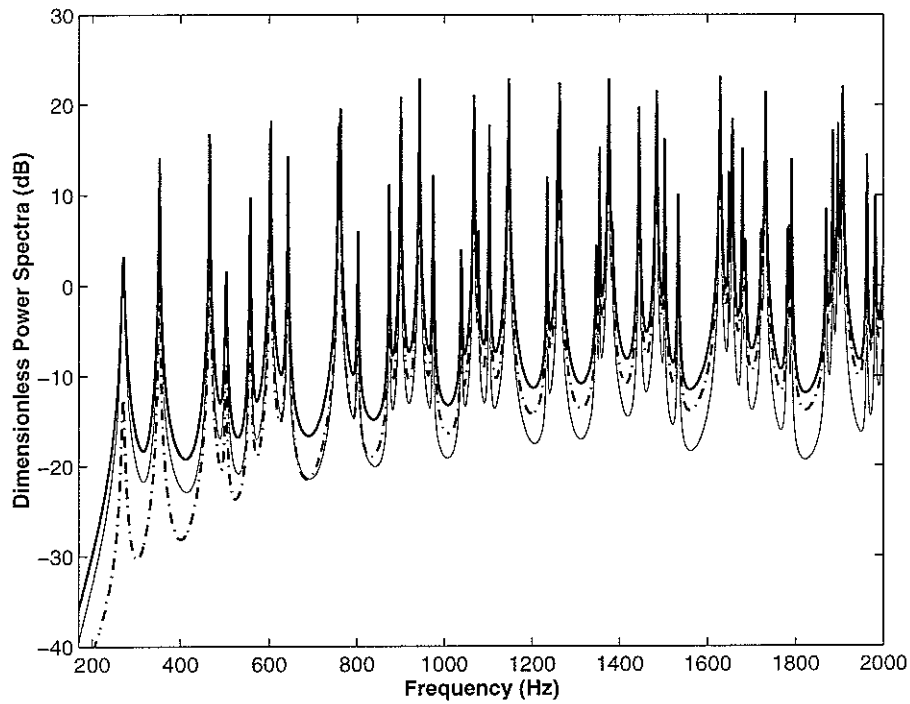
Figure 6.6 Energy balance of the power spectral quantities for the lightly damped panel ($\varsigma = 0.001$): boundary-layer input power (bold), structurally dissipated power (dash-dotted) and inwardly radiated power (thin).
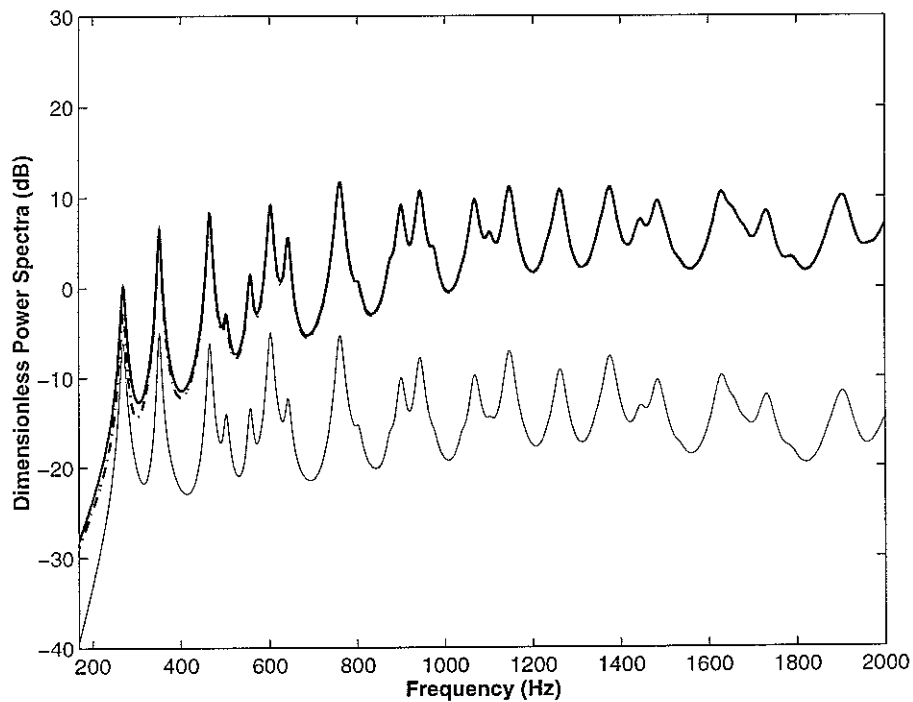

Figure 6.7 Energy balance of the power spectral quantities for a more heavily damped panel ($\varsigma = 0.01$): boundary-layer input power (bold), structurally dissipated power (dash-dotted) and inwardly radiated power (thin).

53
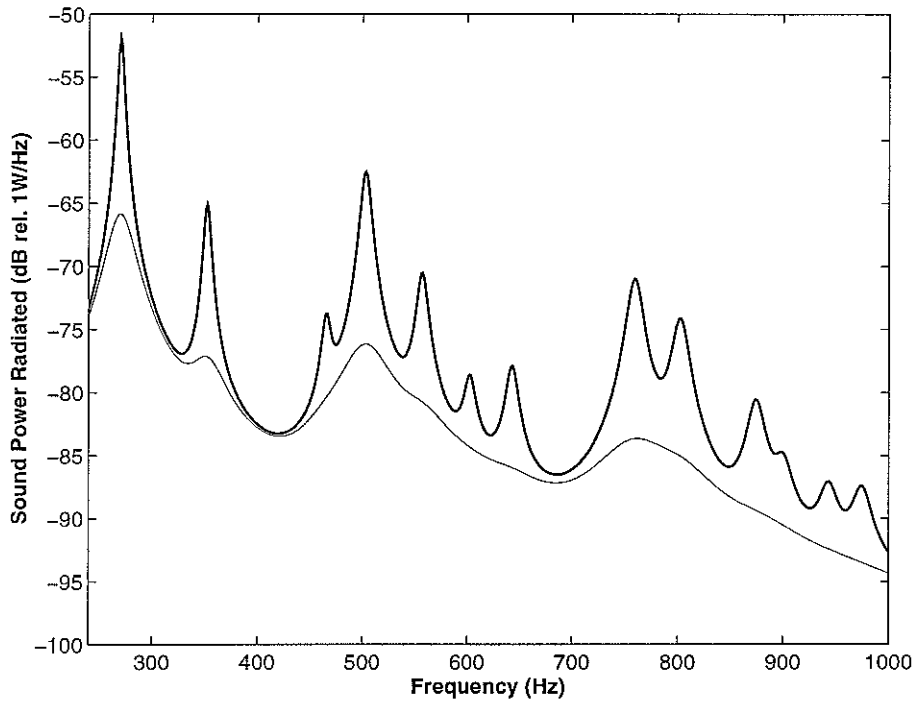
Figure 6.8 Influence of an increased structural damping on the sound power inwardly radiated by an aircraft panel: bold ($\varsigma = 0.01$) and thin ($\varsigma = 0.05$).
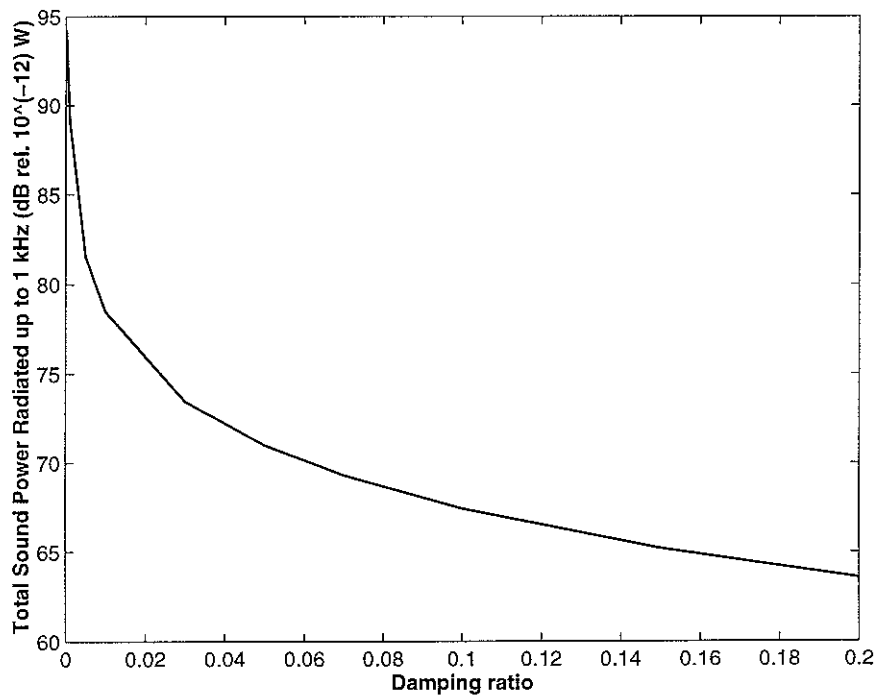
Figure 6.9 Influence of an increased structural damping on the total sound power inwardly radiated by an aircraft panel up to 1 kHz.
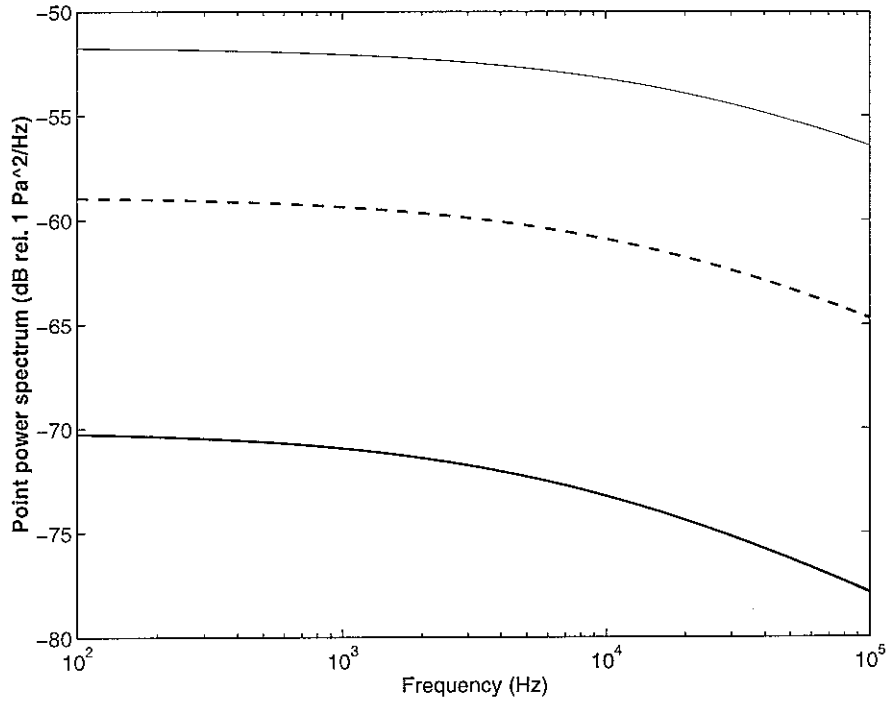
Figure 6.10 Evolution with flow velocity (thin, $U_\infty = 225\,\text{m/s}$; dashed, $U_\infty = 130\,\text{m/s}$; bold, $U_\infty = 55\,\text{m/s}$) of the point-power spectrum of the wall-pressure fluctuations beneath a turbulent boundary layer and described by the Efimtsov model.
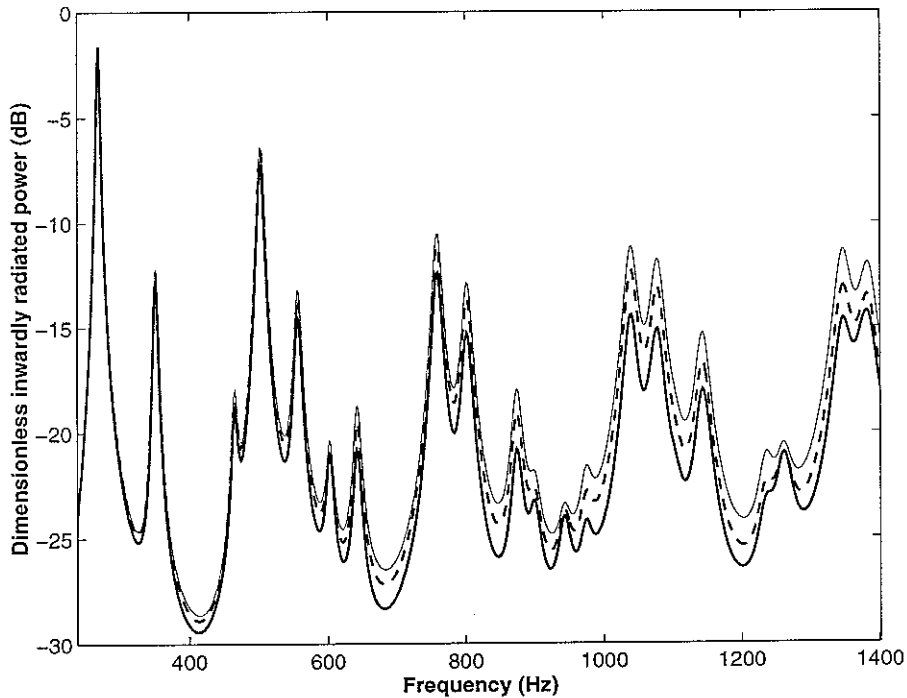

Figure 6.11 Influence of an increased flow velocity on the dimensionless sound power inwardly radiated by an aircraft panel ($\varsigma = 0.01$): $U_\infty = 200\,\text{m/s}$, bold; $U_\infty = 225\,\text{m/s}$, dashed; $U_\infty = 250\,\text{m/s}$, thin.
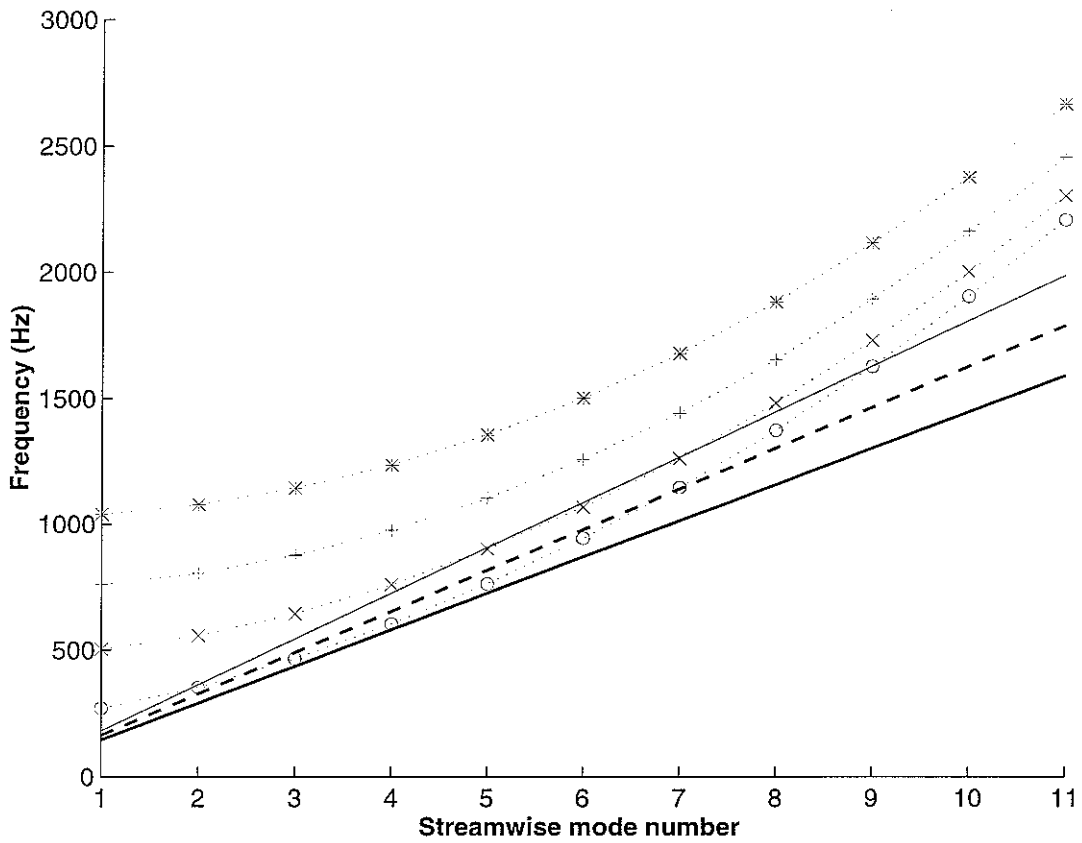
Figure 6.12 Hydrodynamic matching effect between the modal resonances for spanwise mode numbers of m=1 (o), m=2 (×), m=3 (+), m=4 (*) against streamwise mode number and the hydrodynamic matching lines $\omega/U_c = n\pi/a$ *for three flow velocities:* $U_\infty = 200\,\mathrm{m\,/\,s}$, *bold;* $U_\infty = 225\,\mathrm{m\,/\,s}$, *dashed;* $U_\infty = 250\,\mathrm{m\,/\,s}$, *thin.*
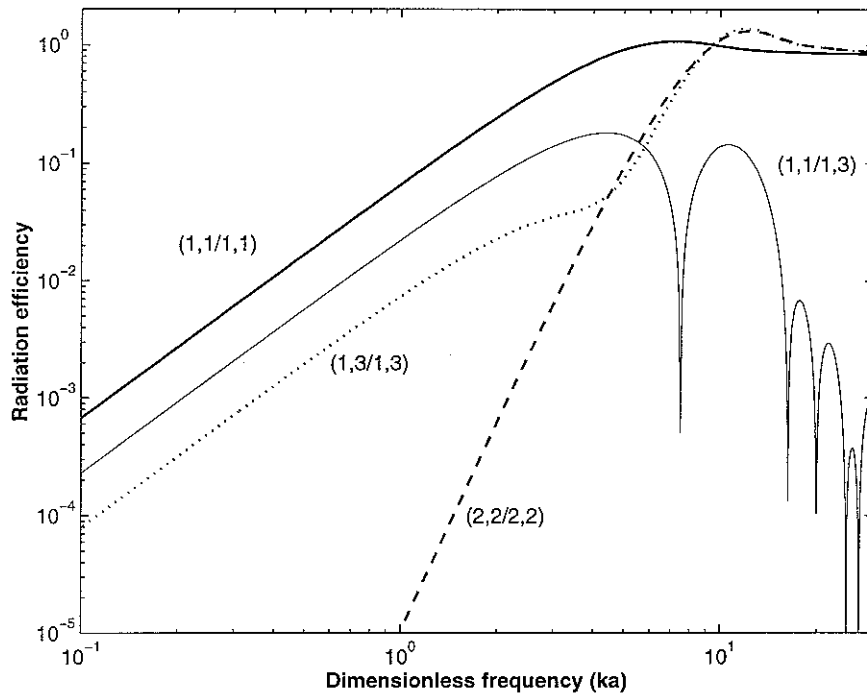
*Figure 6.13 The self-radiation efficiencies of the (1,1) (bold), (1,3) (dotted) and (2,2) (dashed) **structural** modes of the panel, and the mutual-radiation efficiency between the (1,1) and the (1,3) **structural** modes (thin).*
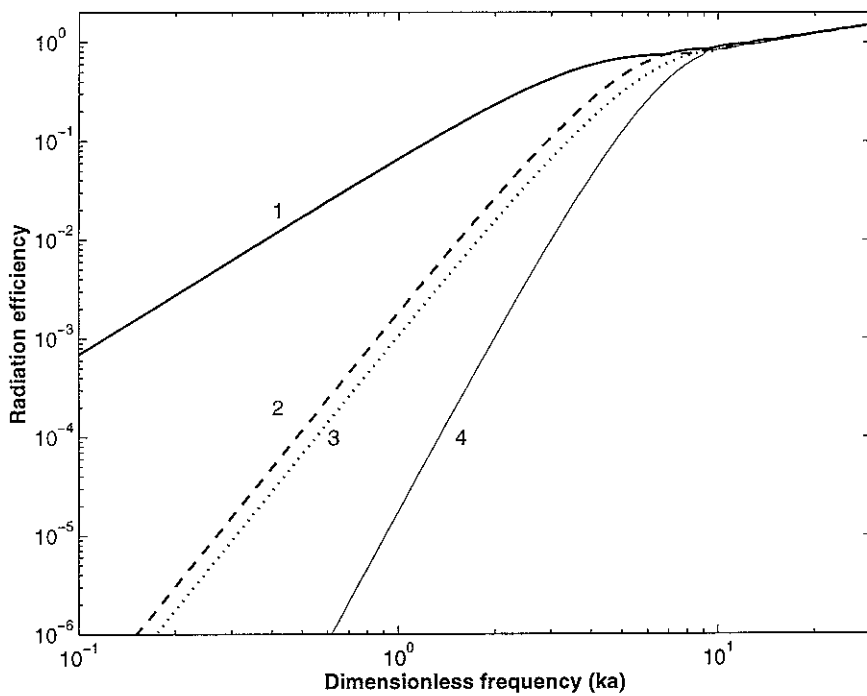

*Figure 6.14 The radiation efficiencies of the first four **radiation** modes of the panel.*
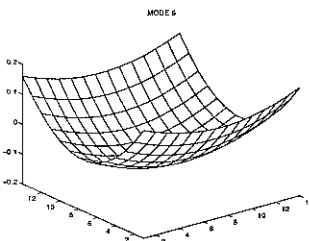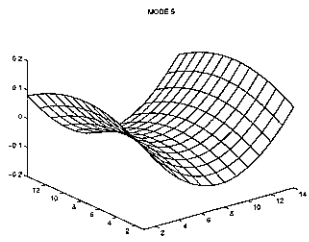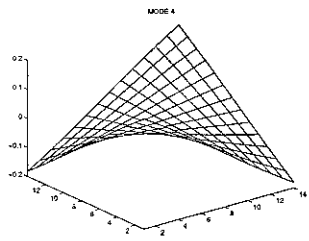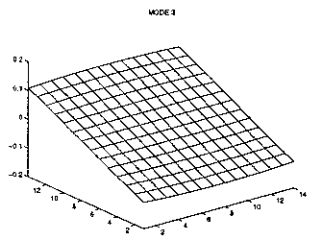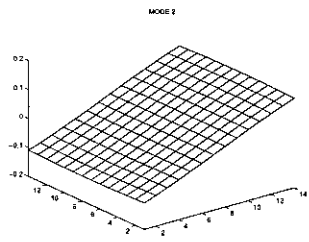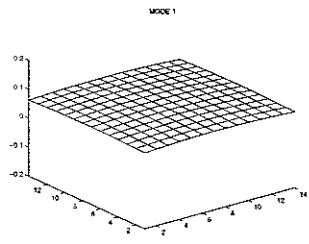
f=250 Hz   **f=1000 Hz**
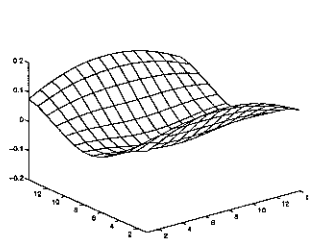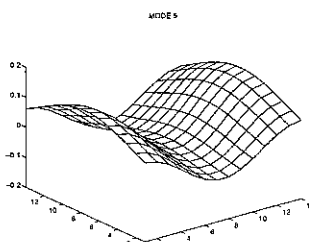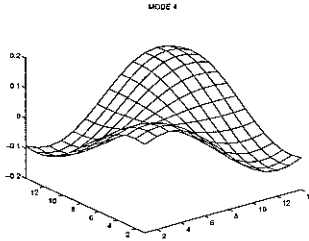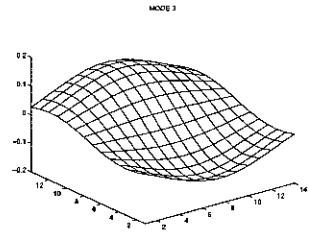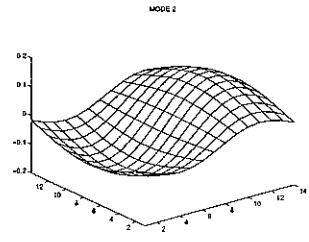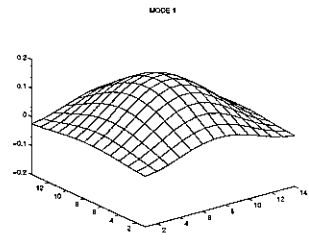
*Figure 6.15 The mode shapes of the first six radiation modes of the panel for excitation frequencies corresponding to ka = 1.9 (left column) and ka = 7.6 (right column).*
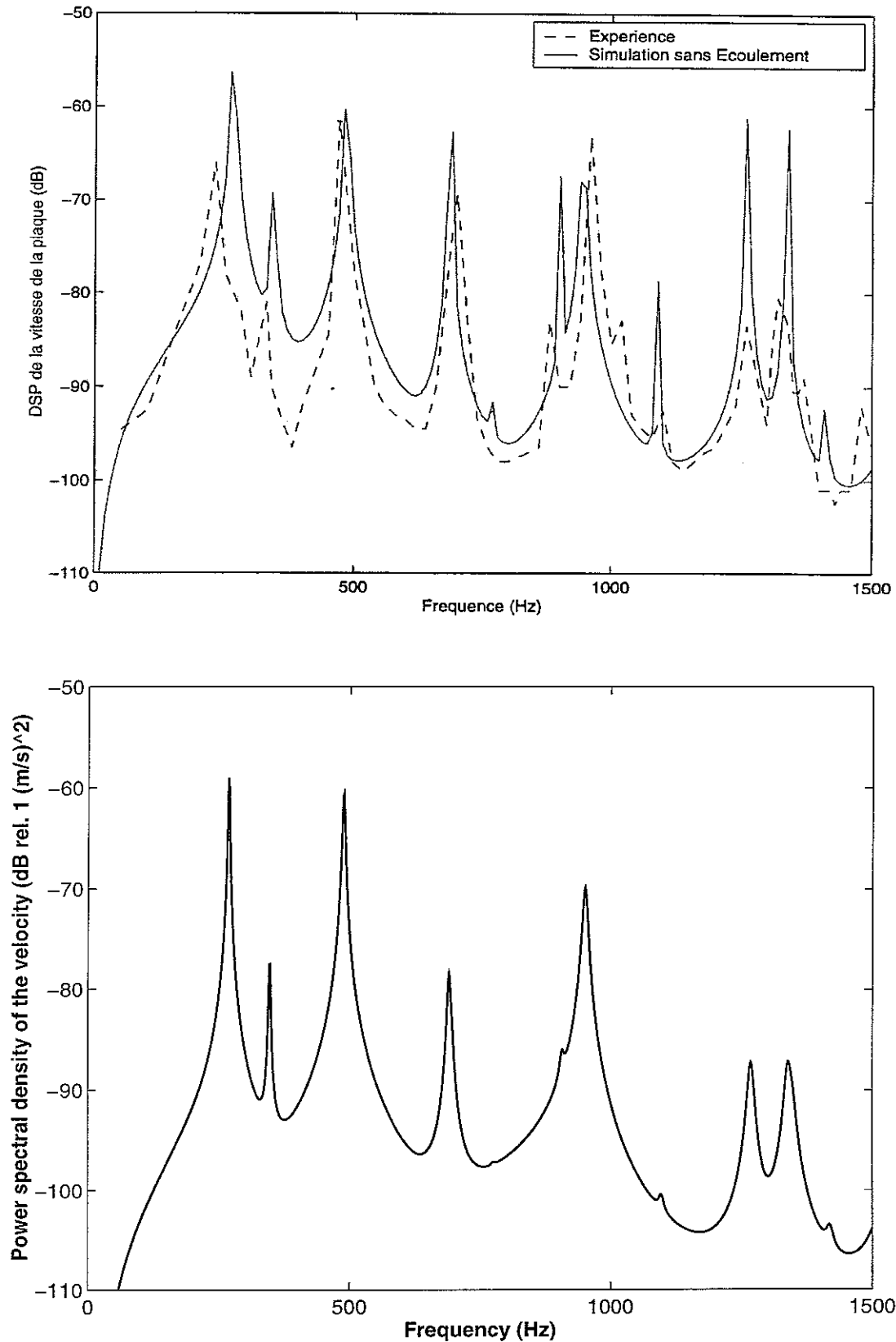
Figure 6.16 The power spectral density of the velocity, at the point R1, of a clamped plate excited by a TBL: comparisons between measurements by G. Robert (top fig., dashed line) and predictions obtained either by a Boundary Integral Equation method (top fig., thin line) or a modal formulation (bottom fig.).
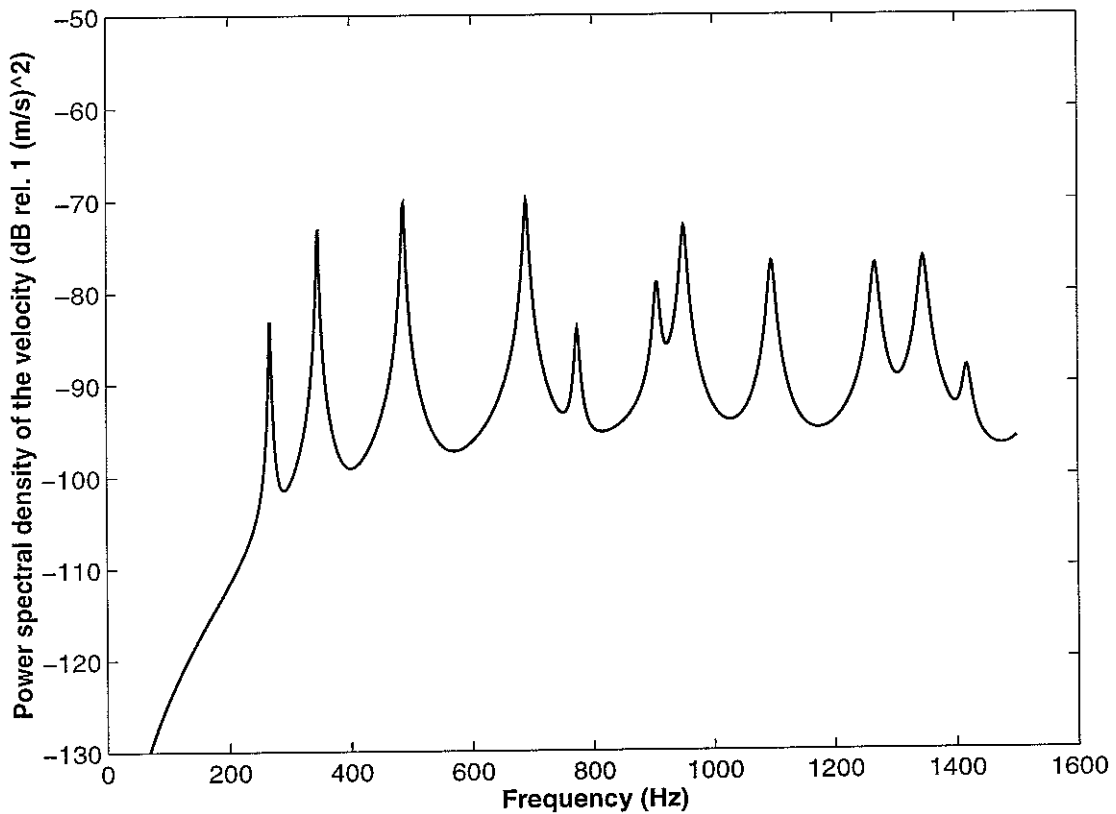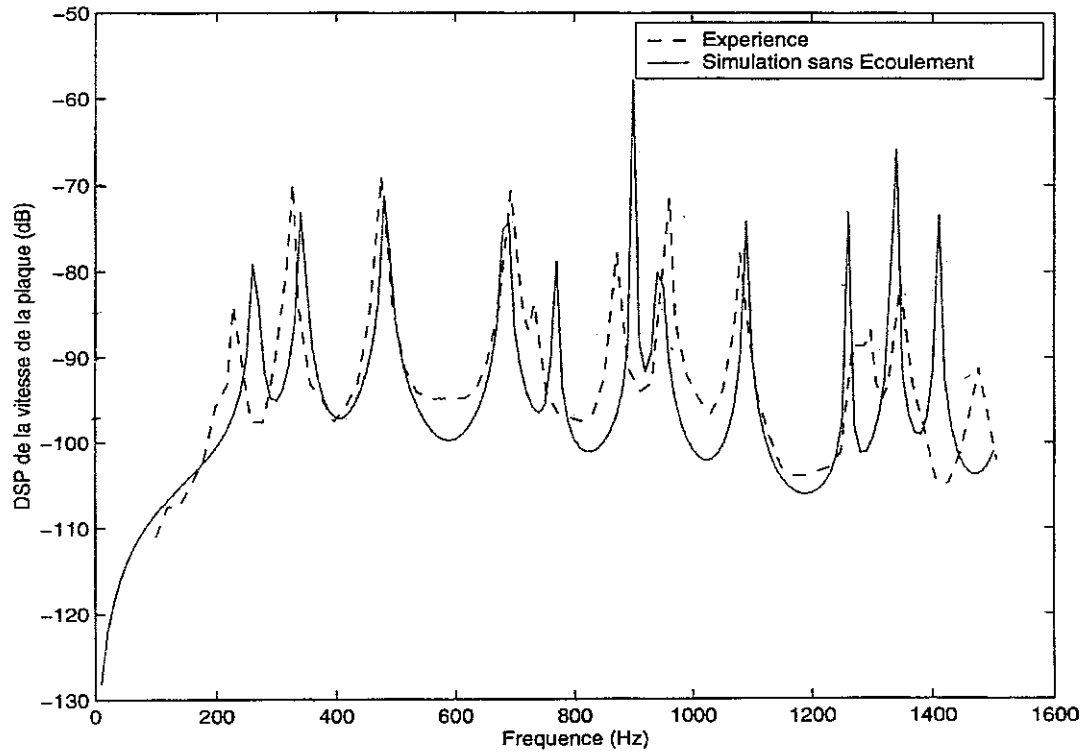
Figure 6.17 The power spectral density of the velocity, at the point R2, of a clamped plate excited by a TBL: comparisons between measurements by G. Robert (top fig., dashed line) and predictions obtained either by a Boundary Integral Equation method (top fig., thin line) or a modal formulation (bottom fig.).
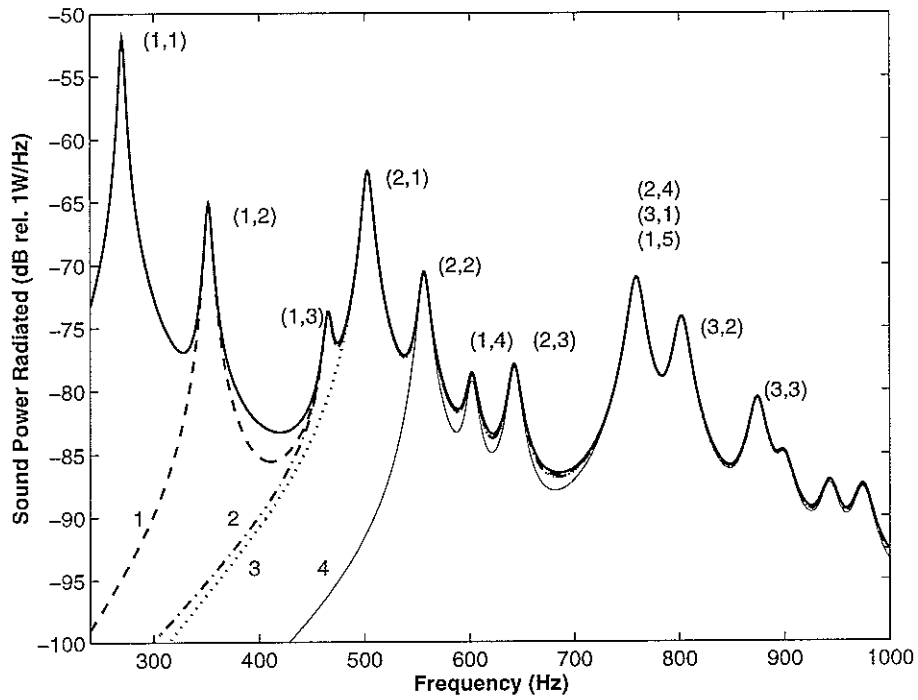
Figure 6.18 The sound power inwardly radiated by an aircraft panel ($\varsigma = 0.01$) before control (bold) and after cancellation of a number of **structural** modes: the first mode (dashed), the two first modes (dash-dotted), the three first modes (dotted) and the four first modes (thin).
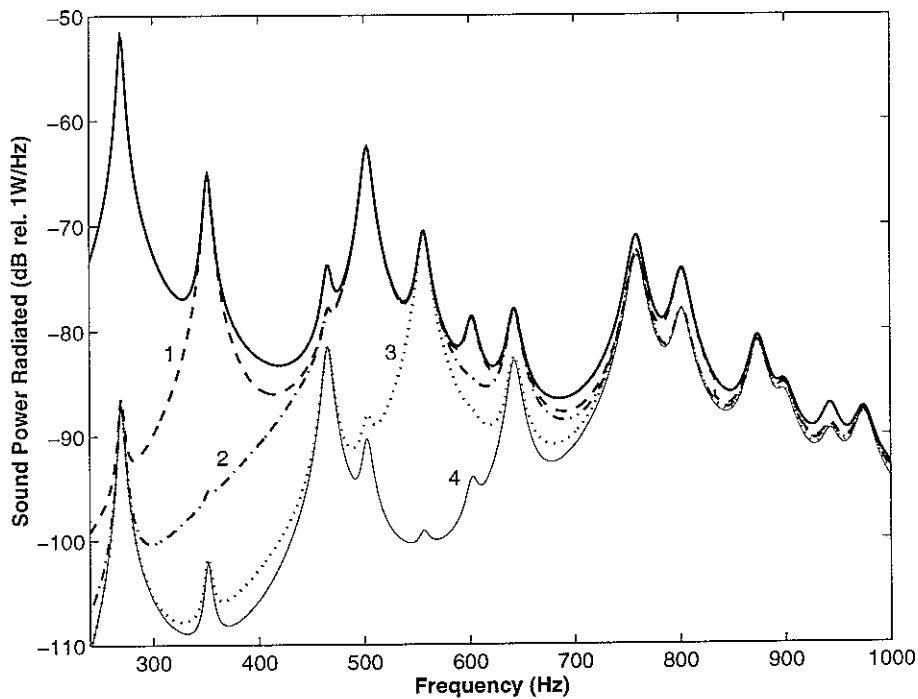
Figure 6.19 The sound power inwardly radiated by an aircraft panel ($\varsigma = 0.01$) before control (bold) and after cancellation of a number of **radiation** modes: the first mode (dashed), the two first modes (dash-dotted), the three first modes (dotted) and the four first modes (thin).
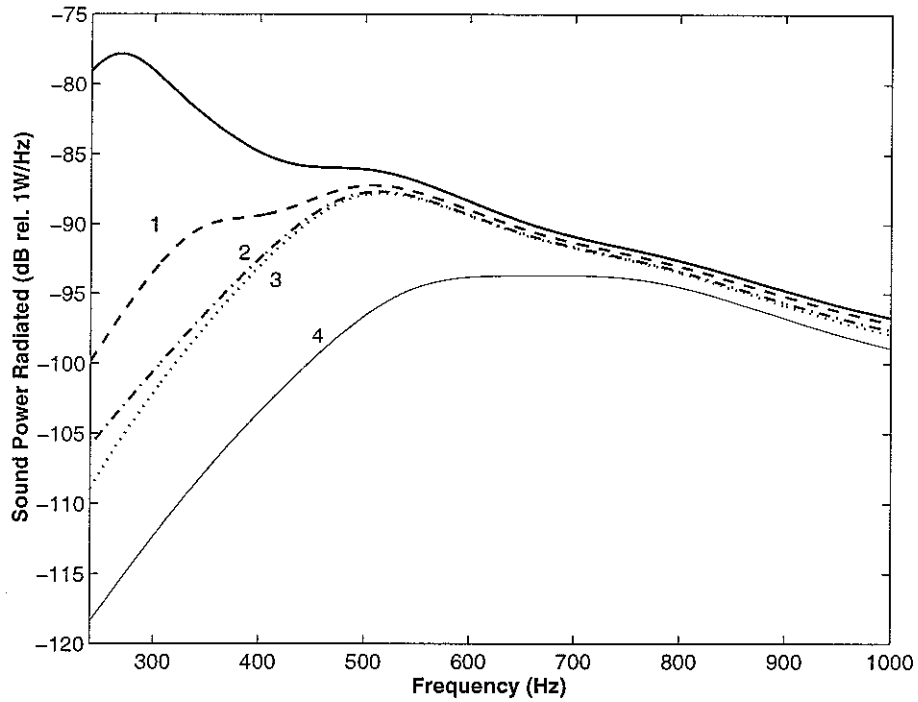
*Figure 6.20 The sound power inwardly radiated by an aircraft panel ($\varsigma = 0.2$) before control (bold) and after cancellation of a number of **structural** modes: the first mode (dashed), the two first modes (dash-dotted), the three first modes (dotted) and the four first modes (thin).*
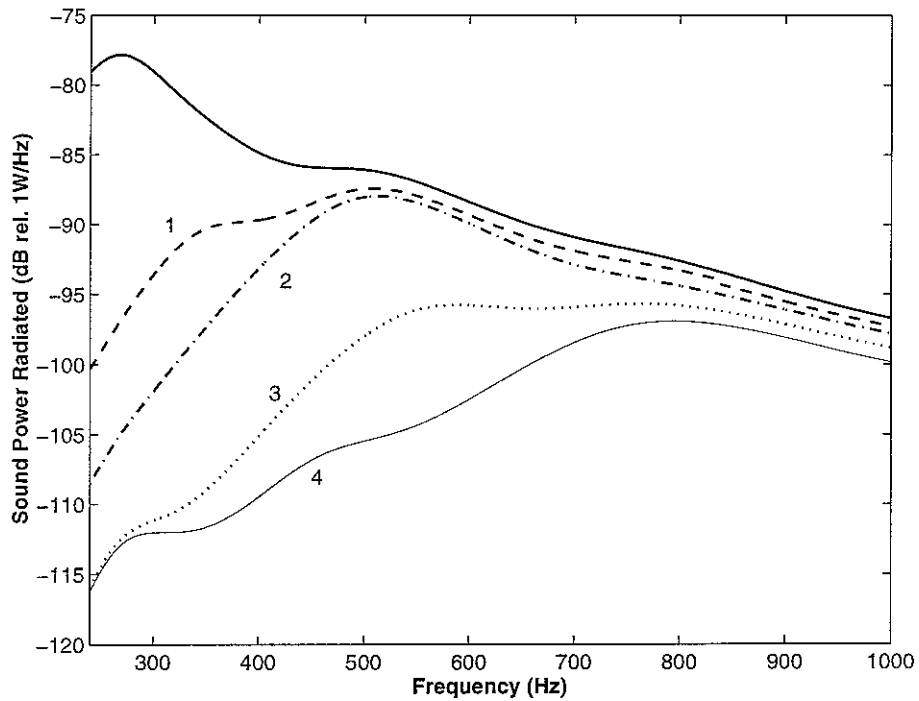
*Figure 6.21 The sound power inwardly radiated by an aircraft panel ($\varsigma = 0.2$) before control (bold) and after cancellation of a number of **radiation** modes: the first mode (dashed), the two first modes (dash-dotted), the three first modes (dotted) and the four first modes (thin).*
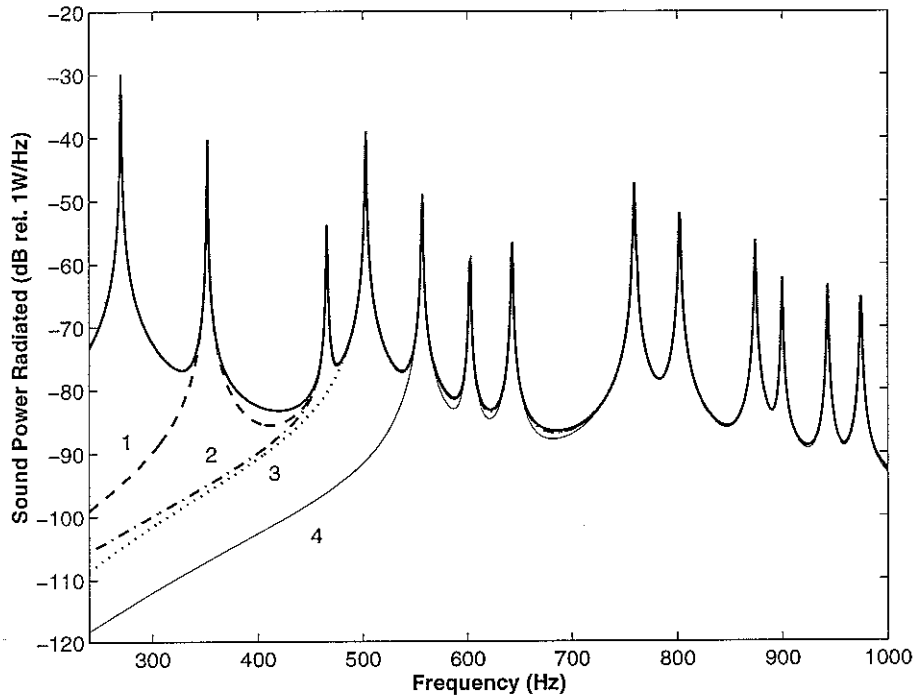
*Figure 6.22 The sound power inwardly radiated by an aircraft panel (ç = 0.0005) before control (bold) and after cancellation of a number of **structural** modes: the first mode (dashed), the two first modes (dash-dotted), the three first modes (dotted) and the four first modes (thin).*


*Figure 6.23 The sound power inwardly radiated by an aircraft panel (ç = 0.0005) before control (bold) and after cancellation of a number of **radiation** modes: the first mode (dashed), the two first modes (dash-dotted), the three first modes (dotted) and the four first modes (thin).*

Figure 6.24 Attenuation in the sound power radiated by an aircraft panel ($\varsigma = 0.01$): after cancellation of the first radiation modes (dash-dotted) and after cancellation of the first structural modes (dashed).

*Figure 6.25 Attenuation in the sound power radiated by a TBL-excited panel after cancellation of the first **structural** modes for different values of the damping ratio:* $\varsigma = 0.0005$ *(bold),* $\varsigma = 0.01$ *(dash-dotted),* $\varsigma = 0.05$ *(dashed) and* $\varsigma = 0.2$ *(dotted).*

*Figure 6.26 Attenuation in the sound power radiated by a TBL-excited panel after cancellation of the first **radiation** modes for different values of the damping ratio:* $\varsigma = 0.0005$ *(bold),* $\varsigma = 0.01$ *(dash-dotted),* $\varsigma = 0.05$ *(dashed) and* $\varsigma = 0.2$ *(dotted).*

8. REFERENCES

[1] S.J. ELLIOTT, P.A. NELSON, I.M. STOTHERS and C.C. BOUCHER (1990) *Journal of Sound and Vibration*, **140**, 219-238. In-flight experiments on the active control of propeller-induced cabin noise.

[2] C.F. ROSS and M.R.J. PURVER (1997) *Proceedings ACTIVE 97*, XXXIX-XLVI. Active cabin noise control.

[3] T.J. SUTTON, S.J. ELLIOTT, M.J. BRENNAN, K.H. HERON and D.A.C. JESSOP (1997) *Journal of Sound and Vibration*, **205**, 81-101. Active isolation of multiple structural waves on a helicopter gearbox struts.

[4] M.J. BRENNAN, R.J. PINNINGTON and S.J. ELLIOTT (1994) *ASME Journal of Vibration and Acoustics*, **116**, 548-554. Mechanism of noise transmission through helicopter gearbox struts.

[5] D.R. THOMAS and P.A. NELSON (1995) *Journal of the Acoustical Society of America*, **98**(5), 2651-2662. Feedback control of sound radiation from a plate excited by a turbulent boundary layer.

[6] W.T. BAUMANN, W.R. SAUNDERS and H.H. ROBERTSHAW (1992) *Journal of the Acoustical Society of America*, **92**, 1998-2005. Active structural acoustic control of broadband disturbances.

[7] R.L. CLARK and K.D. FRAMPTON (1997) *Journal of the Acoustical Society of America*, **102**(3), 1639-1647. Aeroelastic structural acoustic coupling: Implications on the control of turbulent boundary-layer noise transmission.

[8] S.J. ELLIOTT and M.E. JOHNSON (1993) *Journal of the Acoustical Society of America* **94**(4), 2194-2204. Radiation modes and the active control of sound power.

[9] T.C. SORS and S.J. ELLIOTT (1999) *Smart Materials Structures*, **8**, 301-314. Modelling and feedback control of sound radiation from a vibrating panel.

[10] W.R. GRAHAM (1996) *Journal of Sound and Vibration* **192**(1), 101-120. Boundary layer induced noise in aircraft, Part I: the flat plate model.

[11] W.V. BHAT (1971) *Journal of Sound and Vibration* **14**(4), 439-457. Flight test measurement of exterior turbulent boundary layer pressure fluctuations on Boeing model 737 airplane.

[12] J.F. WILBY and F.L. GLOYNA (1972) *Journal of Sound and Vibration* **23**(4), 443-466. Vibration measurements of an airplane fuselage structure, part I: turbulent boundary excitation.

[13] W.R. GRAHAM (1995) *Journal of the Acoustical Society of America* **98**(3), 1581-1595. The influence of curvature on the sound radiated by vibrating panels.

[14] L. CREMER, M. HECKL and E.E. UNGAR (1988) *Structure-borne Sound*. Second Edition, Springer-Verlag, Berlin.

[15] W.R. GRAHAM (1996) *Journal of Sound and Vibration* **192**(1), 121-138. Boundary layer induced noise in aircraft, Part II: the trimmed flat plate model.

[16] A. CUMMINGS, H.J. RICE and R. WILSON (1999) *Journal of Sound and Vibration* **221**(1), 143-167. Radiation damping in plates, induced by porous media.

[17] H.G. DAVIES (1971) *Journal of the Acoustical Society of America* **55**, 213-219. Sound from turbulent boundary layer excited panels.

[18] G. ROBERT (1984) *Modélisation et simulation du champ excitateur induit sur une structure par une couche limite turbulente.* Thèse 84-02, Ecole Centrale de Lyon, France.

[19] S. BANO, R. MARMEY, L. JOURDAN et J.-P. GUIBERGIA (1992) *Journal d'Acoustique* **5**, 99-124. Etude théorique et expérimentale de la réponse vibro-acoustique d'une plaque couplée à une cavité en fluide lourd.

[20] W.R. GRAHAM (1997) *Journal of Sound and Vibration* **206**(4), 541-565. A comparison of models for the wavenumber-frequency spectrum of turbulent boundary layer pressures.

[21] Y.F. HWANG and G. MAIDANIK (1990) *Journal of Sound and Vibration* **142**(1), 135-152. A wavenumber analysis of the coupling of a structural mode and flow turbulence.

[22] R.L. CLARK and K.D. FRAMPTON (1999) *Journal of the Acoustical Society of America* **105**(2), 743-754. Aeroelastic structural acoustic control.

[23] P.L. SHAH and M.S. HOWE (1996) *Journal of Sound and Vibration* **197**, 103-115. Sound generated by a vortex interacting with a rib-stiffened elastic plate.

[24] M.S. HOWE (1989) *Journal of Fluids and Structures* **83**, 83-96. Sound produced by turbulent boundary layer flow over a finite region of wall roughness, and over a forward facing step.

[25] M.S. HOWE (1998) *Journal of Sound and Vibration* **209**(3), 519-530. On the contribution from skin steps to boundary-layer generated interior noise.

[26] A.O. BORISYUK and V.T. GRINCHENKO (1997) *Journal of Sound and Vibration* **204**(2), 213-237. Vibration and noise generation by elastic elements excited by a turbulent flow.

[27] B.M. EFIMTSOV (1982) *Soviet Physics Acoustics* **28**(4), 289-292. Characteristics of the field of turbulent wall pressure fluctuations at large Reynolds numbers.

[28] M.K. BULL (1996) *Journal of Sound and Vibration* **190**(3), 299-315. Wall-pressure fluctuations beneath turbulent boundary layers: some reflections on forty years of research.

[29] D. HABAULT and P.J.T. FILIPPI (1999) *Journal of Sound and Vibration* **213**(2), 333-374. Light fluid approximation for sound radiation and diffraction by thin elastic plates.

[30] M.B. PRIESTLEY (1981) *Spectral analysis and time series.* Academic Press, London.

[31] R. OHAYON and C. SOIZE (1998) *Structural acoustics and vibration: mechanical models, variational formulations and discretization.* Academic Press, San Diego.

[32] D.M. CHASE (1987) *Journal of Sound and Vibration* **112**(1), 125-147. The character of the turbulent wall pressure spectrum at subconvective wavenumbers and a suggested comprehensive model.

[33] D. MAZZONI and U. KRISTIANSEN (1999) *Flow, turbulence and combustion* **61**, 133-159. Finite-difference method for the acoustic radiation of an elastic plate excited by a turbulent boundary layer: a spectral domain solution.

[34] D.G. CRIGHTON, A.P. DOWLING, J.E. FFOWCS WILLIAMS, M. HECKL and F.G. LEPPINGTON (1992) *Modern methods in analytical acoustics.* Lecture notes, Springer-Verlag, Berlin.

[35] A.W. LEISSA (1969) *Vibrations of plates*. Washington D.C. Office of Technology Utilisation, National Aeronautics and Space Administration, NASA SP-160.

[36] G.B. WARBURTON (1951) *Proceedings of the Institute of Mechanical Engineering* **168**, 371-384. The vibration of rectangular plates.

[37] P. GARDONIO and S.J. ELLIOTT (1998) *Driving Point and Transfer Mobility Matrices for Thin Plates Excited in Flexure*. ISVR Technical Report No. 277.

[38] R.F. KELTIE and H. PENG (1987) *ASME Journal of Vibration and Acoustics* **109**, 48-54. The effects of modal coupling on the acoustic power radiation from panels.

[39] F.G. LEPPINGTON, E.G. BROADBENT, K.H. HERON and S.M. MEAD (1986) *Proceedings of the Royal Society of London* A **406**, 139-171. Resonant and non-resonant acoustic properties of elastic panels.

[40] R.A. MKHITAROV (1972) *Soviet Physics Acoustics* **18**, 123-126. Interaction of the vibrational modes of a thin bounded plate in a liquid.

[41] W.R. GRAHAM (1995) *Proceedings of the Royal Society of London* A **352**, 1-43. High-frequency vibration and acoustic radiation of fluid-loaded plates.

[42] I. DYER (1959) *Journal of the Acoustical Society of America* **31**, 922-928. Boundary layer induced flow noise.

[43] G.M. CORCOS (1964) *Journal of Fluid Mechanics* **18**, 353-378. The structure of the turbulent pressure field in boundary layer flows.

[44] D.M. CHASE (1980) *Journal of Sound and Vibration* **70**(1), 29-67. Modelling the wavevector-frequency spectrum of turbulent boundary layer wall pressure.

[45] G. COUSIN (1998) *Sound from TBL-induced vibrations*. Paper No. 98-2216 in Proceedings of the 4th AIAA/CEAS Aeroacoustics Conference, 2-4 June, Toulouse, France.

[46] W.K. BLAKE (1986) *Mechanics of Flow-Induced Sound and Vibration: Complex Flow-Structure Interactions*, **II**. Academic Press, New-York.

[47] C. DURANT, G. ROBERT, P.J.T. FILIPPI and P.-O. MATTEI (2000) *Journal of Sound and Vibration* **229**(5), 1115-1155. Vibroacoustic response of a thin cylindrical shell excited by a turbulent internal flow: comparison between numerical prediction and experimentation.

[48] J.M. WITTING (1986) *Noise Control Engineering Journal* **26**(1), 28-43. A spectral model of pressure fluctuations at a rigid wall bounding an incompressible fluid, based on turbulent structures in the boundary layer.

[49] R.D. BLEVINS (1984) *Formulas for natural frequency and mode shape*. Edited by Robert E. Krieger, Malabar, Florida.

[50] J.C. NEVES, P. MOIN and R.D. MOSER (1994) *Journal of Fluid Mechanics* **272**, 349-381. Effects of convex transverse curvature on wall-bounded turbulence. Part 1. The velocity and vorticity.

[51] C.E. WALLACE (1970) *Journal of the Acoustical Society of America*, **51**(3), 946-952. Radiation resistance of a rectangular panel.

[52] W.H. PRESS, S.A. TEUKOLSKY, W.T. VETTERLING and B.P. FLANNERY (1992) *Numerical Recipes in FORTRAN: The Art of Scientific Computing*. Cambridge University Press, Second Edition, Cambridge.

[53] H.M. HELAL, M.J. CASARELLA and T.M. FARABEE (1989) *ASME Winter Annual Meeting*, NCA-Vol.5, 49-59. An application of noise cancellation techniques to the measurement of wall-pressure fluctuations in a wind-tunnel.

[54] M.P. HORNE and R.A. HANDLER (1991) *Experiments in Fluids* **12**, 136-139. Note on the cancellation of contamining noise in the measurement of turbulent wall-pressure fluctuations.

[55] M. SURGAND (1999) *Rayonnement vibro-acoustique d'une plaque couplée à une cavité et soumise à une couche limite turbulente.* Thèse CNRS-LMA n° 3401-99-195, Marseille, France.

[56] C.K. BARTON and J.S. MIXSON (1981) *Journal of Aircraft* Vol. **18**(7), 570-575. Noise-transmission and control for a light twin-engine aircraft.

[57] C. MAURY, P. GARDONIO and S.J. ELLIOTT (2000) *Active control of the flow-induced noise transmitted through a panel.* Paper n° 2042 in Proceedings of the 6th AIAA/CEAS Aeroacoustics Conference, 12-14 June, Hawaii, USA.

[58] L. SCHWARTZ (1979) *Analyse Hilbertienne*, Hermann, Paris.

[59] K.A. CUNEFARE and N. CURREY (1994) *Journal of the Acoustical Society of America* **96**, 2302-2312. On the exterior acoustic radiation modes of structures.

[60] A. SARKISSIAN (1991) *Journal of the Acoustical Society of America* **90**, 754-778. Acoustic radiation from finite structures.

[61] D.M. PHOTIADIS (1990) *Journal of the Acoustical Society of America* **88**, 1152-1159. The relationship of singular value decomposition to wave-vector filtering in sound radiation problems.

[62] P.T. CHEN and J.H. GINSBERG (1995) *Journal of the Acoustical Society of America* **98**(6), 3343-3351. Complex power, reciprocity, and radiation modes for submerged bodies.

Appendix A

Expressions for the cross-correlation functions involved in the derivation of the power balance equation

$$R_{\mathcal{A}_p(w)\dot{w}}(\mathbf{x},\mathbf{x}';\tau) = \int\limits_{-\infty}^{+\infty}\int\limits_{-\infty}^{+\infty} \iint\limits_{\Sigma} \iint\limits_{\Sigma} \mathcal{A}_p(\gamma(\mathbf{x}-\mathbf{x}'';\tau-t'))R_{p_bp_b}(\mathbf{x}''-\mathbf{x}''';t'-t'')$$

$$\times \frac{\partial\gamma^*}{\partial\tau}(\mathbf{x}'-\mathbf{x}''';\tau-t'')\, d^6\beta$$

$$R_{\ddot{w}\dot{w}}(\mathbf{x},\mathbf{x}';\tau) = \int\limits_{-\infty}^{+\infty}\int\limits_{-\infty}^{+\infty} \iint\limits_{\Sigma} \iint\limits_{\Sigma} \frac{\partial^2\gamma}{\partial\tau^2}(\mathbf{x}-\mathbf{x}'';\tau-t')R_{p_bp_b}(\mathbf{x}''-\mathbf{x}''';t'-t'')$$

$$\times \frac{\partial\gamma^*}{\partial\tau}(\mathbf{x}'-\mathbf{x}''';\tau-t'')\, d^6\beta$$

$$R_{p^{\pm}\dot{w}}(\mathbf{x},\mathbf{x}';\tau) = \int\limits_{-\infty}^{+\infty}\int\limits_{-\infty}^{+\infty} \iint\limits_{\Sigma} \iint\limits_{\Sigma} \mathcal{O}^{\pm}_{\mathbf{x}-\mathbf{x}';\tau-t'}(\mathbf{x}-\mathbf{x}'';\tau-t')R_{p_bp_b}(\mathbf{x}''-\mathbf{x}''';t'-t'')$$

$$\times \frac{\partial\gamma^*}{\partial\tau}(\mathbf{x}'-\mathbf{x}''';\tau-t'')\, d^6\beta$$

where $\mathcal{O}^{\pm}_{\mathbf{x};t}(\gamma) = (\gamma \underset{(t')}{\overset{*}{_{(\mathbf{x}')}}} \mathcal{G}^{\pm})(\mathbf{x};t)$. It is an integral operator defined over space-time domain and associated to the time-domain integral representation of the radiated acoustic field generated by the displacement γ, $\mathcal{G}^{\pm}$ being the inverse Fourier transform of the Green's function.

$$R_{p_b\dot{w}}(\mathbf{x},\mathbf{x}';\tau) = \int\limits_{-\infty}^{+\infty}\int\limits_{-\infty}^{+\infty} \iint\limits_{\Sigma} \iint\limits_{\Sigma} \mathcal{O}^{\pm}_{\mathbf{x}-\mathbf{x}';\tau-t'}(\mathbf{x}-\mathbf{x}'';\tau-t')R_{p_bp_b}(\mathbf{x}''-\mathbf{x}''';t'-t'')$$

$$\times \frac{\partial\gamma^*}{\partial\tau}(\mathbf{x}'-\mathbf{x}''';\tau-t'')\, d^6\beta$$

Appendix B

Construction of an orthonormal set of velocity patterns that diagonalize the radiation operator relating the surface velocity and the acoustic pressure field.

B.1 Spatial representation of the acoustic power radiated.

The weak (energetic) form of the governing equations (3.8) together with the Green's representation (3.10) of the acoustic pressure field lead to an expression for the complex surface power the real part of which corresponds to the acoustic power radiated by the structure in the far-field. It is proportional to the positive form of the radiation operator given by:

$$
<< \mathcal{R}_\omega \, u, v >> = \iint\limits_\Sigma \iint\limits_\Sigma u(x) \, \mathfrak{R}[\mathcal{G}_\omega(x - x')] \, v^*(x') d^2x \, d^2x' \tag{B.1}
$$

where u and v are surface velocity distributions and $\mathcal{G}_\omega$ is the Green's function introduced in paragraph 3.1. For simplicity, the kernel $\mathfrak{R}[\mathcal{G}_\omega]$ of the operator $\mathcal{R}_\omega$ will be denoted R_ω. We notice that the test functions u and v must be square integrable, i.e. belong to $L^2(\Sigma, C)$ where C stands for the set of complex numbers.

B.2 Properties of the radiation operator.

◆ B.2.a: From Eq. (3.11), it can easily be seen that the function $(x, x') \mapsto R_\omega(x, x')$ is *bounded* over $\Sigma \times \Sigma$.

◆ B.2.b: $R_\omega \in L^2(\Sigma \times \Sigma, \mathcal{A}(C))$, i.e. R_ω belongs to the Hilbert space of the functions with values in $\mathcal{A}(C)$ and *square integrable* over $\Sigma \times \Sigma$; $\mathcal{A}(C)$ denotes all the linear applications in C.
It means that:

$$
\iint\limits_\Sigma \iint\limits_\Sigma \|R_\omega(x, x')\|^2_{\mathcal{A}(C)} d^2x \, d^2x' < +\infty \tag{B.2}
$$

that can be proved when expressing (B.2) in a system of cylindrical coordinates. This property results from the analytical expression (3.11) of R_ω that satisfies the energy conservation principle (field of second order).

◆ B.2.c: Finally, from (B.2), it can be shown that the operator $\mathcal{R}_\omega$ is *continuous* from $L^2(\Sigma, C)$ into $L^2(\Sigma, C)$.

From the properties (B.2.a-c), it results, by definition, that $\mathcal{R}_\omega$ is a *Hilbert-Schmidt* linear operator and so it is *compact* [58]. This means that its spectrum is discrete and countable.

Moreover, $\mathcal{R}_\omega$ is a *symmetric* operator:

$$<< \mathcal{R}_\omega u, v >> = << u, \mathcal{R}_\omega v >> \quad \forall (u,v) \in L^2(\Sigma, C) \tag{B.3}$$

It results from the mathematical form of (B.1) and the fact that R_ω satisfies the reciprocity principle. Finally, $\mathcal{R}_\omega$ is *positive* and satisfies, for any ω in R:

$$<< \mathcal{R}_\omega u, u >> \geq 0 \quad \forall u \in L^2(\Sigma, C) \tag{B.4}$$

All these properties enable to justify the *existence of an orthonormal set of eigenvectors* diagonalizing the radiation operator $\mathcal{R}_\omega$ and called the *radiation modes*.

B.3 Diagonalization of the radiation operator.

Since $\mathcal{R}_\omega$ is an Hilbert-Schmidt operator, it admits a discrete and countable set of eigenvalues $\{\lambda_\omega^n\}_n$ and there *exists* a normalized set of eigenvectors $\{\Psi_\omega^n\}_n$ of $\mathcal{R}_\omega$ that form a *Hilbert basis* of $L^2(\Sigma, C)$. Rigorously speaking, each Ψ_ω^n represents the surface velocity pattern associated with each radiation mode $\mathcal{R}_\omega(\Psi_\omega^n)$ through the relation:

$$\mathcal{R}_\omega(\Psi_\omega^n) = \lambda_\omega^n \Psi_\omega^n \tag{B.5}$$

or explicitly, through the integral equation:

$$\iint_\Sigma R_\omega(x, x') \Psi_\omega^n(x') d^2 x' = \lambda_\omega^n \Psi_\omega^n(x), \quad \forall x \in \Sigma. \tag{B.6}$$

where all the eigenvalues are not only positive (since $\mathcal{R}_\omega$ is positive) but they also satisfy the following property: the series of their squares is convergent (since $\mathcal{R}_\omega$ is a Hilbert-Schmidt operator), i.e:

$$\sum_{n=1}^{\infty} \left(\lambda_\omega^n\right)^2 < +\infty.$$

The expression (B.5) requires some comments:
♦ This expression clearly shows why each radiation mode is frequency-dependent and only depends on the surface geometry of the radiating structure and the mechanical properties of the acoustic fluid.

Let us denote $\text{Vect}\{\Phi_n\}$ the space generated by the set of the structural eigenmodes $\{\Phi_n\}$, i.e. all the complex functions square integrable together with their first and second order derivatives over Σ and satisfying the boundary conditions along

73

$\partial\Sigma$. In addition, $\text{Vect}\{\Psi_\omega^n\}$ will stand for the space generated by the set of the radiation modes $\{\Psi_\omega^n\}$, i.e. all the complex functions only square integrable over Σ. It can easily be seen that:

$$\text{Vect}\{\Phi_n\} \subset \text{Vect}\{\Psi_\omega^n\}$$

This means that, unless we manage to exhibit a subset of radiation modes satisfying the boundary conditions along $\partial\Sigma$ and that generates $\text{Vect}\{\Psi_\omega^n\}$, the set of the radiation modes $\{\Psi_\omega^n\}$ cannot be expanded into series of the structural eigenmodes $\{\Phi_n\}$. As expected, the reciprocal proposition is true.

♦ Moreover, if the structure vibrates with a surface velocity proportional to one of the Ψ_ω^n, the surface pressure radiated $\lambda_\omega^n\Psi_\omega^n$, i.e. the corresponding radiation mode, is then in-phase with the velocity distribution. This would not be the case if the surface velocity distribution was proportional to one of the structural modes. This means that *the radiation modes radiate sound independently*. This can be written formerly through the following orthogonality relation:

$$<< \mathcal{R}_\omega\left(\Psi_\omega^n\right), \Psi_\omega^m >> = \lambda_\omega^n\delta_m^n$$

in addition to the orthonormality relation:

$$<< \Psi_\omega^n, \Psi_\omega^m >> = \delta_m^n$$

♦ Since $\mathcal{R}_\omega$ is an operator from $L^2(\Sigma, C)$ into $L^2(\Sigma, C)$, it can then be expanded into a series of the new basis functions as follows:

$$\mathcal{R}_\omega u = \sum_{n=1}^\infty \lambda_\omega^n \Psi_\omega^n << \Psi_\omega^n, u >> = \sum_{n=1}^\infty \lambda_\omega^n \left(\Psi_\omega^n \underset{L^2}{\otimes} \Psi_\omega^n\right) u, \quad \forall u \in L^2(\Sigma, C). \quad (B.7)$$

where the tensor product $v \underset{L^2}{\otimes} w$ of $L^2(\Sigma, C)$ is defined as:

$$\left(v \underset{L^2}{\otimes} w\right)u = v << w, u >>_{L^2}, \quad \forall(u, v, w) \in \left(L^2(\Sigma, C)\right)^3$$

The expression (B.7) can be rewritten in terms of operators as:

$$\mathcal{R}_\omega = \sum_{n=1}^\infty \lambda_\omega^n \Psi_\omega^n \underset{L^2}{\otimes} \Psi_\omega^n \quad (B.8)$$

(B.8) is equivalent to (B.5). This shows that the diagonalization of $<< \mathcal{R}_\omega u, v >>$, for any functions u and v in $L^2(\Sigma, C)$ is equivalent to the application of a **Singular Value Decomposition** to the radiation operator $\mathcal{R}_\omega$, the $\{\lambda_\omega^n\}$ being the singular values of $\mathcal{R}_\omega$.

Several authors [9,59,60] have already performed an eigen-analysis on the real part of the impedance matrix in order to exhibit real radiation modes and so, providing an acoustic modal basis on which the radiated field can be decomposed. Moreover, this approach has been extended [61,62] to the SVD analysis of the impedance matrix to exhibit complex radiation modes for submerged bodies.